Hyaluronic-Acid Based Hydrogels as a Novel Bioscaffold for Cell Encapsulation and Angiogenic Growth Factor Delivery onto Moving Tissue and Organs

A thesis

submitted by

Roberto Elia

In partial fulfillment of the requirements
for the degree of

Master of Science

In

Biomedical Engineering

TUFTS UNIVERSITY

August 2011

Advisor: Robert A. Peattie

Abstract

A series of experiments were carried out to address the lack in therapeutic cell/drug delivery devices capable of targeting moving tissues and organs. First the *in vivo* angiogenic response to dual growth factor delivery by an *in situ* polymerizing hyaluronic acid hydrogel was investigated via direct elicited microvessel counts. Second a HA-silk biocomposite was fabricated, physically characterized and its potential use as an implantable drug or cell delivery vehicle established. Finally, hydrogel composition was optimized for survival and growth of cells encapsulated prior to hydrogel polymerization. The combination these experiments should lead to the development of a securable non-tissue site specific biocomposite capable of sustained cell growth and drug delivery as well as fostering an angiogenic response in and around the implant site.

Acknowledgments

I would like to thank my thesis committee Dr. Robert Peattie, Dr. David Kaplan and Dr. Barry Trimmer for the freedom to pursue this exciting research. I would also like to thank Dr. Glenn Prestwich and Dr. Matthew Firpo for their assistance and generosity. This project was supported by NSF award CBET-0932456, by an NIH award (EB004514), and a Tufts Graduate Student Award.

I wish to thank Mrs. Rebecca Scholl Hayden and Dr. David Wilbur for assistance with the scanning electron microscopy, Ms. Michaela R Reagan for assistance with sample lyophilization, and Dr. Peggy Cebe for assistance with the thermal characterization measurements. A special thanks to Thomas Dabrowski and Eugene Nebelitsky for all of their hilarious comments and priceless advice. I would also like to thank the Peattie lab members, Christa Margossian, Rodrigo Jose and Ethan Golden, for all their support. As well as fellow officemates at 200 Boston Ave. Lee Tien, Shannon Smith, Andrew Reeves, Cinzia Metallo and Kathleen Martinick for making these past few years so enjoyable. I would like to thank all of the undergraduate students which helped me with various aspects of this work, Francis Ball, Danny Newhide and Paul Pedevillano. Finally and most importantly I would like to thank my family for all of their encouragement, inspiration and unending support.

Table of Contents

Table of Contents

Table of Contents

List of Figures

List of Figures

List of Figures

List of Figures

1 Introduction

1.1 Problem statement

Although *in vivo* delivery of therapeutic cell lines has been attempted by many other groups, at present limited success has been reported[2]. A scaffold is critical for cell delivery because it allows for among other things; cell attachment, cell migration and exchange of vital metabolic material. The use of hydrogels as cell delivery matrices is one of the most widely employed delivery approaches because of they are biocompatible and have mechanical properties similar to soft tissue [3, 4]. However, two major problems arise with such systems. The first is that as with all hydrogel scaffolds, they are too weak to be fixed onto tissue, effectively limiting application to areas accessible via injection. The second major difficulty in maintaining encapsulated cell lines in scaffolds is ensuring the cells are able to receive nutrients or eliminate waste products. A potential solution to the first issue is the incorporation of a stiff biocompatible material that would allow fastening of the hydrogel to moving or expanding tissue, such as heart or lungs. To address the second concern, the incorporation of angiogenic growth factors could be used to stimulate a new vascular network to grow in and around the cell containing matrix.

1.2 Background

1.2.1 Biomaterials

1.2.1.1 Hyaluronic Acid

Of the naturally occurring extracellular matrix (ECM) proteins and glycosaminoglycans (GAGs) that have been used to fabricate biocompatible implants and devices, hyaluronan (HA) is especially interesting for its biocompatibility and well studied physico-chemical properties. HA is an anionic biopolymer that forms the major GAG component of the ECM. HA is the only non-sulfated GAG, HA consisting of repeating disaccharide units, (Figure 1a), with an overall molecular weight (MW) between 100 kDa and 5000 kDa.[5-7]. The adult human body contains approximately 15 g of HA, 33% of which is replaced daily[8]. Present in all connective tissues, HA forms a scaffold for binding other large GAGs and proteoglycans [9], which are maintained through specific HA-protein interactions.

HA is degraded *in vivo* by hyaluronidases (HAses), a family of six different enzymes that each differently cleave HA chains by hydrolysis into shorter fragments[10 1]. Short (<20 monomers) HA oligomers (o-HA) are an important example of products generated via hyaluronidase mediated HA degradation[11]. It has been shown that presence of these short chains increases dramatically at sites of injury, inflammation and in tumors[12]. This increase is thought to be caused by increased HA content, HA receptor availability, and presence of HAses[12, 13] . These shorter HA fragments are highly bioactive and have been shown to interact with a variety of cellular pathways, including angiogenesis. These interactions are not otherwise possible with long chain HA (n-HA)[14].

HA also supports maintenance of the extracellular space and provides an open, hydrated structure for the passage of nutrients. HA promotes cell motility and proliferation, influences morphogenesis, wound repair, inflammation and metastasis, all through direct cell-cell and cell-matrix interactions[13, 15, 16]. HA-cell specific interactions occur through cell-surface HA receptor glycoproteins, often times cluster determinant molecule-44 (CD44)[16]. Specifically o-HA can cluster and thus activate the CD44 receptors which activate intracellular signaling cascades[16]. Other receptors that mediate the cellular response to HA fragments are Receptor for Hyaluronan-Mediated Motility (RHAMM)[17] and Toll-Like-Receptor-4[18]. These receptors allow high molecular weight n-HA and o-HA to promote endothelial cell proliferation and migration[17, 19], promote and inhibit[20] angiogenesis[21] and sprout formation[22, 23]. These properties are of critical importance in tissue repair and cell viability, making HA an excellent building block for therapeutic biomaterials.

1.2.1.2 Heparin and Gelatin

Heparan sulfates are known to sequester growth factors in the ECM. Heparin (Hp) is a mimic of these heparin sulfate and also shows the ability to sequester growth factors, primarily through electrostatic interactions between N- and O-sulfated residues of heparin and the lysine and arginine residues of growth factors (GFs)[24-28]. Heparin binding is thought to control GF release *in vivo* and stabilize GFs against thermal denaturation and degradation by ECM proteinases, while retaining their bioactivity[24]. In addition, small amounts Hp in HA-based gels have successfully regulated the rate at which growth factors are released from the gels *in vitro*[24] and augmented elicited *in vivo* vessel maturation and functionality[24, 25, 29]. Initial studies of

in vivo delivery of two cytokines in a mouse ear pinna model produced microvessels organized into recognizable tubular networks filled with erythrocytes[30, 31].

Gelatin (Gtn) is hydrolyzed collagen, and as with natural collagen, gelatin has often been chosen as a bioscaffold base or as a supplemental scaffold constituent. Such is the case because gelatin retains much of the native collagens ability to serve as a substrate for cell adhesion and promote expansion[29, 32, 33]. Collagen is the main fiber constituent of mammalian connective tissue [34] and has long been used as a tissue engineering material due to its biocompatibility[35], biodegradability[35, 36], abundance in nature[36], and natural ability to bind cells[37].

1.2.1.3 Chemically modified HA, HP and Gtn

Recently chemically-modified forms of HA, Hp and Gtn have been created that allow for intra- and intermolecular crosslinking[38]. Thiol- modified variants can be used to produce hydrogels that are greater then 96% water[38], making them a modular[39], clinically-relevant[40] material which can be customized with specific compliance to recreate a three-dimensional cell culture environment[41]. The thiol modified ECM components are crosslinked using poly(ethylene glycol)-diacrylate (PEDGA) (Figure 1b). This allows for the creation of chemically crosslinked HA-Gtn hydrogels along with Hp containing gel variants. As described above the Gtn often serves as a supplement to many other biomaterials because of it biocompatibility and natural ability to augment cell binding, while addition of Hp can help modulate hydrogel drug release.

In an *in vivo* study injectable thiol-modified HA hydrogels were evaluated for effectiveness in repair of osteochondral defects in rabbits[42]. It was found that

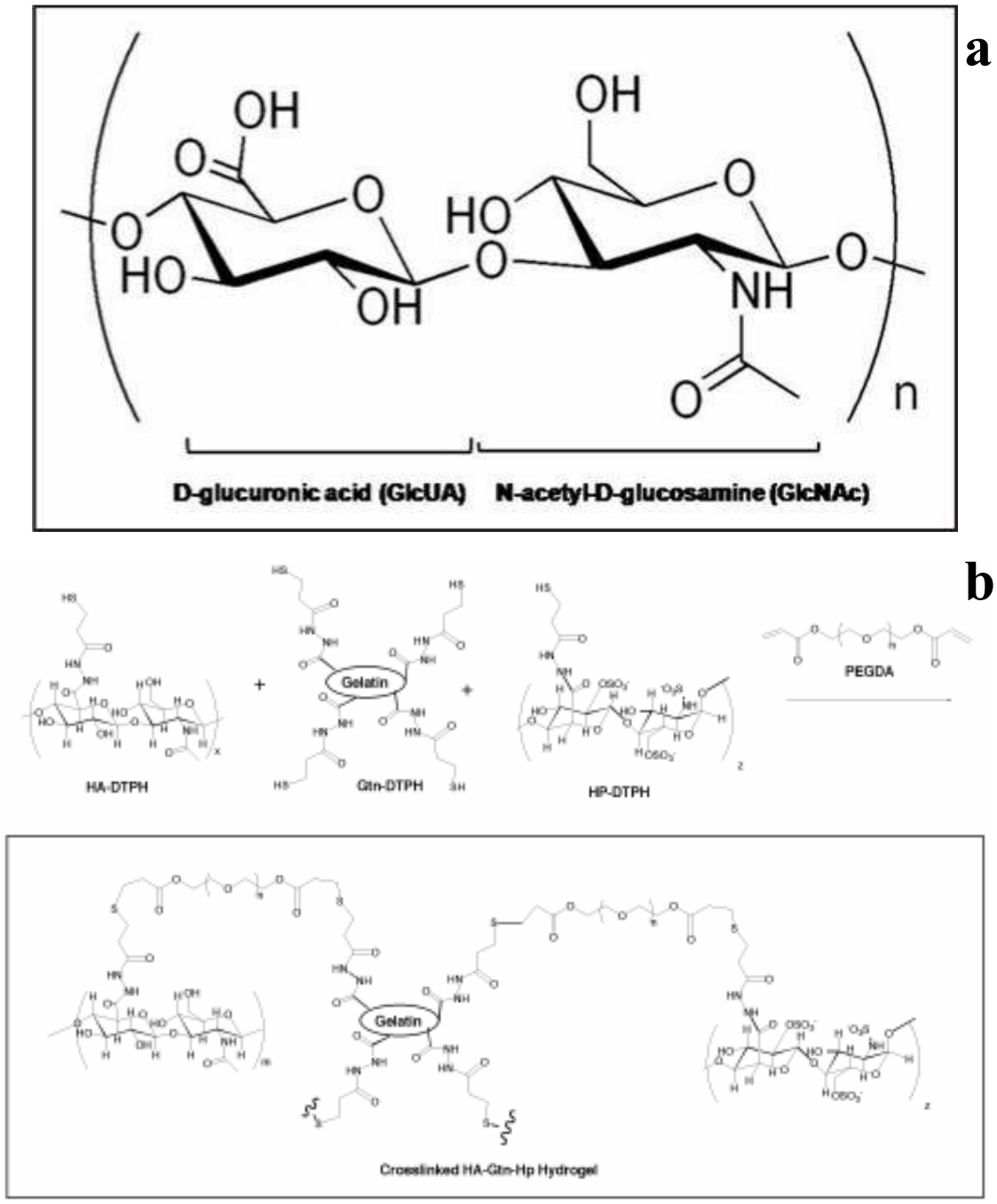

Figure 1. (a) Chemical structure of single repeating disaccharide hyaluronan unit. Adapted from Pardue et al.[1] (b)Chemical structure of modified HA, Hp and Gtn, as crosslinked by PEGDA

filling the defects with the hydrogel produced regeneration of both bone and cartilage tissue[42]. In the same osteochondral study injectable gels containing mesenchymal stem cells (MSCs) were injected into the defects. It was found that the addition of MSCs completely filled the osteochondral groove, producing a firm, elastic, cartilage with better integration of the new and original cartilage compared to the hydrogel alone[42]. Finally numerous studies evaluating the *in vivo* angiogenesis response to HA based hydrogel have been conducted. This research has demonstrated modified HA-based hydrogel gels can be effectively used as drug storage and delivery vehicles[7, 24, 30]. Specifically these studies looked at hydrogel based growth factor delivery into mouse ear pinnae. These gels produced a strong neovascularization response and minimal immune response[7, 24, 30]. Modified HA-based gels can successfully support cell growth[43], and demonstrate numerous applications in tissue engineering and drug delivery[30, 38, 44] making them a good biomaterial candidate for an engineered ECM .

1.2.1.4 Silk

Silk produced by the silkworm *Bombyx mori* is a fibrous protein with at least two major components, light and heavy chains of MW 25 and 390 kDa, respectively[45, 46]. Fibroin chains form tightly packed fibers as long as 2 km, which derive structural integrity from extensive interchain H-bonding. Natural silkworm fibers are encased in a coat of sericin, a family of glue-like proteins[47] which must be purified, degummed, from the fibroin for use in tissue engineering[47-49]. Even after degumming, the silk fibers maintain high mechanical integrity. The tensile strength of de-sericinized fibroin is 15-17 GPa[50], at

elongations of up to 16% at breaking[50]. Silk fibroin can be solubilized and processed into various formats including porous sponges, films, gels, fibers and mats[49, 51-54]. The silk fibroin can be designed to degrade over controlled periods of time, ranging weeks to years, depending on processing protocols[55-57].

Of particular interest are silk mats generated using electrospinnig techniques. Electrospinning is a process developed in 1914, in which a liquid solution is charged with a high electric potential[58], and extruded to create fibers. Briefly the charged solution is forced through a capillary needle, via a syringe pump, under which lies a grounded collector plate. The electric potential between the charged solution and the grounded plate exerts a tensile force on the solution pulling it from the capillary tip[59]. Surface tension between the solution and the needle will keep the droplet from falling until a critical voltage is reached. At this point, a fiber jet ejects from the suspended droplet[60]. The fiber is believed to dry as it is whipped around on its way towards the collector plate[61, 62]. By tuning various solutions and processing parameters, (i.e applied voltage potential, collector plate distance, pump rate, solution concentration and humidity) the fiber diameter and strength can be manipulated[60, 63].

Once processed to become water insoluble, usually by methanol treatment[63], the resulting randomly align fiber mats can be used for numerous tissue engineering applications. Tubular variants of silk electrospun mats have been evaluated for potential applications as small diameter vascular grafts[64-67]. Wound healing applications have used functionalized electrospun silk mats-based dressings to induce cell growth and accelerate wound healing process[68-71]. Additionally silk mats have been used for bone[72-74] and cartilage[75, 76] regeneration applications, demonstrating the versatility of these silk based scaffolds in tissue engineering.

1.2.2 Angiogenisis

Angiogenesis is the process of new blood vessel formation from existing blood vessels, and is essential in providing nourishment to newly forming tissue both during normal development as well as during tissue regeneration[1]. The body balances vessel formation via both angiogenic -stimulating and inhibition factors[1]. Stimulating factors, often times cytokine growth factors (GF), can be delivered *in vivo* or *in vitro* to initiate local angiogenesis[1]. Of the numerous available GF vascular endothelial growth factor (VEGF), keratinocyte growth factor (KGF) angiopoiten-1 (Ang-1) and platelet-derived growth factor (PDGF) have been shown to strongly stimulate a mature angiogenic response[77, 78].

VEGF is a strong promoter of angiogenesis, but large doses tend to produce highly fenestrated capillary vessels similar those found in tumors[79, 80]. KGF appears to act in the latter stages of blood vessel maturation by stabilizing epithelial borders aiding to create a mature vessel[81]. Ang-1 is associated with the Tie family of receptors, and appears to play a role in organization, vessels survival as well as stabilization[82-84]. PDGF has been shown to aid up regulation of VEGF mRNA expression and thus indirectly stimulate angiogenesis[85-87]. Supplying these growth factors individually or in combination has been demonstrated to produce a substantial neovascularizton *in vitro* and *in vivo* [24, 33, 88, 89]. In addition o-HA fragments have been implicated in variety of cellular pathways, including stimulating VEGF expression[7, 90]. HA-based GF delivery vehicles, including films and hydrogels, have produced increases in the initial and long term neovascularization response[7, 33].

1.3 Current State of the Cell Delivery Field

Microencapsulation is a technique in which cells and potential drugs of therapeutic value are embedded into small spherical bodies, usually composed of a hydrogel center and a more robust stiff outer shell[34]. Variants of these microcapsules have been used to successfully deliver therapeutic cells for a number of diseases. One study made use of chinese hamster ovary cells engineered to express VEGF, and deliver them via micocapsules into infarcted myocardiums of mice[91]. Twenty-one days post delivery, there was minimal inflammation, augmented angiogenic response and improved overall heart function[91]. Goren et al. encapsulated genetically engineered cells that expressed an angiogenesis inhibitor, hemopexin like protein. The results of this study revealed a significant reduction in the tumor volume, increase in tumor cell apoptosis, decrease in blood vessel formation and tumor cell proliferation[92].

Although microencapsulation has demonstrated a good capability for cell delivery, it has two major drawbacks. The first is the fabrication of these carriers often requires multiple steps and depending on the materials used, treatments can be quite harsh[34]. These harsh conditions have been shown to affect cell survival and eventual success of the implants[34]. The second major issue is that the microcapsules must be injected directly into the target site, which depending on the disease may not be trivial.

To overcome the above problems, a biological composite, much like the one described in this work, has recently been developed. Amanadine et al. used decellularized human myocardium sheets, composed of only ECM elements, upon which they placed a cell-doped fibrin hydrogel glue[93]. The idea was that the gel

would act as the cell encapsulating component and the decellularized tissue would serve to fix the gel onto a variety of sites in the body. This composite could overcome the limitations associated with delivery of microcarriers and gels only to areas accessible via injection. Mesenchymal progenitor cells were used as the therapeutic cell line. The implants produced an enhanced vascular network around the infarcted site[93].

The major issues with this composite are related to concerns accompanying the use of decellularized tissue. Decellularization processes, regardless of intensity or method, causes at least some ECM disruption[94]. Chemical decellularization removes cell surface antigens but interferes with basement membrane proteins necessary for cell sustainability, as well as mechanical integrity[95, 96]. Additionally sterilization techniques such as autoclaving, gamma irradiation, or ethylene oxide gas exposure are often damaging to the ECM, or leave behind toxic residues[97-100] .

1.4 Encapsulated Cells

The delivery of cells via any biological transport vehicle is not an insignificant problem. Cells seeded for therapeutic activity often produce a strong host immune response [101, 102]. The accompanying inflammatory reaction in the microenvironment surrounding the implant is frequently enough to cause the death of the encapsulated cells[103, 104]. To overcome such issues two approaches have been examined. The first approach involves co-administration of cells and anti-inflammatory drugs, aimed to suppress eventual immune responses [104, 105]. L292-fibroblast cells were encapsulated into dexamethasone containing alginate gels. It was found that the dexamethasone capsules prevented fibroblast overgrowth in the capsules *in vivo*[105]. In a similar *in vitro*

study antifugal amphomericin B, was incorporated into liquid spheres and small airway epithelial cells were exposed to the drug containing spheres[106]. These drug loaded spheres did not induce toxicity or production of inflammatory cytokines and nitric oxide[106]. These co-encapsulation techniques have been successful in decreasing macrophage adherence to the along with increasing cell viability and therapeutic efficacy[104-106].

The second approach makes use of naïve cells such as stem cells, in order to reduce or completely avoid an immune response. In one study, human mesenchymal stem cells were successfully used as long-term *in vivo* sources of cancer therapeutic factors, demonstrating improved biocompatibility of the implants tested[92]. In the hydrogel-decellularized tissue composite described above, mesenchymal progenitor cells were used to promote a strong *in vivo* vascular network while at the same time producing a minimal immune response [93].

1.5 Research Aim

The aim of this research is to develop a bioscaffold which can be directly fastened to moving or expanding tissue, and can sustain cell growth and vascularization while at the same time serving as a delivery vehicle for drugs and therapeutically relevant cells. The first objective is to quantify the elicited microvascular response of growth factor delivery *in vivo*. The second objective is to develop a silk reinforced hydrogel with mechanical properties sufficient to allow fastening to moving tissue. If the implant is capable of establishing its own microvascular network, as is ultimately intended, this should allow for effective therapeutic delivery as well as potential cell ingrowth and tissue regeneration. This

potential for tissue regeneration and effective drug delivery serves as the motivation for the first set of experiments. The motivation for combined aims one and two was to create a novel biocompatible, biodegradable device that can be used to target most tissue or organs in the body. Currently there are few devices capable of delivering therapeutic drugs to organs or moving tissue, such as the heart, lungs or stomach. The devices that do exist are difficult to administer, often times painful, and not effective when the target site is deep with in the body.

It is the goal of the last series of experiments to generate a hyaluronic acid-based hydrogel which can best support cell growth *in vitro* in the presence of angiogenic growth factors intended for eventual *in vivo* delivery. The motivation for these experiments is to ultimately incorporate cell lines capable of producing and releasing products of therapeutic relevance. Currently effective treatments to conditions caused by organ or tissue dysfunction are direct replacement of the lacking product. The replacement is most commonly delivered via injection or an oral format such as a pill. However these treatments are often painful, ineffective and require constant monitoring. The hope is that by incorporating therapeutic cells we can regulate the production of the drug depending on physiological conditions and deliver it to the target site with minimal patient discomfort and involvement.

The sequential incorporation of what is learned from the three independent experiments will add to the current scientific knowledge base for cell viability and encapsulation. It is hoped that the developed biocomposite may one day be a viable delivery vehicle for therapeutic cell lines capable of targeting a broad spectrum of diseases.

2 Materials and Methods

2.1 Hydrogel Solution Preparation

Hydrogel solutions were prepared using commercially available thiol modified hyaluronic acid, (Glycosil ®; Glycosan Biosystems), gelatin, (Gelin-S ®; Glycosan Biosystems) and heparin (Heprasil ®; Glycosan Biosystems). Lyophilized Glycosil Gelin-s, and Heprasil were separately dissolved according to manufacturer's instruction in DPBS (Invitrogen) to obtain 50 mg/ml solutions. Poly(ethylene glycol)-diacrylate (Mw 3400; Glycosan Biosystems) was used as a cross-linker for the HA and Gtn solutions (Figure 1b). Lyophilized PEGDA was prepared at 25 mg/ml in DPBS. To obtain the recommended 1:2 ratio of acrylate to thiol functionalities HA and Gtn were mixed in a volume ratio of 4:1 to the PEGDA.

When described, growth factors were non-covalently incorporated into the hydrogels prior to the addition of PEGDA crosslinker. The lyophilized growth factors VEGF (human recombinant, 165 amino acid, MW = 38.2 kDa; Peprotech), KGF (human recombinant, 163 amino acid, MW = 18.9 kDa; Peprotech0, Ang-1 (human recombinant, 476 amino acid, MW = 66 kDa; Peprotech) PDGF-AA (human recombinant, 25 amino acid, MW = 25 kDa; Peprotech) were reconstituted according to the vendor's instructions and then diluted to a working concentration of 25 μg/ml.

2.2 Experiment 1: Stimulation of in vivo Angiogenesis

In this experiment all steps other than data analysis were carried out by students and staff at Oregon State University. Data analysis was carried out by Roberto Elia

2.2.1 Chemical Synthesis and Hydrogel Preparation

Thiol-modified HA, Gtn and Hp were used to create *in situ* curing hydrogels. Briefly, four sets of HA-based hydrogels were prepared: HA, HA:Hp, HA/Gtn and HA/Gtn:Hp. HA and Gtn were incorporated in a 1:1 volumetric ratio, while Hp-containing set, gels were fabricated with different Hp concentrations, 0%, 0.03% or 0.3% w/w relative to total HA or HA/Gtn. In all case reconstituted PEGDA crosslinker was added in a volume ratio of 4:1.

As described previously, growth factors were non-covalently incorporated by mixing them with the dissolved HA-DTPH solution before crosslinking. Experiments were performed with concentrations that resulted in 25 ng of each growth factor delivered to the animal for non-heparinized gels. However, 100 ng of each was delivered in heparin-containing gels, to compensate for the slower anticipated release. Non-heparinized cases included (i) an HA gel preloaded with VEGF and KGF (ii) an HA gel preloaded with VEGF and Ang-1 (iii) an HA gel preloaded with VEGF and PDGF (iv) an HA/Gtn gel preloaded with VEGF and KGF (v) an HA/Gtn gel preloaded with VEGF and Ang-1 and (vi) an HA/Gtn gel preloaded with VEGF and PDGF. Heparinized cases included the same GF and HA/Gtn combinations as experiments (i-vi), but with either 0.03% or 0.3% Hp (experiments vii-xviii). There was also a sham surgical case in which a pocket was

formed but no implant was delivered (experiment xix).

2.2.2 Surgical and Experimental Procedures

All procedures were carried out with the full approval of the Oregon State University Institutional Animal Care and Use Committee. Male Balb/C mice aged 6-8 weeks were anesthetized using 2.5% isoflurane with an inhalation anesthesia system (Summit Medical Equipment, Inc., Bend, OR). Once a deep general anesthetic plane had been reached, a shallow 4-5mm incision was created through the superficial skin on the posterior pinna of the right ear. A blunt probe was inserted through the incision, and a 5-mm pocket created under the skin.

Hydrogel solutions were mixed at room temperature immediately prior to delivery, and 50 μL aliquots of the gel solutions were injected into the ear pocket prior to curing. The ear was held in a fixed position until a gelled bolus formed *in situ* in the pocket, and the incision was allowed to close without sutures. Mice recovered without incident within 5-10 minutes after these brief surgeries, and the incisions healed in 2-3 days (Figure 2).

On days 7 or 14 post implantation, the mice were anesthetized by overdose of isofluorane (5%) and sacrificed by cervical dislocation. Both the surgical (right) and contralateral ears were retrieved and fixed in formalin. The ears were then embedded in paraffin, thin sectioned parallel to the pinna surface, and stained with hemotoxylin and eosin (H&E). Microvessels were counted directly from the slides at 400× magnification after identification marks on each slide were covered so the observer was blind to treatment group under observation. Ten locations per ear

from within the pocket area, were selected at random for quantification resulting in microvessel density representative of that ear.

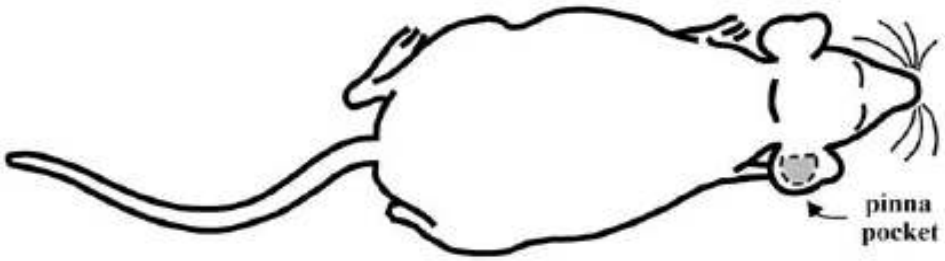

Figure 2. Diagram of mouse model, showing implant placement / injection site in the ear pinna

2.2.3 Data Analysis

A total of 6 animals ($n = 6$) received implants for each treatment case and each time point. Microvessel density data are presented as mean ± standard deviation. To minimize the effects of intra-observer variability, a protocol had previously been developed in the Peattie lab to standardize vessel counts. A standard set of 22 slides from 11 treatment cases were set aside and vessels in them counted by each member of the laboratory. Group averages were then calculated, and a correction factor determined for each individual observer. This correction procedure has been applied to all the data presented in this thesis work. The vessel counts were performed independently by two observers, and data from both observers is presented in the results.

To distinguish between the number of vessels present before surgery, those induced by the surgical procedure alone and those produced by the individual treatments, a dimensionless *Neovascularization Index* (*NI*) was defined as[7, 29],

$$NI = \frac{\overline{(treatment - CL)} - \overline{(sham - CL)}}{mean\ \ CL} \quad (1)$$

where $\overline{(treatment - CL)}$ refers to the vessel count from the implanted ear of a particular animal minus that of its contralateral ear, averaged over all the animals in a particular treatment group, $\overline{(sham - CL)}$ represents the same quantity for a sham surgery control case that underwent pocket formation but received no implant, and *mean CL* is the average count from all contralateral ears over all treatment groups. *NI* represents the number of additional vessels present post-implant in a treatment group, minus the additional number due to the surgical procedure alone, normalized by the average contralateral count. Statistical significance was determined using a two-way ANOVA and post hoc Fisher's PLSD analysis (StatView 5.0, SAS Institute Inc., Cary, NC), with significance taken at the level $p \leq 0.05$.

2.3 Experiment 2: Composite Hydrogel

2.3.1 General Silk Fibroin Solution Preparation

Japanese *Bombyx mori* silk cocoons were cut and placed into boiling 0.02M Na2CO3, (Sigma Aldrich, ≥99.5%, anhydrous) for 40 minutes to degum the sericin component and isolate the silk fibroin protein, as previously described[48, 53]. Isolated silk fibroin was then washed three times for 20 minutes in deionized water and allowed to dry for 24 h. Dried silk was dissolved in 9.3M LiBr at 60°C for 3 h, producing a 20% w/v solution. The silk solution was then placed into dialysis

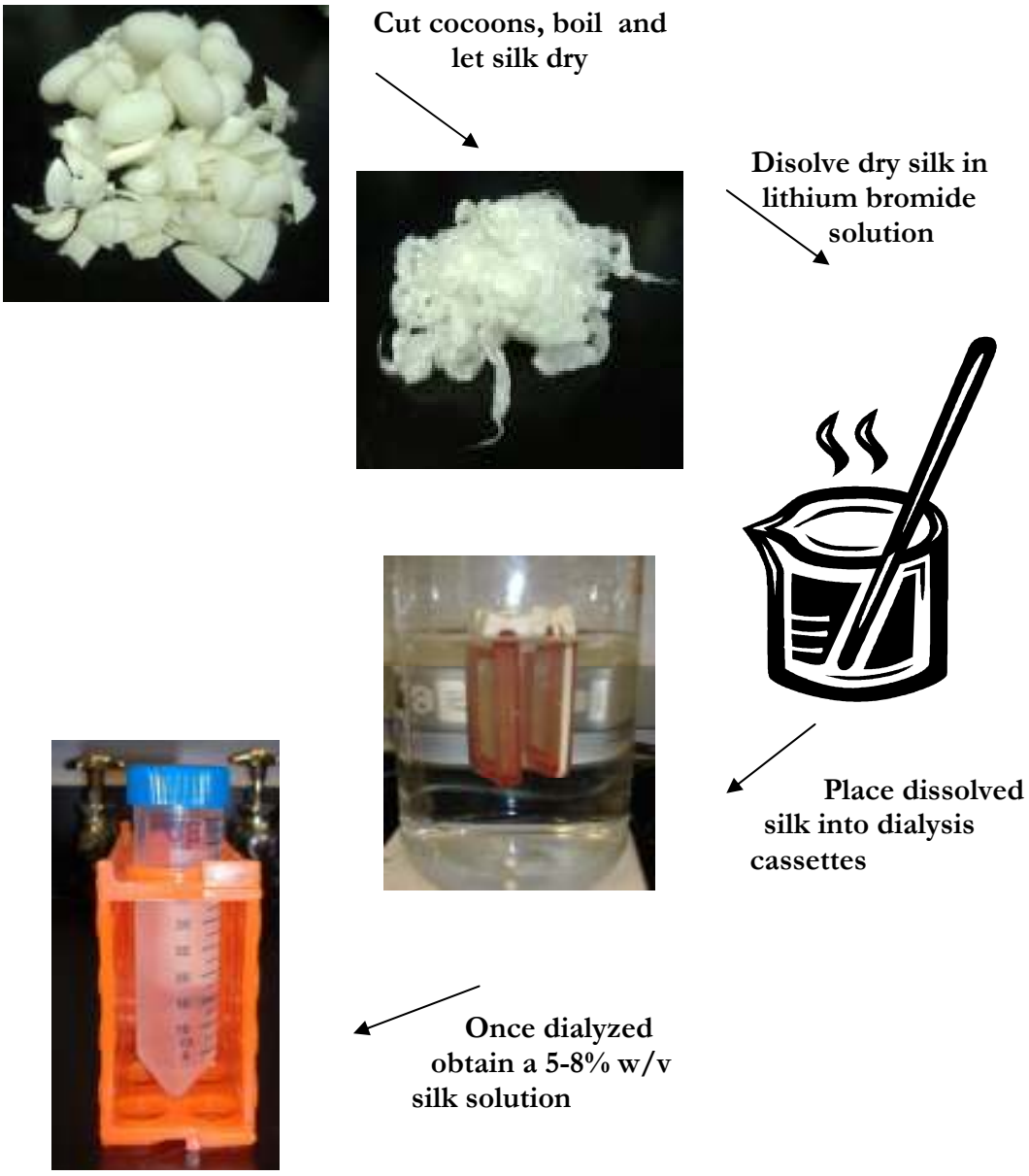

Figure 3. Silk processing overview

cassettes (Slide-a-Lyzer dialysis cassettes 3500 MW-cutoff; Pierce) and dialyzed against deionized water for three days to remove excess ions (Figure 3). After dialysis the solution was removed from the cassettes and centrifuged at 10,000 rpm to remove remnant non-dissolved fibroin or debris. Typical concentration of post-

dialysis silk fibroin solutions ranged from 5.0-8.0 wt%, which was calculated by weighing the remaining solid silk film after drying.

2.3.2 Silk Electrospinning and Mat Preparation

2.3.2.1 Silk Solution Preparation

In order to be effectively electrospin low concentration silk solutions, typically lower than 15% w/v, require the addition of polyethylene oxide (PEO 900,000 g/mol; Sigma Aldrich)[53]. The PEO serves to increase viscosity, improve solution constancy and generate stable, continuous spinning[72]. 5% w/v PEO solution was created and added to the dialyzed silk fibroin in a volume ratio of 4:1, generating a final 7.5% w/v solution[72].

2.3.2.2 Silk Electrospinning and Processing

Fibrous silk mats were created following previously described silk electrospinning techniques [107, 108]. Briefly electrospinning was performed with a 1.5mm steel capillary tube mounted on a fixed, stainless steel circular focusing plate. A high voltage power supply was used to maintain both the capillary tube and focusing at a high electric potential relative to a grounded collector plate, ~12 kV. The collector plate was covered with a sheet of non-stick aluminum foil, which was grounded to the power supply using 18 gauge wire. Silk/PEO solutions were then delivered through the capillary tube at a semi-constant volumetric flow rate via a syringe pump (Thermo Orion Sage Inc., model 361). As the silk solution comes in to contact with the capillary tube it is charged, creating an electric potential between the solution and the grounded collection plate (Figure 4a). The distance between the

capillary tube and the collection plate was maintained at 2 cm/kV, allowing for a stable jet to form and deposit randomly oriented fibers[74]. Approximately 20 ml of silk/PEO were used to make initial circular mats approximately 100μm thick and with a radius of 5 cm.

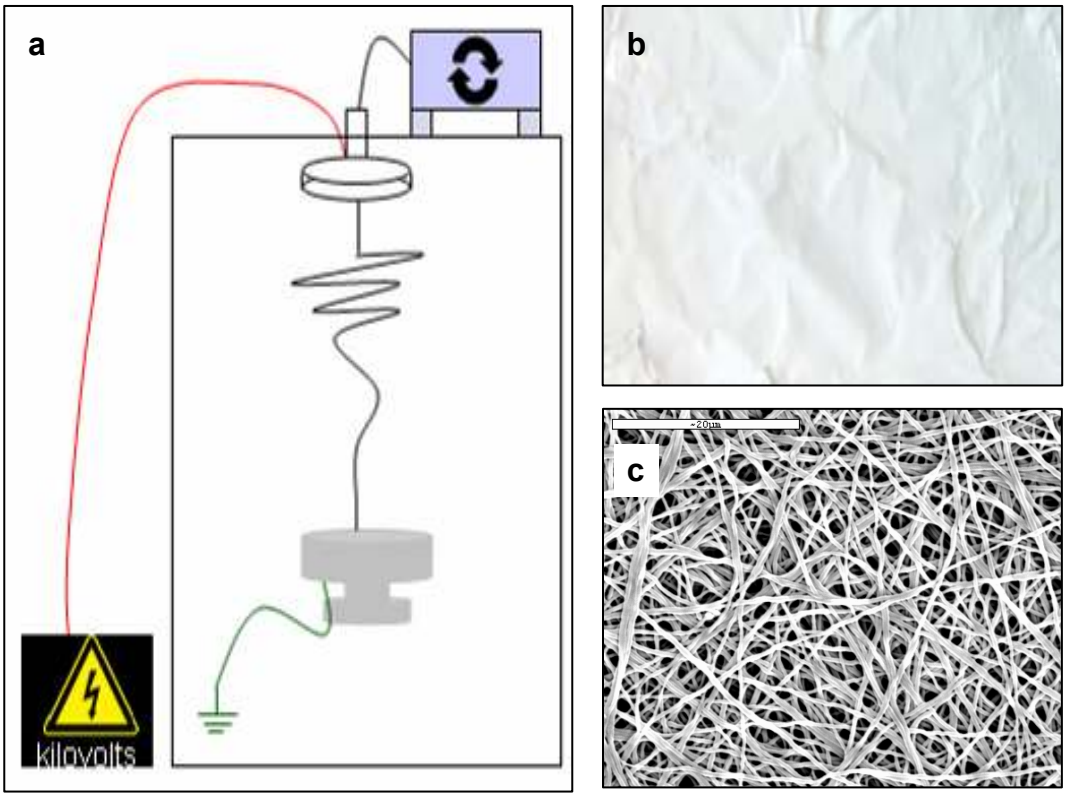

Figure 4. Creation of electrospun mats (a) Schematic diagram of elecrospinner, high voltage power supply charges silk solution. The solution is pumped through capillary needle and dries as it is wiped toward the grounded collector plate. (b) Surface image of electrospun silk mat. (c) Surface SEM of silk electrospun mat

The electrospun mat was then soaked in 70% methanol for 10 minutes to induce β-sheet formation, making the mats resistant to dissolution in water[63]. While wet, the mats were removed from the collector plate and allowed to air dry for 30 minutes on a sheet of parafilm (Figure 4b). A series of 25 mm disks were then cut from the larger silk mat, and pores were punched through the silk disks using an 18

gauge needle to allow the hydrogel solution to crosslink through the silk mat (Figure 4c), improving the integrity of the eventual composite.

2.3.3 Composite Gel Preparation

As with the *in vivo* experiments, thiol modified hyaluronic acid based hydrogels were crosslinked using PEGDA. Both HA and Hp were reconstituted in aqueous 5% glycerol to give a concentration of 50 mg/ml. This solution was again crosslinked to form a hydrogel by mixing with 25 mg/ml PEGDA in a volume ratio of 4:1. Hp was included in all drug containing gels, and HA only gels were used for all other experiments.

The 25mm silk disks mat was set on the bottom of a 26mm diameter cylinder, and HA/Hp solution was mixed with PEGDA and injected under the silk mat. As the hydrogel solution was injected, it lifted the mat from the base of the cylinder. Slow injection of the hydrogel solution allowed hydration of the silk mat and flow of solution through the prepunched channels as well as through the mat meshes itself. In order to create a composite with a centrally encapsulated silk mat, hydrogel solution was also injected directly on top of the mat. Gel thickness above and below the silk mat was typically 4mm (Figure 5 upper).

For implantation and characterization small gels 8mm were punched from the 25 mm composite. An 8 mm biopsy punch was used to extract 5 individual gels from each larger composite (Figure 5 lower). These composites were allowed to fully cure at room temperature for 3h.

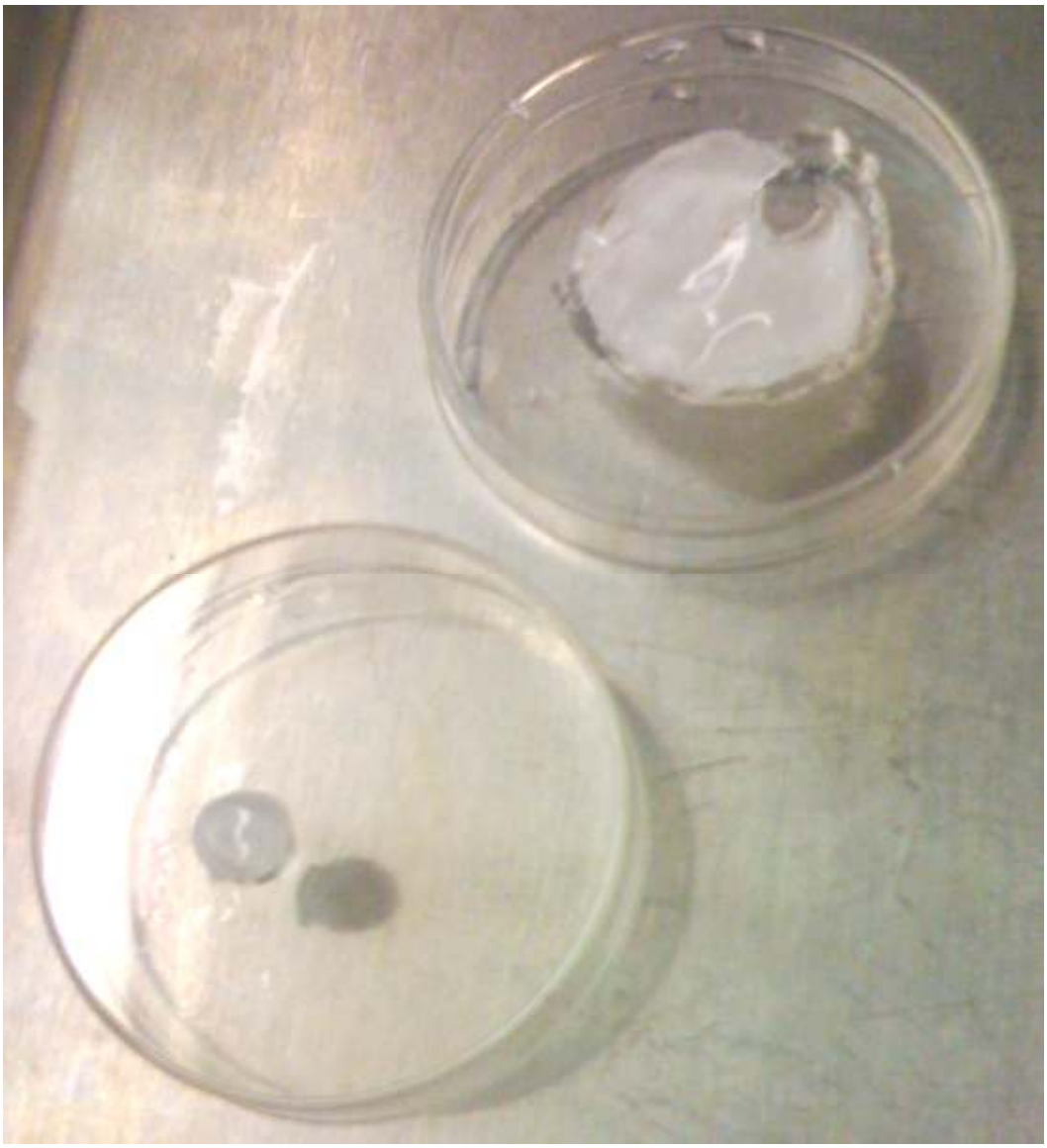

Figure 5. Composite hydrogel containing physically crosslinked silk mat in center, Top 25 mm composite, Bottom 8 mm punched gel for implantation and testing

2.3.4 Gel Cure Time and Density

The cure time was considered to be the amount of time for the gel solution to become too viscous to pour. Composite hydrogels were cast as described above and the cylinder containing the hyrdrogel was slowly tilted and momentarily held at 45^{O}. This process was repeated every 15 seconds until the gel was no longer fluid.

The above described 8mm gels were used to evaluate composite gel densities. The hydrated thickness (T_w) of each hydrogel was measured using a uniaxial mechanical tester (Instron Inc., Model 3366) set up in compression configuration. Gels were placed on a fixed bottom platen while the top platen was slowly lowered onto the hydrogel, the computer was used to carefully control top platen displacement. Density was calculated as gel weight per unit volume, and was evaluated for both wet and dehydrated gels.

2.3.5 Equilibrium Swelling Ratio and Swelling Kinetics

For swelling ratio calculations, a cured 25mm composite gel was submerged in a petridish containing pH 7.4 PBS and allowed to equilibrate for 72h at room temperature. 8mm gels were cut from the large composite and the thickness, diameter and weight were measured (T_w, D_w and W_w, respectively). Thickness was obtained using the Instron as described above, the diameter was considered to be 8mm and weight was measured using a digital balance. (Acculab AL-104). The gels were then allowed to dry for 7 days in an open petridish at room temperature, and dry thickness, diameter and weight were measured (T_d, D_d and W_d). The swelling ratio was defined as the ratio of the hydrated to dehydrated gel volumes, $SW = V_w/V_d$.

To quantify swelling kinetics, the thickness and diameter of the composite gels were monitored simultaneously. In order to make the gel boundary stand out on camera a small amount of dye was incorporated into the hydrogel, prior to the addition of PEGDA crosslinker . This colored gel was allowed to dry at room temperature for 7 days. Using an 8mm punch, disks were cut from the dehydrated

composite. Dry disks were placed in a Petri-dish positioned on a microscope stand, with a camera (Olympus Inc., Model BX41) oriented to image the top of the disk. This camera was used to measure the diameter of the gels. A second camera was positioned to record the gel thickness. The two cameras were synchronized, and swelling was initiated by addition of PBS. The gel volume was the calculated from still images and swelling kinetics tracked every minute for the first 10 minutes and then at 20 and 60 minutes.

2.3.6 Scanning Electron Microscopy

Scanning electron microscopy was used to observe gel micro-morphology for both intact composites and composites exposed to hyaluronidase (HAse). Previously described 8mm gels were allowed to equilibrate in pH 7.4 PBS buffer or complete media for 24h. A third 8mm gel was allowed to equilibrate for 24h in the presence of HAse in PBS. The three hydrated samples were frozen on dry ice, and then lyophilized (Labconco Inc., Model 796002). To observe the intact dehydrated gel state, a forth 8mm gel was equilibrated in water, then allowed to air dry for 72h at room temperature and then lyophilized. Environmental scanning electron microscopy was used to avoid the necessity of sample sputter coating, allowing for visualization of native surface features (Carl Zeiss Inc**.,** model Supra 55VP).

2.3.7 Thermal Behavior

Thermostability of the composite gels was evaluated by thermal gravimetry (TA Instruments Inc., Model TGA Q500). The weight loss of 8 mm composite gel samples was obtained during heating from 23ºC to 800°C at a rate of 10ºC/min.

Differential Scanning Calorimeter analysis was carried out on a TA Instruments Model DSC Q100 calorimeter. Profiles of 8 mm dried composite gels were obtained as the temperature increased from 23ºC to 250ºC at a rate of 10ºC/min under a N_2 atmosphere.

2.3.8 Mechanical Characterization

Compressive properties of the HA-silk composite gel were determined using a uniaxial mechanical tester (Instron Inc., Model 3366) set up in a parallel plate conformation. Five 8mm gel samples were produced as described above and allowed to equilibrate in PBS for 60 minutes. Uniaxial compression tests were performed in a PBS bath to prevent hydrogel fluid loss during compression (Figure 6a). Data was obtained via a 100 N load cell. Gels were first precycled three times at a rate of 0.5 mm/min for 0.5 millimeters. For the fourth cycle, the compression of the gel via the top platen was run to completion, again at a rate of 0.5 mm/min. Young's Modulus of compression, E_c, was calculated using the slope at the linear portion of the stress (σ) *vs.* strain (ε) plot, between 10% - 25% stain. (Figure 14 a)

Tensile character of composite hydrogels was quantified by measuring the tear strength of the hydrated gels. Three individual 14mm composite gels were fabricated in the same manor as 25mm composite. Once these 14mm gels had cured two strands of surgical silk suture were looped through opposite ends of the samples. The free ends of the sutures were fixed in the clamps (Figure 6b), and the samples were stretched at a rate of 0.25 mm/min. Data were obtained with a 100 N load cell. Tensile stiffness, E, was calculated for the linear region of the stress-strain curve

over 10-20% strain. Ultimate tensile strength (UTS) was also obtained from the measurements.

Figure 6. Gel mechanical characterization (a) composite gel in PBS bath compressed to failure at 0.5mm/min (b) Composite gel with sutures placed on opposite ends of the composite, gels pulled to tensile failure at a rate of 0.5mm/min.

2.3.9 Enzymatic Degradation

The rate of composite gel breakdown was analyzed in two ways, first by direct measurement of mass and then indirectly by evaluation of the rate of FITC-dextran release

2.3.9.1 Direct Mass Measurement

As described above, 8mm diameter composite gel disks were fabricated and placed in sealable, pre-weighed vials with complete medium. A single HAse dose of 0, 2, 5, 10, 50, 100, or 150 U/ml was added to individual vials. The gels were stored

in an incubator at 37°C and 5% CO_2. Gels degradation was obtained by removing the liquid from the vials and weighing the remaining gel mass. The liquid from each vial was reused for the full time course of the experiment, and HAse doses were not supplemented. Mass measurements were obtained at twelve hours post-HAse exposure and once every twenty-four hours thereafter for six days.

2.3.9.2 FITC-Detxran Release

Fluorescein isothiocyanate-dextran samples of molecular weight 4,000, 70,000 or 250,000 Da (FITC-dextran; Sigma Aldrich) were non-covalently incorporated into HA-silk composite gels prior to crosslinking, at a loading of 0.5 or 1.0 wt%, and allowed to homogenously mix. After gel curing, 5mm disks were cut from the gels and placed in wells containing PBS loaded with 0, 3 or 75 U/ml HAse. Spectrophotometric measurements of FITC-dextran containing supernatant were used to quantify composite degradation (SpectraMax M2e UV-Vis). For FITC-dextran readings 200µl aliquots of the supernatant were placed into a cuvette and both absorbance (493nm) and fluorescence (Exc. 490nm / Emi. 520nm) measurements were obtained. The 200µl aliquots were then returned to the original wells. HAse was administered once with the initial PBS solution, and never supplemented over the time course of the experiment. Measurements were performed every two hours for the first 12 hours, then once every twelve hours for four days.

2.3.10 *In vitro* Drug Release

2.3.10.1 Hydrophobic Drug Release

The rate of release of six model hydrophobic drugs from HA-silk composite gels in was characterized using spectrophotometric readings. The drugs (cortisone, hydrocortisone, prednisolone, prednisone, dexamethasone and 6α-methylprednisolone) were dissolved in ethanol and non-covalently incorporated into the HA-DTPH prior to crosslinking. Drug loading was 5mg per 1ml of HA-DTPH or 10.0 wt% relative to the dry weight of the HA in each gel. 5mm drug-loaded gels were punched from the as cast 25mm composite and placed into individual wells containing 2 ml PBS buffer at 37ºC. At a series of times after PBS exposure, 200μl aliquots of the supernatant were withdrawn from the wells, and drug content measured via absorbance. The absorbance interrogation wavelength depended on the drug and ranged from 238-243nm. The 200μl aliquot was returned to the original well. After completion of the release study, gels were degraded using HAse solutions and the remaining drug content determined by absorbance.

The 2ml of PBS were considered to be a constant sink given the small initial drug loading and size for sample composite gel. Drug release was modeled using the first order kinetic release equation: $m(t) = A\,(1 - e^{-t/\tau})$. Here $m(t)$ represents percent of drug present in solution at the time (t). τ is the time constant describing the release rate of the drug, A is the initial drug loading. For ease of comparison, concentrations were converted to percentages thus A was taken to be ~100 %

2.3.10.2 ELISA VEGF Release

As an example of cytokine release from the HA-silk composite gels, the rate of release of VEGF was evaluated by Enzyme-Linked Immunosorbent Assay (ELISA; R&D Systems). Fabrication of these gels was similar to previously described methods, however small gels were individually cast and not punched from the large composite. Silk electrospun mats were placed into individual wells of a 96 well plate. Gels were produced using either Glycosil or Heprasil, and VEGF was non-covalently incorporated into these solutions at 10ng/mg relative to the dry weight of HA. PEGDA crosslinker was added, and as with the large composites, hydrogel solution was injected through and directly on top of the silk mat. Cases tested included HA/VEGF 0.0% Hp and HA/VEGF 0.3% Hp. After curing, PBS was added to each well and the plate was placed on a shaker in a 37°C incubator. At days 0, 1, 4 7, 14, 21 and 42, set of 4 gels were terminated by removing the supernatant and storing at 80ºC. After all samples were collected, the released VEGF concentration at each time point was evaluated by ELISA, following manufacturer's instructions.

2.3.11 Statistical Analysis

Unless otherwise stated, all measurements were repeated in triplicate (n = 3).Mean and standard deviations were calculated for each experiment. Where appropriate, two-tailed unpaired Student's t-tests were performed using StatGraphics (Herndon, VA). Statistical significance was taken at $p < 0.05$

2.4 Experiment 3: Encapsulation of Cell in Hydrogels

2.4.1 Cell Culture

Recombinant HEK293 cells transfected with red fluorescent protein were available in the laboratory, and were used for all cell experiments. Cells were grown on standard tissue culture flasks. Briefly, frozen cells were thawed and resuspended in DMEM (Sigma Aldrich) medium. The cell suspension was centrifuged for 10 minutes at speeds ranging for 10,000-15,000 RPM. After centrifugation, a pellet of cells was obtained on the bottom of the centrifuge tube. The cell pellet was resuspended in complete media consisting of DMEM supplemented with 10 % fetal bovine serium (FBS; American Type Culture Collection) and 1% Penicillin/streptomycin (Invitrogen). The cells were seeded onto flasks at a density of 4,000 cells/cm^2. Cells were split or harvested for experiments when 75-85% confluence was reached. Trypsin-EDTA (0.25%; Invitrogen) was used to detach the cells for the tissue culture plastic. The cell solution was diluted 10 fold in complete medium to inactivate the trypsin. A hemocytometer slide was used to estimate number of trypsinized cells.

2.4.2 *In vitro* Hydrogel Fabrication

For *in vitro* cell studies hydrogels were fabricated and cast into individual wells of tissue culture treated 96 well plates. To fabricate the hydrogels stock 50 mg/ml solutions of HA-DTPH and Gtn-DTPH were combined in a 2.0 mL vials. HA-Gtn solution was aliquoted into individual wells along with previously trypsinized HEK293 cells. Cell seeding densities varied based on individual

experiments; however cell solutions were adjusted to ensure every gel received exactly 2 μl of cell solution regardless of experimental seeding density. PEGDA crosslinker was added to each solution at the recommended 4:1 volumetric ratio. The solutions were mixed by gentle pipetting the mixture up and down for 60 seconds. Once mixed, the hydrogels were allowed to fully cure at 37°C for 30 minutes. After gelation, the gel containing wells were filled with complete medium.

In one experiment, the effects of gel thickness and cell seeding were simultaneously evaluated. For that purpose, hydrogels composed of 1:1 HA-DTPH: Gtn-DTPH were cast in well plates to constrain gel diameter, allowing for the creation of thick gels approximately ~500μm and thin gels approximately ~70μm in height after the addition of cells and PEGDA crosslinker. After curing, 200μl of complete media was added to the 70μm hydrogels and 100 μl of media was added to the 500μm gels. The hydrogels were seeded with either 50,000 cells/gel or 25,000 cells/gel, creating 4 cases, thick or thin gels with either high or lower cell seeding density.

In a separate experiment, hydrogel composition was further altered by varying HA:Gtn content and growth factor incorporation. For the remaining studies the final hydrogel height was keep constant at ~100 μm thickness, while the relative amounts of HA-DTPH and Gtn-DTPH was altered. 50 mg/ml solutions of HA-DTPH and Gtn-DTPH were combined in 2.0 mL vials at ratios of 1:1, 4:1, 9:1 and 1:0, 50%, 80%, 90% and 100% HA-DTPH respectively.

Finally, to observe the effects of cytokine presence on *in vitro* cell viability, growth factors were incorporated at concentration of 1 ng/μl. Using a working

concentration of 50 ng/ml, approximately 0.5 µl of growth factor solution was added to the HA-Gtn-cell solution prior to the addition of PEGDA.

2.4.3 *In vitro* Hydrogel Tissue Culture Maintenance

In order to maintain cell growth and survival, complete media changes were performed on each hydrogel for the duration of the experiment. Briefly, 96 well plates were brought into a sterile tissue culture hood and spent media was carefully removed using a manual pipetter. 200µl of complete media was added to the 70µm and 100µm gels and 100µl of media was added to the 500µm gels.

2.4.4 Cell Viability Assays: Alamar Blue and MTS

Cell concentration within the hydrogels was measured using Alamar Blue ® and MTS cell viability and proliferation assays. The Alamar Blue ® and MTS assays were performed on alternating days for the first week as well as on day 10, 14, 18 and 21. 150µl of media was removed from the hydrogels and 20µl of assay was added. After 2 hours of incubation the plate was read on a spectrophotometer plate reader (SpectraMax M2e UV-Vis). For the Alamar Blue treatments, the cells were excited at 570nm and the emission measured at 610nm. For the MTS, gels absorbance was measured 490nm. Mean +/- standard deviations were calculated based on the three independent gel readings. Emission and absorbance were correlated to cell numbers and used for growth ratio calculations

2.4.5 Growth Ratio

Growth ratios were calculated by dividing the number of cells at day three, five, seven and fourteen by the initial number of cells seeded. Direct comparisons of

$$GR = \frac{\text{Cell count day X}}{\text{Cell count day 0}} \quad (2)$$

growth ratios were used to determine the optimal hydrgel composition. Where appropriate, two-tailed unpaired Student's t-tests were preformed using StatGraphics (Herndon, VA). Statistical significance was taken at $p < 0.05$

3 Results and Discussion

3.1 Experiment 1 Stimulation of *in vivo* Angiogenisis

In vivo microvessel development in response to implantation of gels that were allowed to undergo *in situ* gelation was assessed in an ear pinna model for a series of control and experimental conditions. Cases included (i) a HA gel preloaded with VEGF and KGF (ii) a HA gel preloaded with VEGF and Ang-1 (iii) a HA gel preloaded with VEGF and PDGF (iv) a HA/Gtn gel preloaded with VEGF and KGF (v) a HA/Gtn gel preloaded with VEGF and Ang-1 and (vi) a HA/Gtn gel preloaded with VEGF and PDGF. Heparinized cases included the same GF and HA/Gtn combinations as experiments (i-vi), but with either 0.03% or 0.3% Hp (experiments vii-xviii). There was also a sham control surgical case in which a pocket was formed but no implant was delivered (experiment xix). These cases provide controls allowing the neovascular effects attributable to the individual gel components as well as the interaction between preloaded gels and cytokine combinations to be separately identified.

Representative photographic images of tissue microvasculaturization show significant differences that characterized the tissue response to each treatment (Figure 7). For all animals, the appearances of microvascular networks in contralateral ear sections were very similar regardless of the treatment of the surgical ear (Figure 7a). No evidence of any systemic response to the implant was observable at either time point for any of the treatment cases. Chondrocytes were widely distributed in this tissue, along with numerous hair follicles and other glands typical of ear pinnae. Contralateral ear sections contained relatively low capillary densities,

but the endothelial borders of these capillaries were well defined. Red cells were confined within fully intact, well-developed capillary walls (Figure 7a).

Figure 7

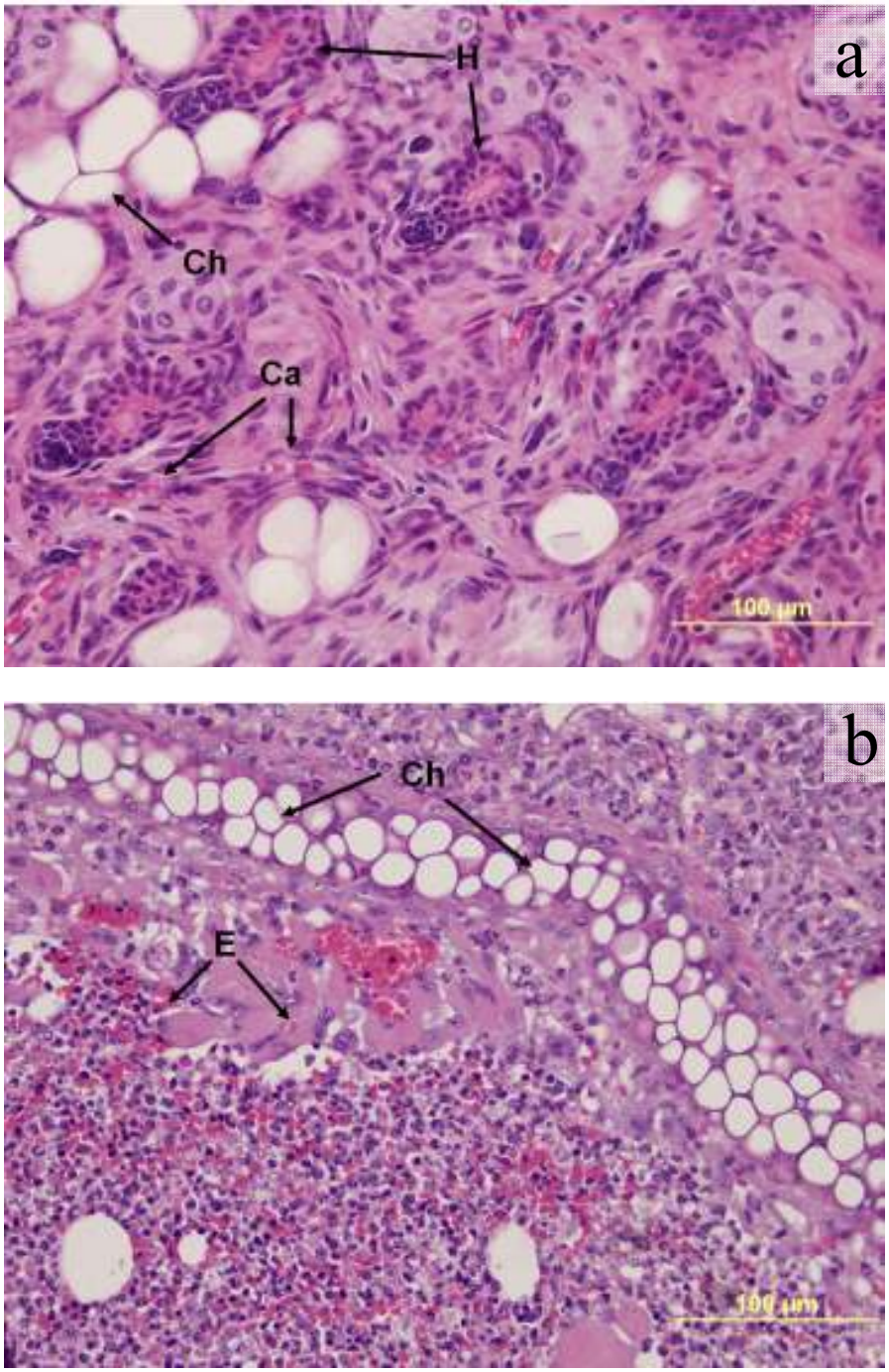

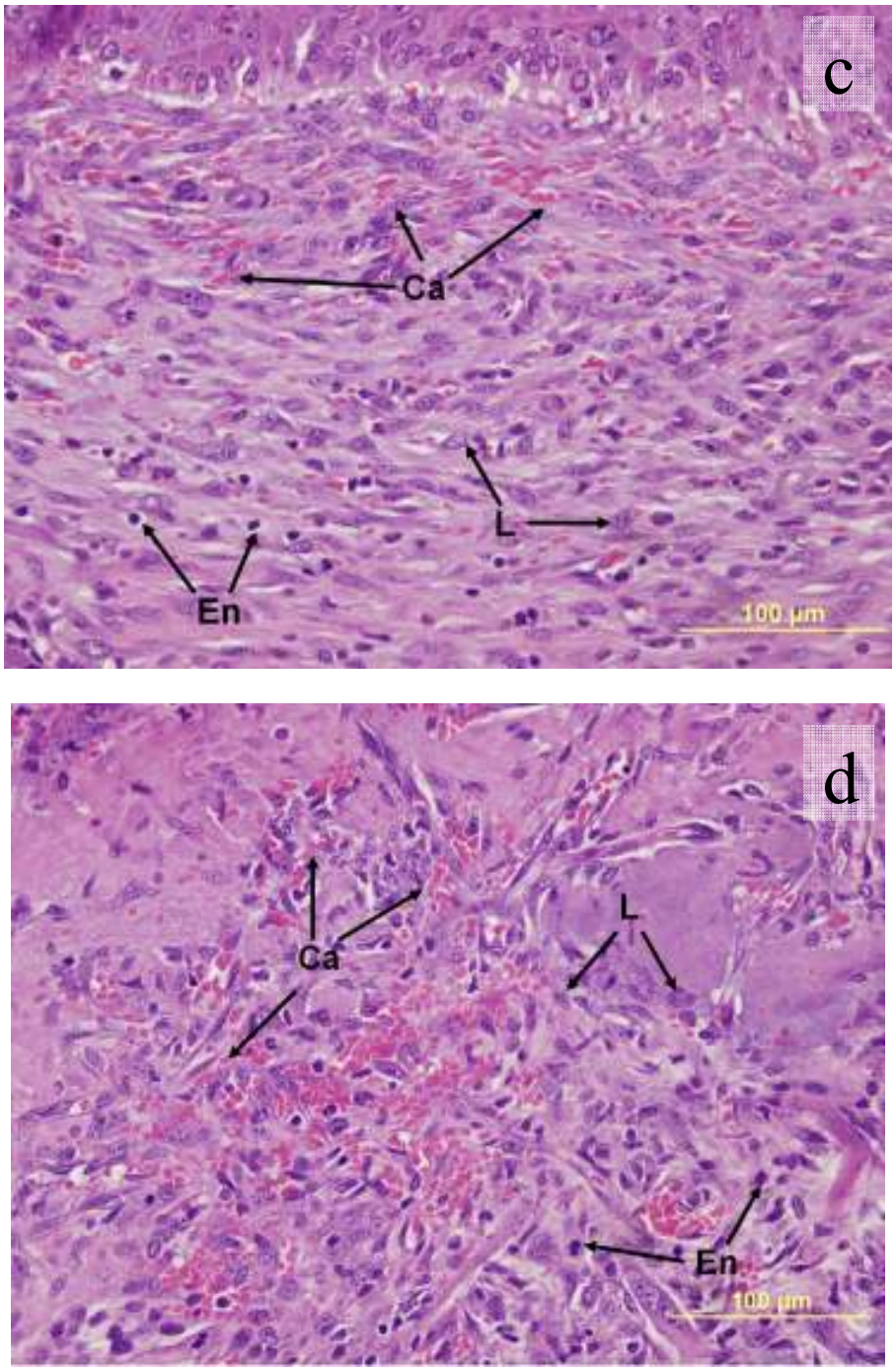

Figure 7. Hematoxylin and eosin stained representative images of ear tissue for different implant types, 400 x, **(a)** Contralateral ear, day 7 post-surgery, **(b)** HA:0.03% Hp-VEGF+KGF implant day 7, **(c)** HA:Gtn-VEGF+PDGF implant day 14, **(d)** HA:Gtn:0.3% Hp-VEGF+KGF implant day 14.

Ca—capillary, Ch—chrondrocyte lacunae, E—erythrocytes, En—endothelial cell, H—hair follicle, L—polymorphonuclear leukocyte.

In the ears receiving hydrogel implants, distinct histological differences from the contralateral ear tissue were observed (Figure 7b-d). In addition to chondrocytes, hair follicles and glands there were many apparently partially formed new microvessels. As can be seen in figure 7b, the presence of many extravasated erythrocytes indicated that the endothelial borders of these newly formed vessels had not fully developed by day 7.(Figure 7b, treatment with HA:Hp-VEGF+KGF).

By day 14 neovessel walls were more mature and much less permeable (Figure 7C and D, treatment with HA/Gtn:VEGF+PDGF and HA/Gtn:Hp-VEGF+KGF respectively). The density of microvessels remained high in these treatments, and far fewer extravasated red cells were observed. Instead, the erythrocytes appeared to form continuous chains of cells, confined within microvessels. Additionally there appeared to be few leukocytes in the surgical treatments, indicating that the implants were well tolerated, with reduced or no inflammation, no signs of exudation and with no cases of failure.

Elicited microvessel density was analyzed initially through direct counting of microvessels in the implanted ears of each treatment group (Figure 8). Microvessel density remained unchanged at both day 7 and 14 in the contralateral ears of all treatment groups (Figure 8, control). This indicated that the tissue response to the implants was localized to the region of the implant, with no systemic reaction. Significant growth of new microvessels occurred in response to surgical intervention, as sham surgical ears showed approximately twice the vessel density of contralateral ears ($p < 0.05$). Finally the sham surgical ears showed reduced numbers of vessels on day 14 compared to day 7, which would be expected for tissue recovering from surgical operation. Most importantly, the data in figure 8 indicates that at both day 7

and 14, all ears receiving implants showed significantly higher microvessel counts than did ears receiving only sham surgery ($p < 0.05$).

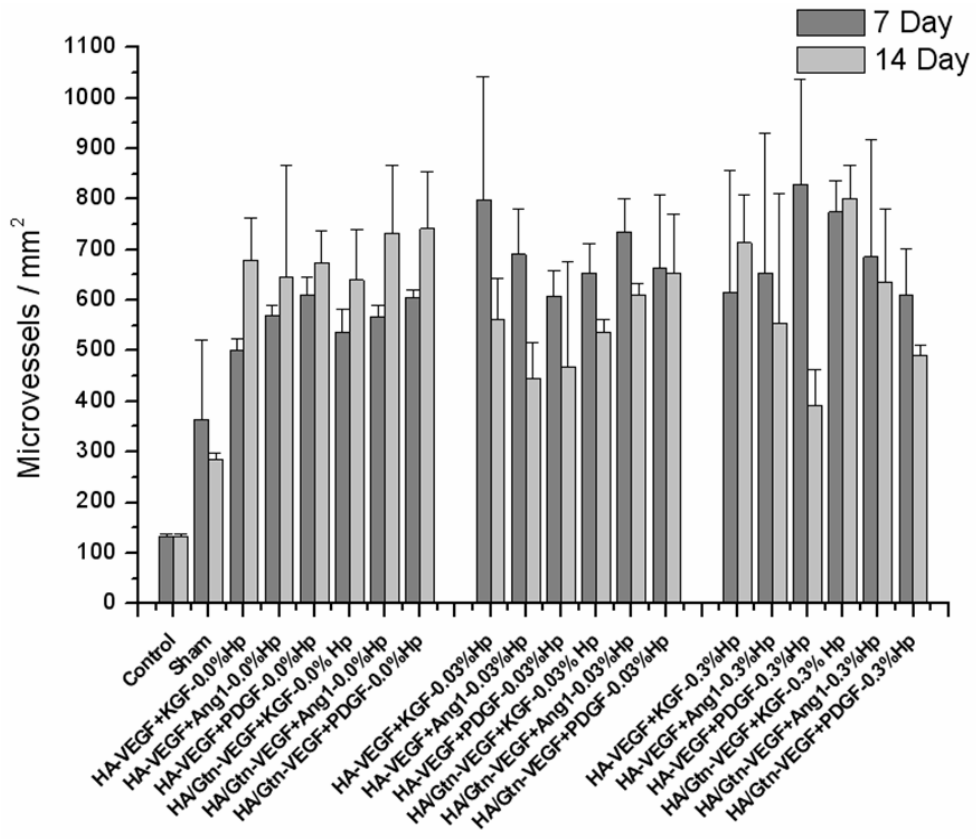

Figure 8. Microvessel density for HA:Gtn:Hp-cytokine loaded treatment groups at days 7 and 14 post-implantation. Control cases represent contralateral ears. Mean ± s.d., $n = 6$.

At day 7 post-implantation (Figure 8, dark bars), the greatest density of microvessels was found for the treatment case HA:0.3%Hp-VEGF+PDGF (829.84 microvessels/mm^2), although several other groups were not statistically significantly different from this case (HA:0.03%Hp-VEGF+KGF, 799.0 microvessels/mm^2, and HA/Gtn:0.3%Hp-VEGF+KGF, 775.06 microvessels/mm^2). At day 14 (Figure 8, light bars), the treatment group HA/Gtn:0.3%Hp-VEGF+KGF showed the highest microvessel density, (801.01 microvessels/mm^2), though again many other groups

were not statistically different. Further, ears with HA/Gtn:0.3%Hp-VEGF+KGF implants showed microvessels with defined borders, non-fenestrated vessels and representative presence of chondrocytes, hair follicles and glands (Figure 7d).

To distinguish tissue response to the different implants from the surgical induced response, vessel growth was rexpressed through the neovascularization index (Figure 9). Positive *NI* values indicate a tissue response greater than that of sham control, while a negative value would indicate treatments producing fewer vessels than sham surgery. Figure 9 (dark bars) showed that on day 7 post-implantation the highest *NI* values were produced by the HA:0.3%Hp-VEGF+PDGF (*NI* = 3.52 ± 0.38), HA:0.03%Hp-VEGF+KGF (*NI* = 3.29 ± 0.65) and HA/Gtn:0.3%Hp-VEGF+KGF (*NI* = 3.11 ± 0.73) treatment groups. These three groups correspond exactly with the findings based on raw microvessel counts (Figure 8). At 14 days post-implantation the highest overall *NI* value was observed for the HA/Gtn:0.3%Hp–VEGF+KGF (*NI* = 3.91 ± 0.68), HA/Gtn:VEGF+PDGF (*NI* = 3.46 ± 0.62) and HA/Gtn:VEGF+Ang-1 (*NI* = 3.39 ± 0.68). Again these trends correspond to the direct microvessel counts.

However with the exception of the above three cases, Figure 9 shows that many of the treatment cases which appeared to produce a similar micvovessel stimulation response based on the vessel counts (Figure 8) when normalized showed distinct differences. For example, the case HA/Gtn:VEGF+Ang-1 produced 567 ± 23 microvessels/mm^{2}at day 7 while the case HA:0.03% Hp-VEGF+KGF produced 562 ± 80 microvessels/mm2 at day 14. However, HA/Gtn:VEGF+Ang-1, produced a neovascularization index of 1.54 whereas, HA:0.03% Hp-VEGF+KGF, produced an *NI* of 3.28. As a result, many

treatment cases that appeared to generate similar vessel densities between days 7 and 14 may have undergone major changes during that period. For example, the treatment HA:Gtn:0.03% Hp-VEGF+PDGF produced 664 ± 143

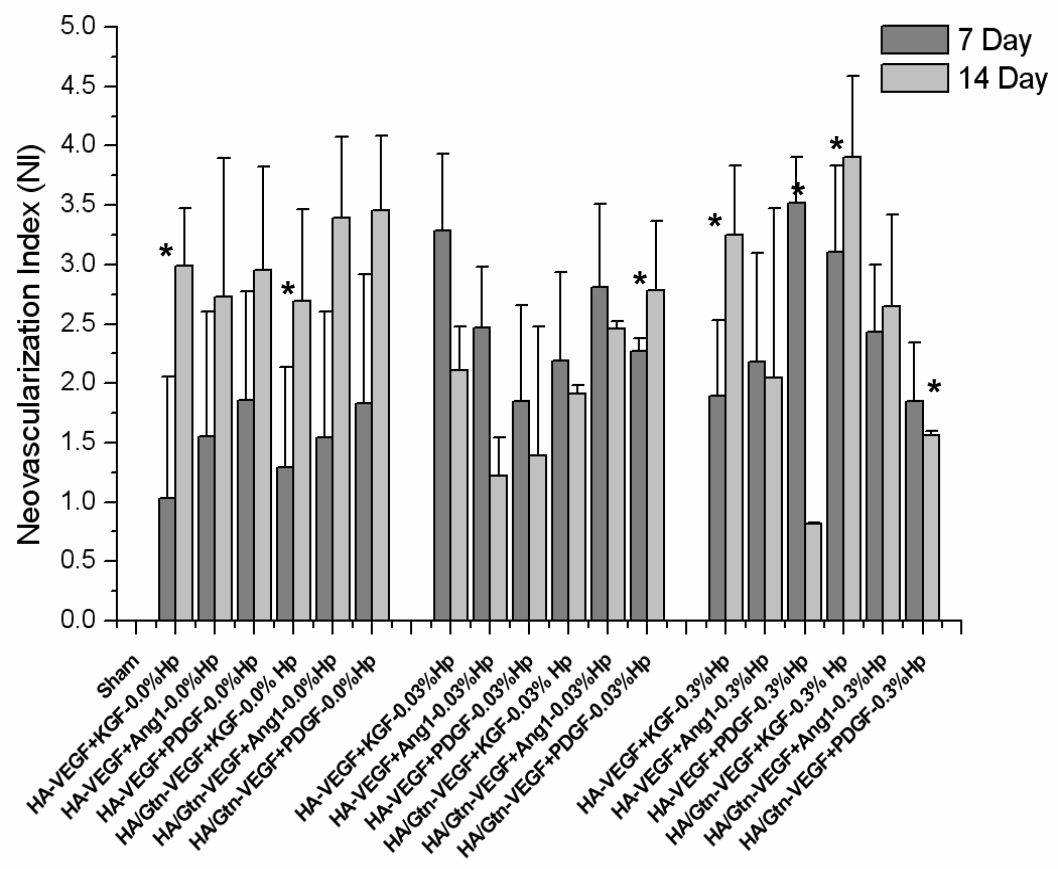

Figure 9. Neovascularization index for HA:Gtn:Hp-cytokine loaded treatment groups at days 7 and 14 post-implantation. Sham cases represent surgery without implant placement. *NI* is defined in the text, Eq. (1). Mean ± s.d., $n = 6$. * indicates statistical significance for comparison with sham, ** indicates statistical significance for comparison between two individual treatment cases as well as sham (only comparisons discussed in the text are identified).

microvessels/mm^2 at day 7, while for day 14 it showed a similar count of 652 ± 116 microvessels/mm^2. However, the *NI* values at the two time points were significantly different ($p < 0.05$), 2.27 for the day 7 treatment but 2.79 at day 14. Similarly, the treatment HA:Gtn:0.3% Hp-VEGF+KGF produced very similar microvessel

density of 775 ± 61 microvessels/mm^2 and 801 ± 67 mcrovessels/mm^2 a day 7 and 14 post-implantation respectively. The corresponding *NI* values were 3.11 at day 7 and 3.91 at day 14, which are again significantly different ($p < 0.05$).

Using direct comparisons, the effect of gelatin and heparin on neovascularization could be isolated at both day 7 and 14 (Figure 10a and b). Figure 10a shows the *NI* of treatment groups at day 7 post-implantation. Gels not containing Hp all produced similar neovascularization responses on day 7 post implantation regardless of Gtn content (Figure 10a), and all cases showed an increase in *NI* from day 7 to day 14 (Figure 10b). Inclusion of 0.03% Hp in the gel also resulted in no intra-group differences at day 7. However five of the six treatments showed a decrease in *NI* from day 7 to day 14, all Gtn containing gels produced decreased *NI's* by day 14 (Figure 10b).

The groups containing 0.3% Hp showed no distinct trends in *NI* with the incorporation of Gtn. HA:0.3% Hp-VEGF+KGF showed a higher *NI* when Gtn was incorporated into the gels ($p < 0.05$), while HA:0.3% Hp-VEGF+PDGF produced a lower *NI* value in the presence of Gtn ($p < 0.05$) (Figure 10a). On day 14, only the case HA:0.3% Hp-VEGF+PDGF showed a statistically higher *NI* in the presence of Gtn. The other cases produced statistically identical values regardless of the Gtn content. Between day 7 and 14 *NI* increased for HA:0.3% Hp-VEGF+KGF, was unchanged for HA:0.3% Hp-VEGF+Ang-1, and decreased for HA:0.3% Hp-VEGF+PDGF ($p < 0.05$).

Overall, there appeared to be no single growth factor combination that stood out as most effective irrespective of the presence of Gtn and Hp. However, treatments containing the growth factor combination VEGF+KGF

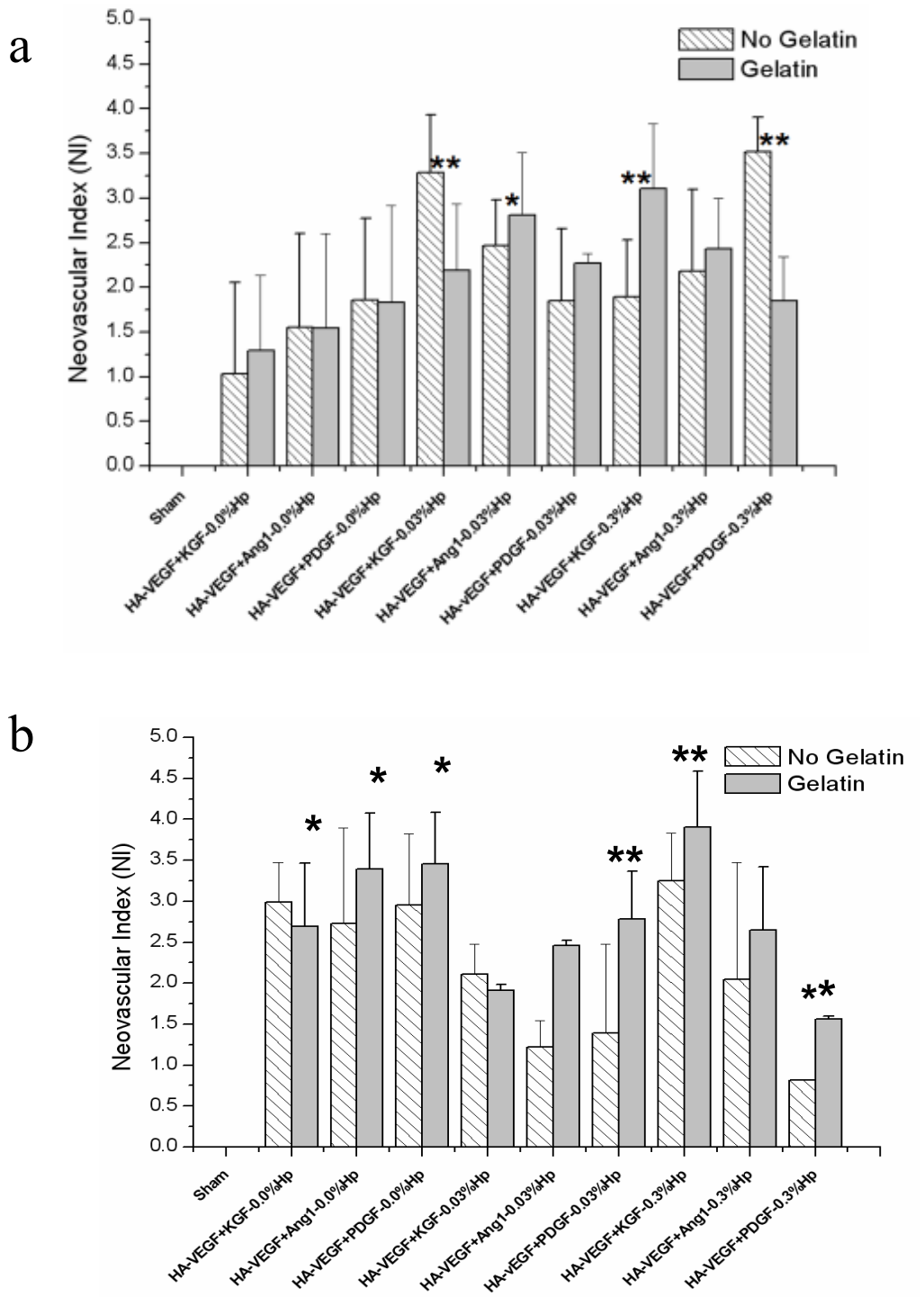

Figure 10. Neovascularization index for HA:Hp-cytokine loaded treatment groups both with and without gelatin at (a)day 7 post-implantation (b) day 14 post-implantation. *NI* is defined in the text, Eq. (1). Mean ± s.d., $n = 6$. * indicates statistical significance for comparison with sham, ** indicates statistical significance for comparison between two individual treatment cases as well as sham (only comparisons discussed in the text are identified).

consistently produced the strongest responses, regardless of gel Gtn or Hp content, a finding consistent with past studies[30].

The results suggest that inclusion of heparin in the gel may have a cytokine-dependent influence on elicited microvessel density levels, improving maturation in some cases but inhibiting maturation in others. In the absence of Hp, all cases showed a significant increase in vessel density from day 7 to day 14 (Figure 10, $p < 0.05$). In the presence of Hp, patterns were less clear, with most treatments producing no change in vessel number. However in some cases the inclusion of Hp produced either significantly higher (HA:Gtn 0.3% Hp, VEGF+KGF) or lower vessel counts (HA:VEGF+Ang-1).

Past studies have shown that the synthetic ECM created by crosslinking modified HA with modified gelatin produces robust, bioresorbable scaffolds that can be implanted to achieve cell and tissue growth *in vivo*[31, 109] However cell viability in these scaffolds was shown to be reduced in the absence of this gelatin component[31, 109]. It turned out that, a 50% HA-DTPH, 50% gelatin mixture provided an optimum mixture for seeding with fibroblasts, chondrocytes, and bone marrow cells *in vivo* [31, 110]. Previous *in vitro* measurements of the rate of release of growth factors from HA-based gels show more rapid release in gels containing gelatin[109]. This effect is likely due to the smaller molecular weight of gelatin compared with long-chain HA. As a result, gelatin-containing gels would be expected to present less steric interference, and therefore less hindered diffusion and less resistance to growth factor release, than non gelatin-containing gels. Additionally the gelatin provides the cells with numerous integrin binding sites. As described previously, cell proliferation and viability depend strongly on cell-ECM integrin interactions. Considering the

angiogenic response *in vivo* begins with endothelial cell proliferation, which is driven by the appearance of VEGF, the presence of integrin binding sites is extremely important. Neovessel development in these gels therefore depends on exposure to the growth factors release as well as the scaffold's ability to support endothelial cell ingrowth.

GF release from the HA-based gels occurs in part through diffusion and in part through gel breakdown mediated by HAse. When Hp is present in the gels, interactions between Hp and the GFs can be expected to retard GF release and alter the patterns of new vessel formation. *In vitro* release measurements indicate that heparin-containing gels release different GFs at specific rates unique to the GF[29]. For example, VEGF and KGF were released from the gels *in vitro* at similar rates while the rate of release of Ang-1 was 5-10 times slower. It is possible that this difference in angiogenic response is due to a variable rate of GF release.

As previously described, HA is degraded *in vivo* bioactive oligomers (o-HA) capable of binding receptors, CD44, RHAMM and TLR-4, that all play a role in mediating cellular responses. The interaction between o-HA chains and these surface receptors have shown to promote endothelial cell proliferation and migration, induce sprout formation and eventually lead to angiogenesis[1, 111-113]. Additionally HA has been shown to be able to augment the effects of VEGF both *in vitro* and *in vivo* [7, 114], although this feature is not universal to all growth factors[24]. GFs are known to be specific and often require specific conditions to situate a response[115-120]. It is possible that with time, fragments resulting from the breakdown of HA, may interact more or less favorably with the incorporated GF. These interactions could be as simple as

exposure or degradation of potential GF binding sites or, more likely, highly complex signaling pathways.

In brief, HA has recently been shown to directly effect VEGF expression[90]. *In vitro* experiments show that o-HA treated atrioventricular explants exhibit a strong increase in mRNA for VEGF[90]. Rogders et al. injected o-HA directly into atriovetricular canals of chickens and monitored parameters such as subsequent VEGF expression. The study showed a drastic increase in levels of VEGF in the myocardium lining[90]. These experiments demonstrate the strong association of o-HA and VEGF, and the previously described roles in angiogenesis. Augmentation of angiogenesis via Ang-1, KFG of PDGF-AA containing HA hydrogel has been well established[7, 24, 109]. It is probable that the increases in vasclarization seen in the above *in vivo* hydrogel studies are due to unknown o-HA-GF interaction that either stimulate vessel production or allow GF activation.

3.2 Experiment 2: Composite Hydrogel

3.2.1 Gelation time, density, and swelling

Mean gelation time based on (n = 3) individual trials was 29 min, 30 sec +/- 57 sec. The density of these hydrated composites was 0.915 +/- 0.094 g/cm^3. The average equilibrium swelling ratio (volume wet/ volume dry) for three composite gel samples in PBS at room temperature and pH 7.4 was 9.05 +/- 2.90, indicating the hydrated gel volume was 9 times that of the dry film state. This result was similar to previously published data showing pure HA-based films to swell over 7 times their dry volume when exposed to PBS[32]. Thus it appears that neither the presence of the

silk component nor the inclusion of glycerol hindered the gel capacity to dry to a film state or swell back to its original size.

The resulting swelling kinetics of three samples are shown in Figure 11. The figure demonstrates that the HA-silk composite gels swelled rapidly, reaching equilibrium in 10 minutes. The swelling was fit to the best fit regression curve of

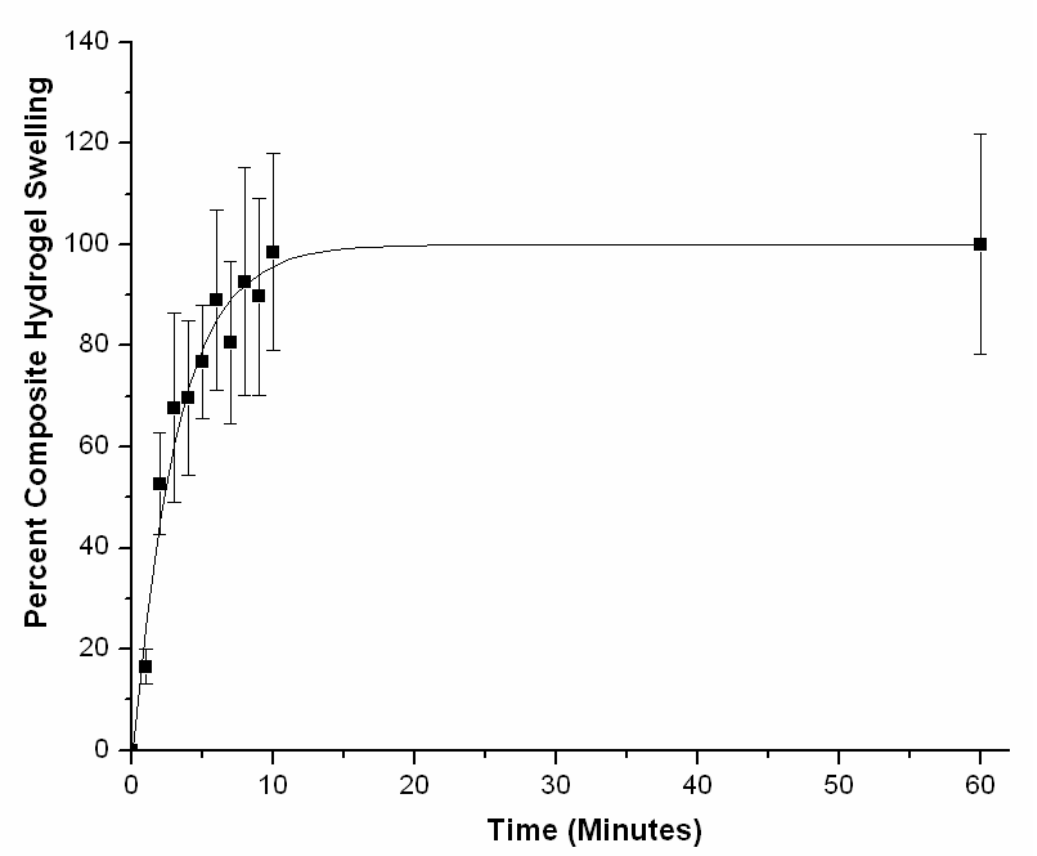

Figure 11. Swelling kinetics of HA-silk composite gels in PBS. The associated curve is the best fit regression of the data to the form $m(t) = A\,(1- e^{-t/\tau})$. Data points represent an average of three independent measurements.

form $m(t) = A\,(1- e^{-t/\tau})$, with A being the initial thickness, t being time after immersion in PBS, and τ representing the time constant.. This equilibrium was six times longer than for pure HA-based gels, which reached equilibrium in

approximately 100 seconds[32]. This delayed swelling character is probably caused by the presence of the hydrophilic glycerol, which likely slowed hydration.

3.2.2 Surface morphology by SEM

Control composite hydrogels exposed to PBS, lyophilized and imaged by SEM without sputter coating at 2000×, showed no signs of physical degradation (Figure 12a). Surface texture appeared smooth at fine scale, with widely separated small surface ripples but no areas of cracking or gel-silk separation. This smooth surface corresponds well with the featureless texture typical of HA-based gels[32]. In contrast, the sample exposed to water and allowed to air dry had a rougher appearance (Figure 12b). This gel had large areas of cracking and missing gel fragments, as well as areas in which the previously encapsulated silk mat was fully exposed. In this case, the slow air drying process led to different drying rates for different areas of the gel. The surface of the gel likely dried first and began to shrink rapidly compared to the interior sections of the gels. This localized shrinking would cause stresses within the gel, and eventual tearing. In the absence of the silk mesh, thiol-modified HA hydrogels cycle from dry to hydrated states without degradation. However, this image shows that the presence of the silk mat, which is inelastic and does not shrink or swell appreciably, sets a limit to the extent to which the hydrogel can shrink without tearing.

The sample exposed to complete media displayed surface characteristics similar to the PBS control gels (Figure 12c), with the exception of the presence of localized micron-sized pores. These samples were intentionally not rinsed in order to observe potential effects of the media components on the gel. As a result, traces of proteins

and salts derived from the media are visible in the images. Although much of the gel surface was intact, a few regions contained sparsely distributed pore-like structures a few micrometers in diameter. These pores were all surrounded by raised circular rings, which are the remaining media components. The presence of these pores and rings suggests that media components, probably originating from the FBS supplement, may have enzymatic activity and are thus able to slowly degrade these gels.

HAse-treated gel samples showed a greater number of pores of substantially larger diameters, when compared to pores seen in the media treated gels. (Figure 12d). Pores varied in size from about 5um up to 80um, and were widely distributed over the gel surface. This degradation pattern was similar to those seen with non-composite gels *in vivo*[121], suggesting the presence of silk does not interfere with HAse-mediated gel degradation.

Silk mat enzymatic biodegradation was not observed with exposure to HAse. However, silk mats but has been demonstrated to be controllably degradable by protease XIV[52, 107, 122]. Fibrin content of these hybrid silk hydrogels had a direct effect on the gel porosity, with increased fibrin producing smaller pores[52]. If desired of small amounts of protease XIV could be included in the HA hydrogel composite to produce controlled silk degradation and potentially alter release kinetics of incorporated drugs.

Figure 12

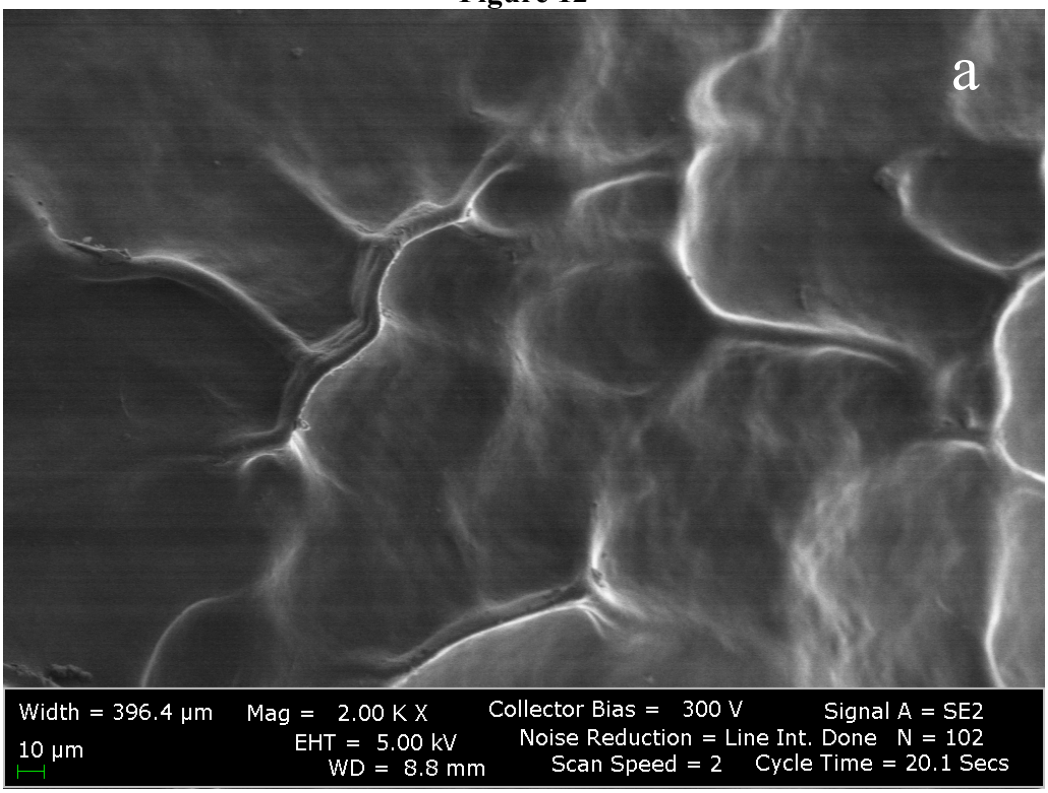
a
Width = 396.4 µm
Mag = 2.00 K X
Collector Bias = 300 V
Signal A = SE2
10 µm
EHT = 5.00 kV
Noise Reduction = Line Int. Done N = 102
WD = 8.8 mm
Scan Speed = 2
Cycle Time = 20.1 Secs

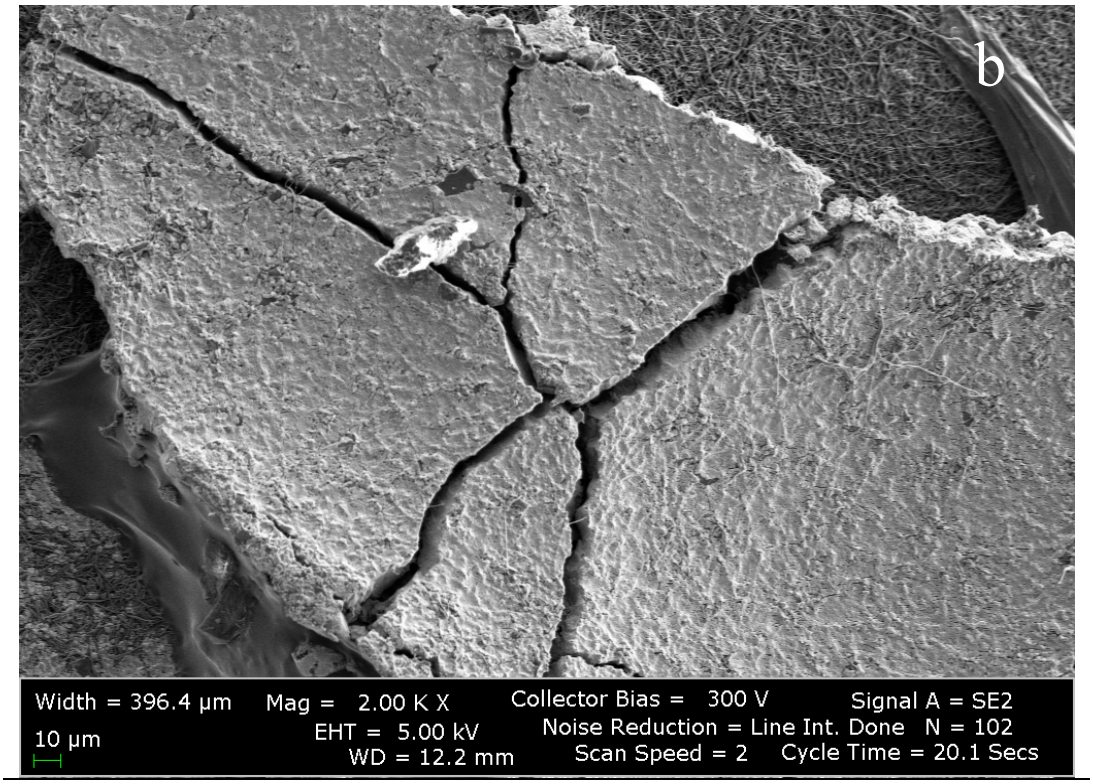
b
Width = 396.4 µm
Mag = 2.00 K X
Collector Bias = 300 V
Signal A = SE2
10 µm
EHT = 5.00 kV
Noise Reduction = Line Int. Done N = 102
WD = 12.2 mm
Scan Speed = 2
Cycle Time = 20.1 Secs

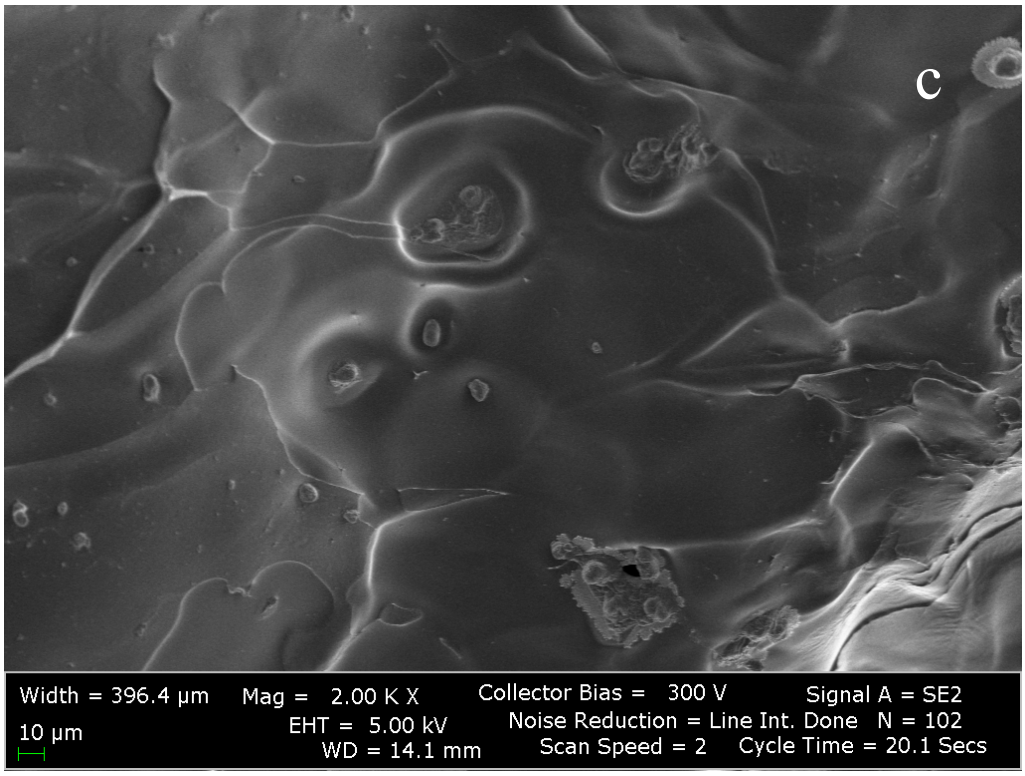

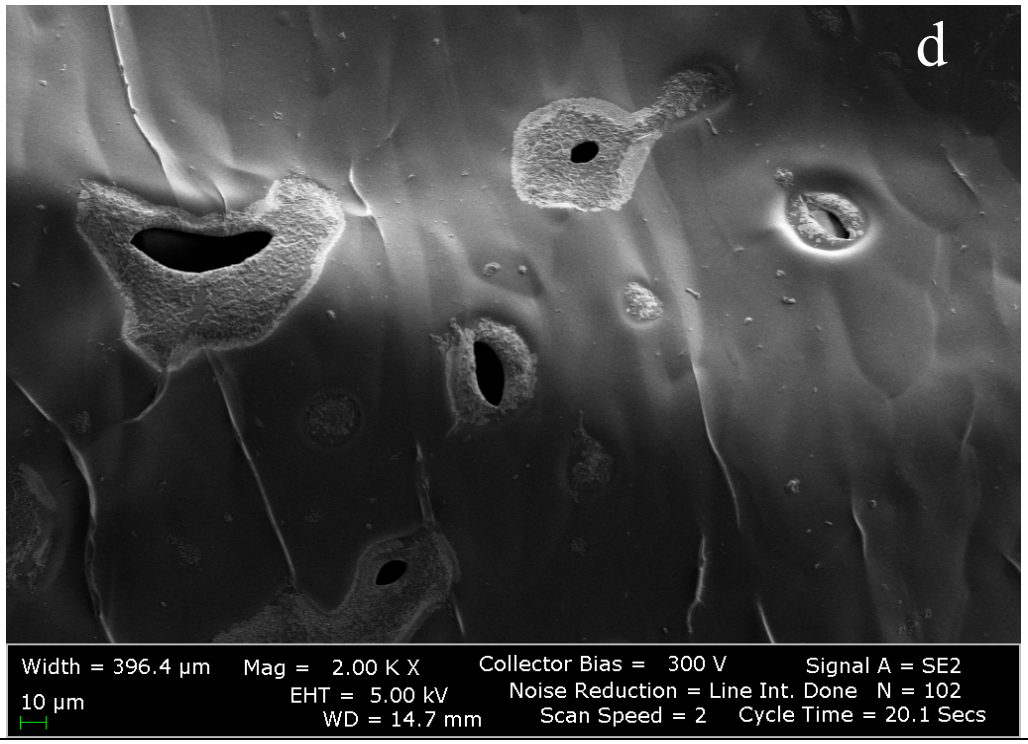

Figure 12. SEM images of lyophilized HA-silk gel surfaces. (a) Composite hydrogel exposed to PBS for 24 hours prior to lyophilization. (b) Composite hydrogel exposed to water for 24 hours and air dried prior to lyophilization. (c) Composite hydrogel exposed to 10% FBS media for 24 hours prior to lyophilization. (d) Composite hydrogel exposed to 75 U/ml HAse for 24 hours prior to lyophilization.

Thermal behavior

Thermal properties of the HA-silk composite gels were examined by Differential Scanning Calorimetry (DSC) and Thermal Gravimetric Analysis (TGA). Figure 13a shows a DSC scan of a composite gel. All samples showed a small endothermic peak around 55°C due to absorption by water, which corresponded to both weight loss and to an increase in the rate of weight loss rate (Figure 13b). Glass transition temperatures, T_g, for the individual components would be expected to be ~110°C for modified HA and ~178°C for electrospun silk [123, 124]. At temperatures above these T_gs, the DSC scan showed major endothermic peaks at 210°C and 240°C, corresponding to the crystallization temperatures for silk and HA, respectively [125]. These peaks matched with observations in other studies[124, 126]. Not surprisingly, the composite gel lost weight most rapidly in the range 150 – 220°C, due to evaporative water losses (Figure 13b). Sample weight then declined much more slowly at higher temperatures, over the duration of the measurements. Because the silk and HA components of the composite gel were physically as opposed to chemically crosslinked, it is not surprising that the DSC and TGA curves reflected the properties of the individual gel components.

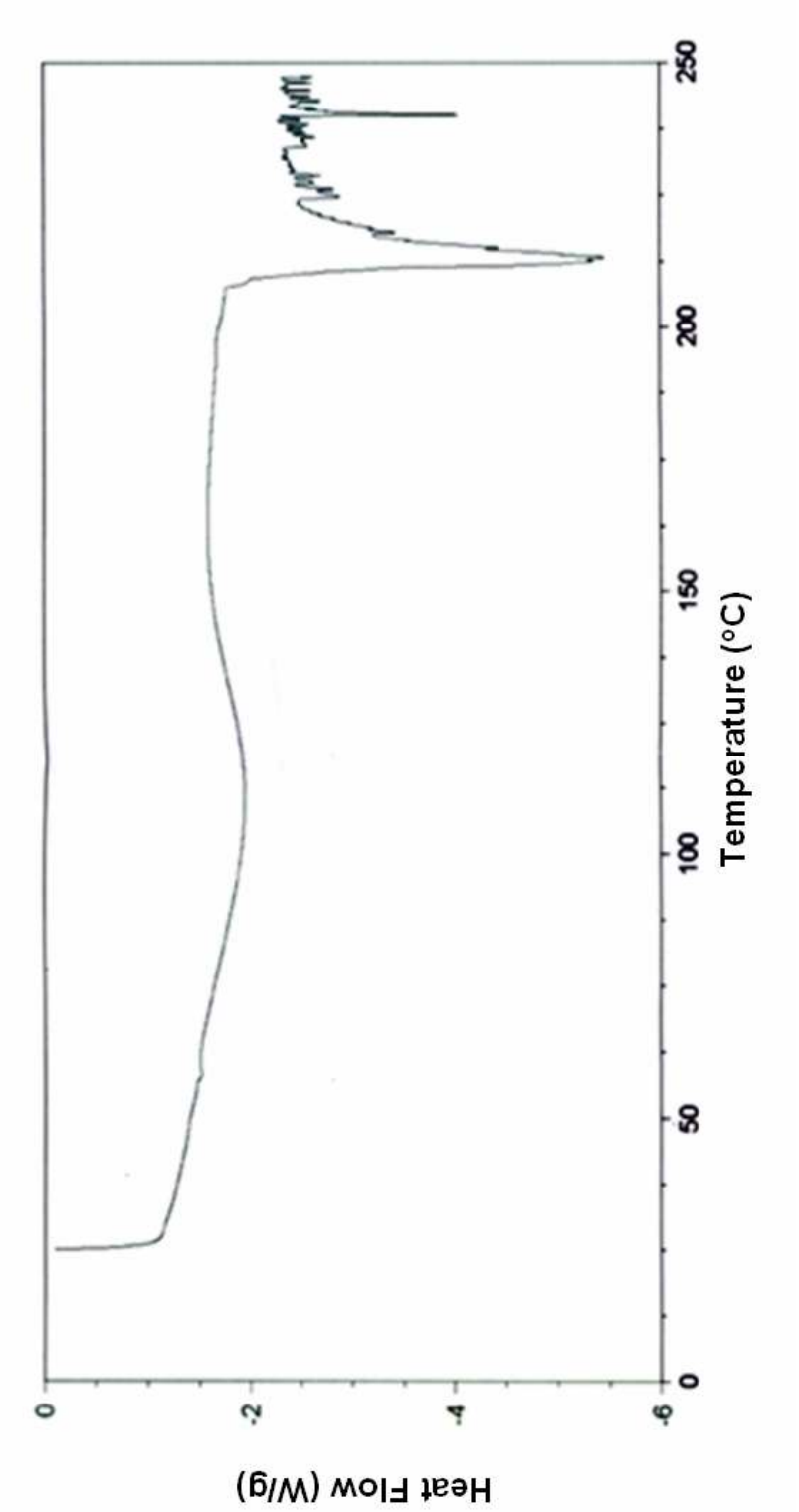

Figure 13a. Differential scanning calorimetry analysis of the HA-silk composite hydrogel.

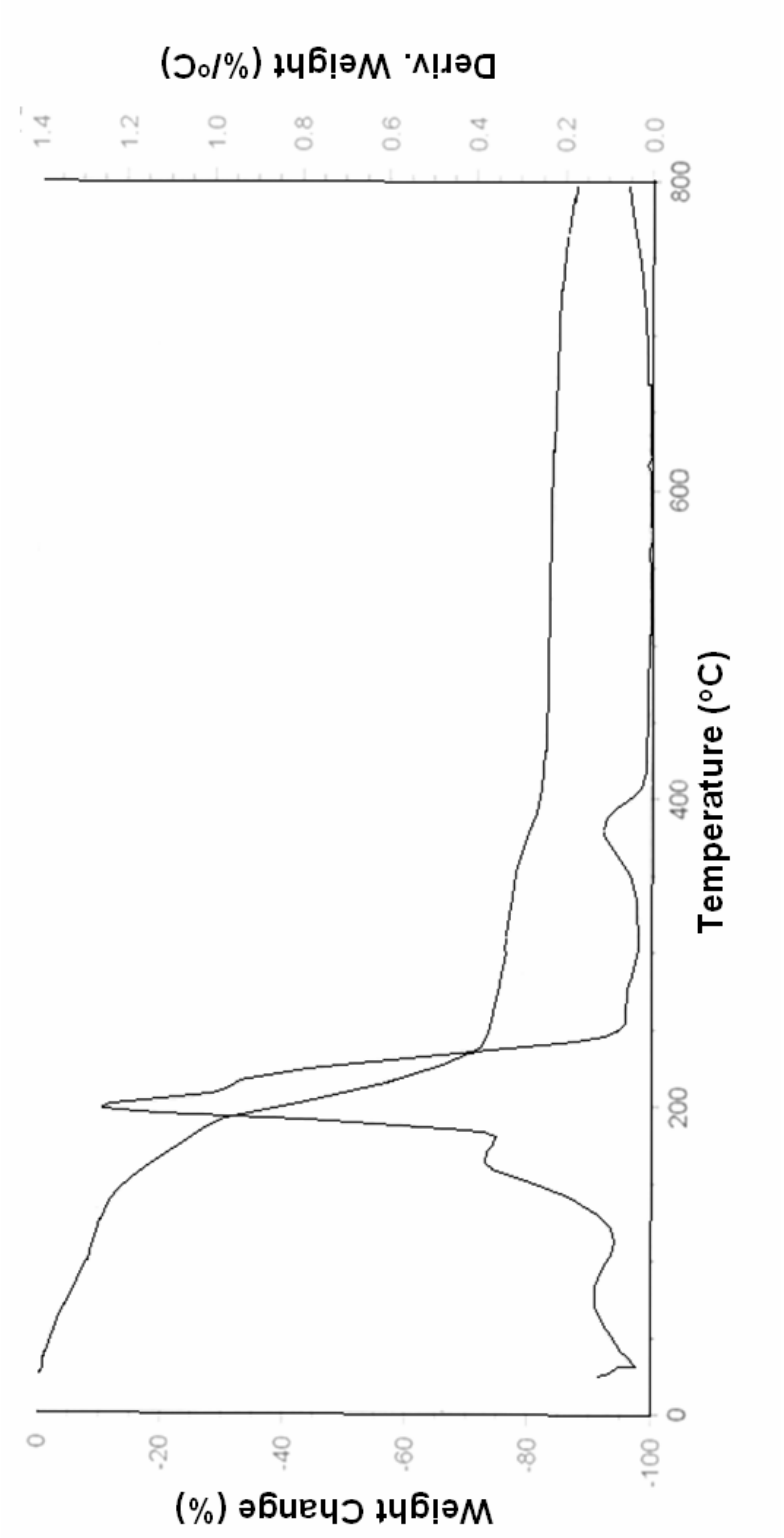

Figure 13b. Thermal gravimetry analysis illustrating percent weight change with increase in temperature

3.2.4 Mechanical Characterization

In compression testing up to 92% strain (Figure 14a), gel stress increased monotonically with strain for all samples tested, after which the gels reached ultimate failure. Over the range of strains tested, the gels showed a characteristic non-linear compressive curve with continuously increasing stiffness. Mean E_c (Young's Modulus) for the initial linear region of the stress v. strain curve, up to 25% strain, was 5.38 ± 1.18 kPa. This value was 20% greater than the stiffness of the corresponding HA-based gels lacking the silk mesh (4.33 ± 1.17 kPa). The inclusion of the silk mesh did not appear to alter the ultimate compressive strength of the composite gels, since failure occurred through the gel component and not through the much stronger silk mesh. Similar sized gels synthesized without glycerol had a compressive modulus of 3.51 ± 1.49 kPa, a 35% decrease. The higher modulus for the composite gels is probably due to retention of water by the glycerol component. The incorporated water requires more applied force for equal compressive displacement and thus produces a higher compressive modulus. Although the properties of hydrogels can vary significantly with the material, crosslinking density and fabrication techniques the mechanical behavior of the composite HA-silk hydrogels fell well within previously published data[127-129].

Tensile behavior of the composite gels is shown in Figure 14b. Testing was only possible for composite gels; corresponding gels without silk mats lacked the strength to support pulling of the sutures. Tensile stress increased monotonically with strain over the range of strains tested for all samples. However, in contrast to compressive behavior, tensile stiffness decreased continuously with strain. Mean E for the composite gels over the range from 10% to 20% strain was

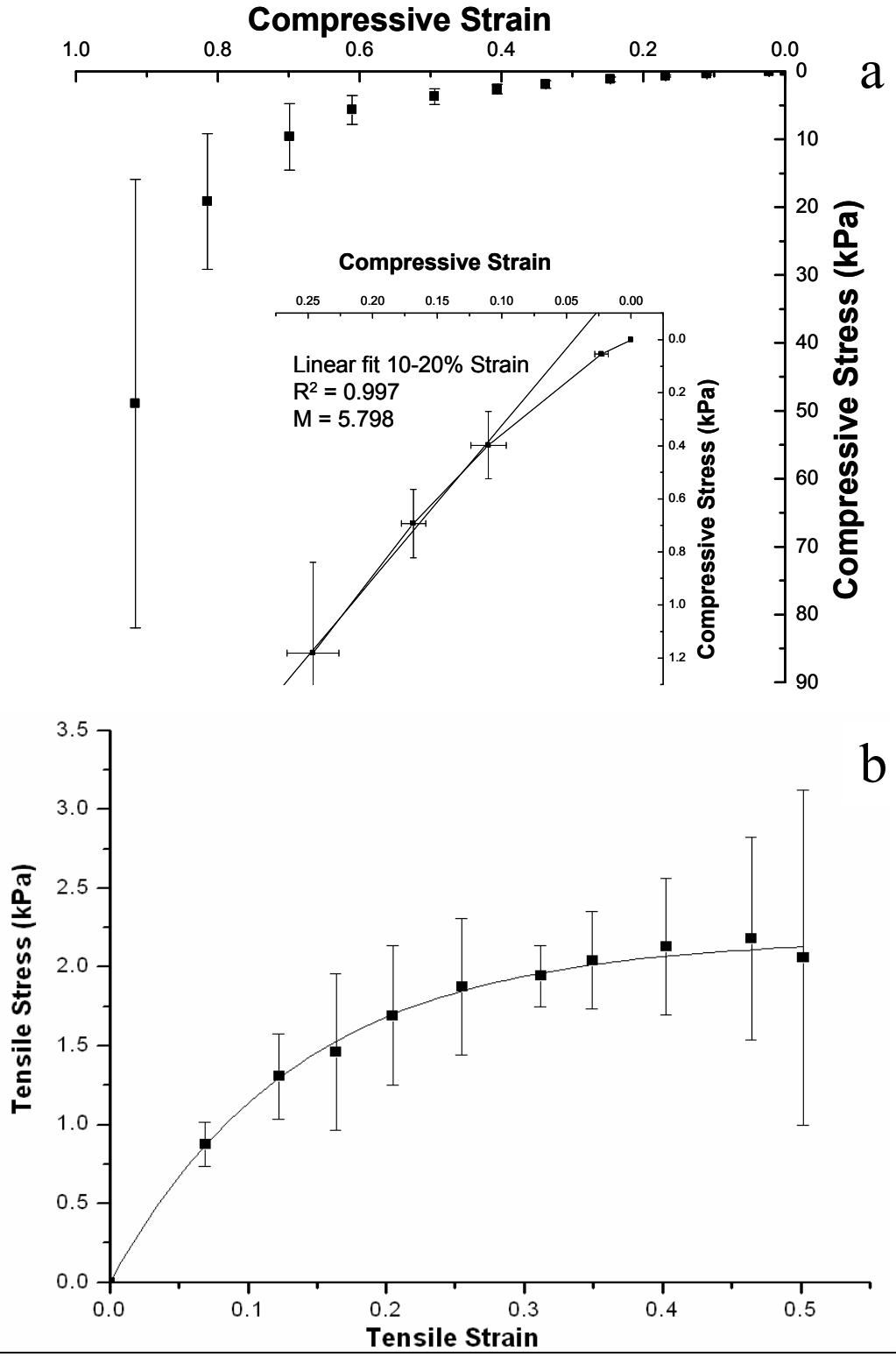

Figure 14. Mechanical behavior of the composite hydrogel. (a) Compressive characteristics. The insert demonstrates the linear region of the stress *vs.* strain curve. The compressive modulus over this range of strain is 5.38 kPa, R2 = 0.997 (n = 3). (b) Tensile characteristics. Mean E for the composite gels over the range from 10% to 20% strain was 4.43 kPa, and the UTS was 2.06 kPa (n = 3).

4.43 ± 2.87 kPa, and the UTS was 2.06 ± 1.06 kPa. Although the presence of the mesh reinforcement did not contribute mechanical integrity in the compressive direction, it is apparent that under tensile stress it provides significant reinforcement to the gels.

The silk mat reinforces the composite, providing strength necessary for the gels to be secured onto tissues and organs, which otherwise might be difficult or impossible to target for localized delivery of therapeutic agents. One potential application is for delivery of drugs or growth factors to ischemic tissue regions. Fiber tension around ischemic tissue is estimated to be close to 15-30 Pa, below the structural properties of the composite by two orders of magnitude[130].

3.2.5 Enzymatic degradation

3.2.5.1 Degradation quantified via composite mass loss

The rate of degradation of the composite gels in the presence of HAse was evaluated by measuring the rate of mass loss as a function of HAse concentration. Direct measurements (Figure 15) showed that the untreated control gels retained more than 90% of their mass for the duration of the experiment. For all other cases, mass decreased with time exposed to the HAse. Gels exposed to 2 U/ml HAse showed a steady loss of gel mass, reaching 54.3 % of original weight by the end of the experiment. Gels in 5 U/ml HAse did not vary significantly from the 2 U/ml gels for the first three days, showing a relatively steady decline in mass. However, between days 3 and 5 these gels lost over 70% of the remaining hydrogel weight. The 10 U/ml HAse gels lost 35% of their mass in the first day, and continued to loss mass over days 2-4, at which point hydrogel mass was completely gone. At higher

HAse concentrations (50, 100 and 150 U/ml), gels lost mass much more rapidly, with all hydrogels being completely degraded by the end of day 3. By comparison, previous *in vivo* studies have shown that pure HA-based gels lacking the reinforcing mesh were partially intact in a subcutaneous environment after a period of seven days, but are fully degraded by day fourteen[29, 33, 43, 109]. These measurements therefore suggest that native *in vivo* degradation conditions are matched most closely by *in vitro* HAse concentrations less than 5 U/ml.

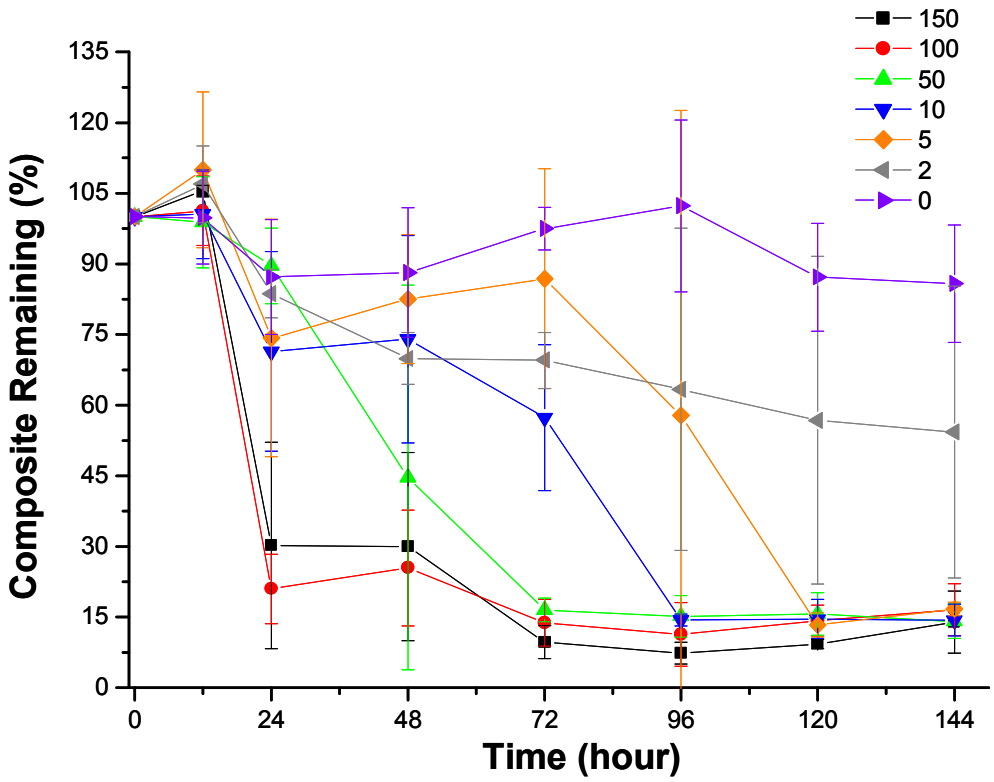

Figure 15. Time course of Hase-mediated composite gel degradation, mean ± s.d of $n = 3$ independent trials.

The hydrogel component accounted for 85% of the composite patch initial weight, with the other 15% of the weight corresponding to the silk mat. Thus,

measurements with 15% composite mass remaining indicated full degradation of gels with only the silk mat remaining. Upon visual inspection with a light microscope the silk mat were found to be non-degraded at the end of the experiment in all cases.

3.2.5.2 Degradation quantified via FITC-Dextran release

Non-covalently incorporated solutes are released from the composite hydrogels through a combination of direct diffusion and breakdown of the hydrogel. To evaluate degradation gel breakdown, FITC-dextran samples of three different molecular weights (4000, 70,000 and 250,000) were loaded into composite gels at two concentrations (0.5 or 1.0 wt %). Figure 16 shows the release rates of FITC-dextrans. For low molecular weight (4000, Figure 16a), the solute showed over 80% release within 2 hours and full release after less than 6 hours, for both loading levels regardless of the presence and concentration of HAse. Release mechanisms were therefore dominated by diffusion. A similar diffusion based escape was previously observed for M_w 4000 FITC-dextran release from HA-based hydrogels lacking the electrospun silk mat[32]. Diffusion occurred within minutes in the non composite gels[32]. Slower release here was most likely due in part to the presence of the silk mat, but primarily to the presence of glycerol. Studies have shown that drugs in glycerol-containing hydrogels display a delayed release profile compared to non-glycerol-containing counterparts, as was observed here[131].

Release was slower for high molecular weight FITC-dextran (250,000, Figure 16b) and appeared to depend on HAse concentration. Release kinetics for high M_w solutes followed nearly first order exponential kinetics, with a release rate of 5.26

$min^{-1/2}$ and 5.00 $min^{-1/2}$ for 0 and 3 U/ml HAse, respectively, while only 3.82 $min^{-1/2}$ for 75 U/ml HAse. This release reflected gel breakdown, since direct measurement showed degradation to be complete by 24 hours in the presence of 75 U/ml HAse (Figure 15). Over 80% of the gel remained intact at 24 hours for both 0 and 2 U/ml HAse (Figure 16), but more than 60% of the solute had been released even without gel breakdown. This indicates that the release of the high molecular weight FITC was driven by a combination of degradation and diffusion. The 70,000 MW loaded gels profiles showed intermediate release profiles to the 4,000 and 250,000 dextran gels.

The fact that release of FITC-dextran followed kinetics profiles that can be explained on a physical basis shows the ability of the gel to store and then release compounds at a controllable rate. Both diffusion and gel breakdown affected release rate. Low M_w solute diffused freely and quickly out of the highly porous hydrated gel. However, high M_w solute was released more slowly and involved both free diffusion and enzymatic degradation. Interestingly, the FITC-Dextran hydrogels did not gel at room temperature, and only after being put in a 60^{O}C oven did full gelation occur. This could be an influential factor in gel behavior, the unexpected breakdown of 0 U/ml and 3U/ml gels.

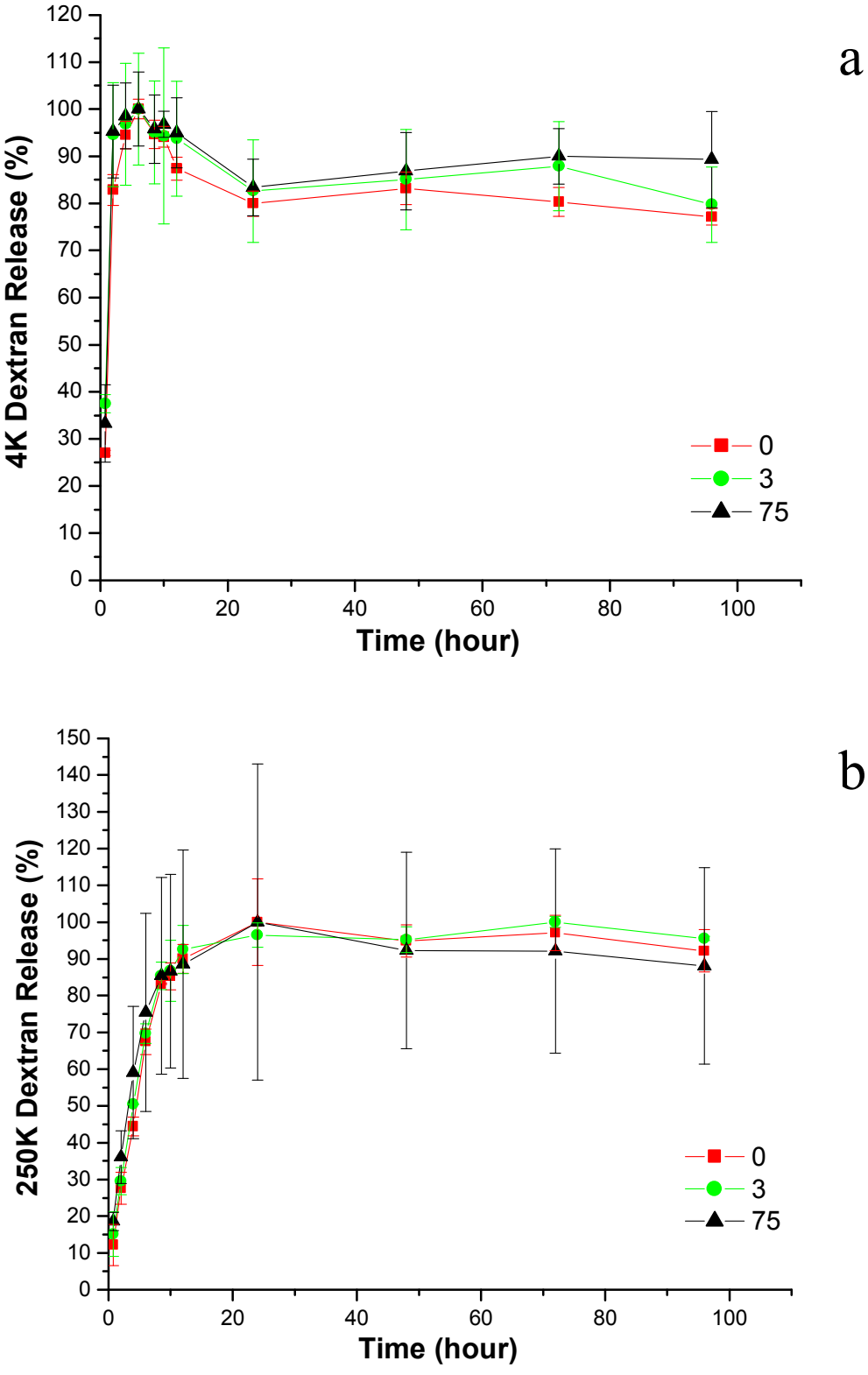

Figure 16a. Composite hydrogel HAse-regulated FITC-dextran release (a) *M*w = 4,000 (b) *M*w = 250,000 mean ± s.d of *n* = 3 independent trials.

3.2.6 *in vitro* Drug Release

3.2.6.1 *in vitro* Hydrophobic Drug Release

To evaluate the capability of the composite for controlled drug delivery, several anti-inflammatory were loaded non-covalently into the gels prior to crosslinking and rate of release *in vitro* measured spectrophotometrically (dexamethasone, hydrocortisone, 6α-methylprednisolone, cortisone, prednisolone and prednisone). Results of these drug release experiments are shown in Figure 17. For all six drugs, release profiles increased monotonically with time, and were well fit by first order exponential kinetics ($R^2 > 0.9$ for all cases). The released drug mass was fit to a kinetic release model appropriate for diffusing molecules, $m(t) = A\,(1- e^{-t/\tau})$, where $m(t)$ represents percent of drug present in solution at the time (t), τ is the time constant characterizing the release rate of the drug and A is the initial drug loading. To compare between drugs, the release rate was taken as the slope of cumulative drug release *vs.* $(\text{time})^{1/2}$ over the range from 0 - 65% release[32]. Cortisone and prednisolone had release rates of 9.89 $\text{min}^{-1/2}$ and 7.79 $\text{min}^{-1/2}$ respectively. In contrast, hydrocortisone and dexamethasone had rate below 4.0 $\text{min}^{-1/2}$. Prednisone and 6α-methylprednisolone fell between these ranges, with release of 6.44 $\text{min}^{-1/2}$ and 4.52 $\text{min}^{-1/2}$.

The observed release rates from the composite gels were lower than those previously observed for HA-based hydrogels lacking a reinforcing mesh[32], indicating that the drugs were retained for a longer period of time in the HA/silk composite. Part of the explanation for this may relate to the drug interaction with the silk mat, thereby slowing its rate of release. Past studies of biofunctionalized electrospun silk mats demonstrated that drug release was dependent on silk fiber contact with an

aqueous environment[71]. Swelling of biofunctionalized fibers exposed to PBS caused swelling and prevented full release of growth factors[71]. Similarly we expect that mat swelling may hinder release of GF near the silk by acting as a diffusion barrier or through direct drug entrapment within the mesh.

In addition, as with the FITC-dextran, the presence of glycerol alters the microenvironment within the gel, increasing the drug residence time and delaying its release. Past studies have demonstrated that increasing glycerol content is associated with increased drug storage and delayed release [131]. Further, previous studies with HA-only-based gels showed a positive correlation between drug hydrophobicity and release rate. That relation was not maintained in the present studies, also presumably because of the presence of glycerol.

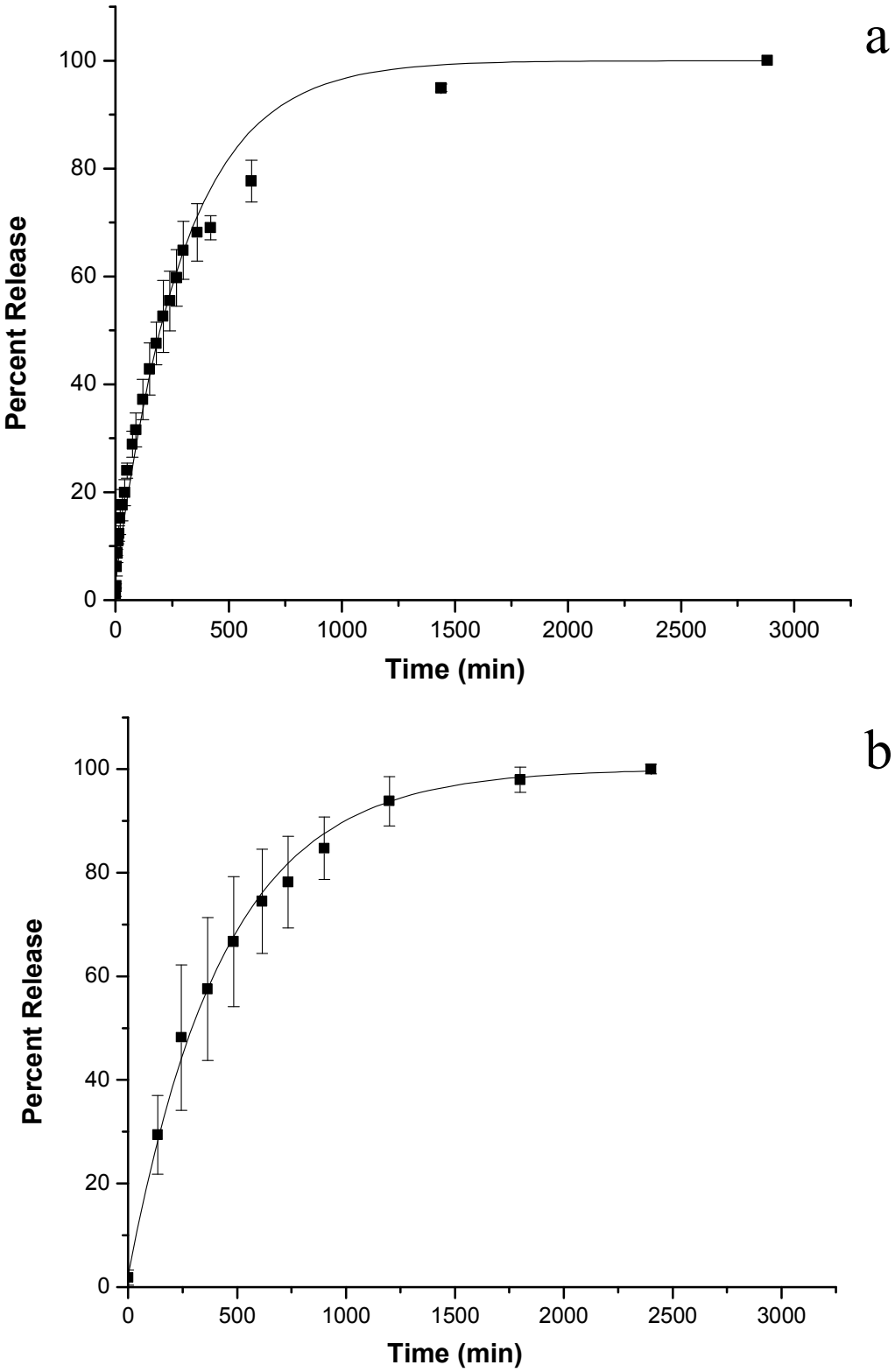

Figure 17. Time course of (a) dexamethasone (b) hydrocortisone release from composite hydrogels *in vitro*. Data points represent mean ± s.d of $n = 3$ independent trials, and the associated curves are best fit regressions to the form $m(t) = A\,(1 - e^{-t/\tau})$.

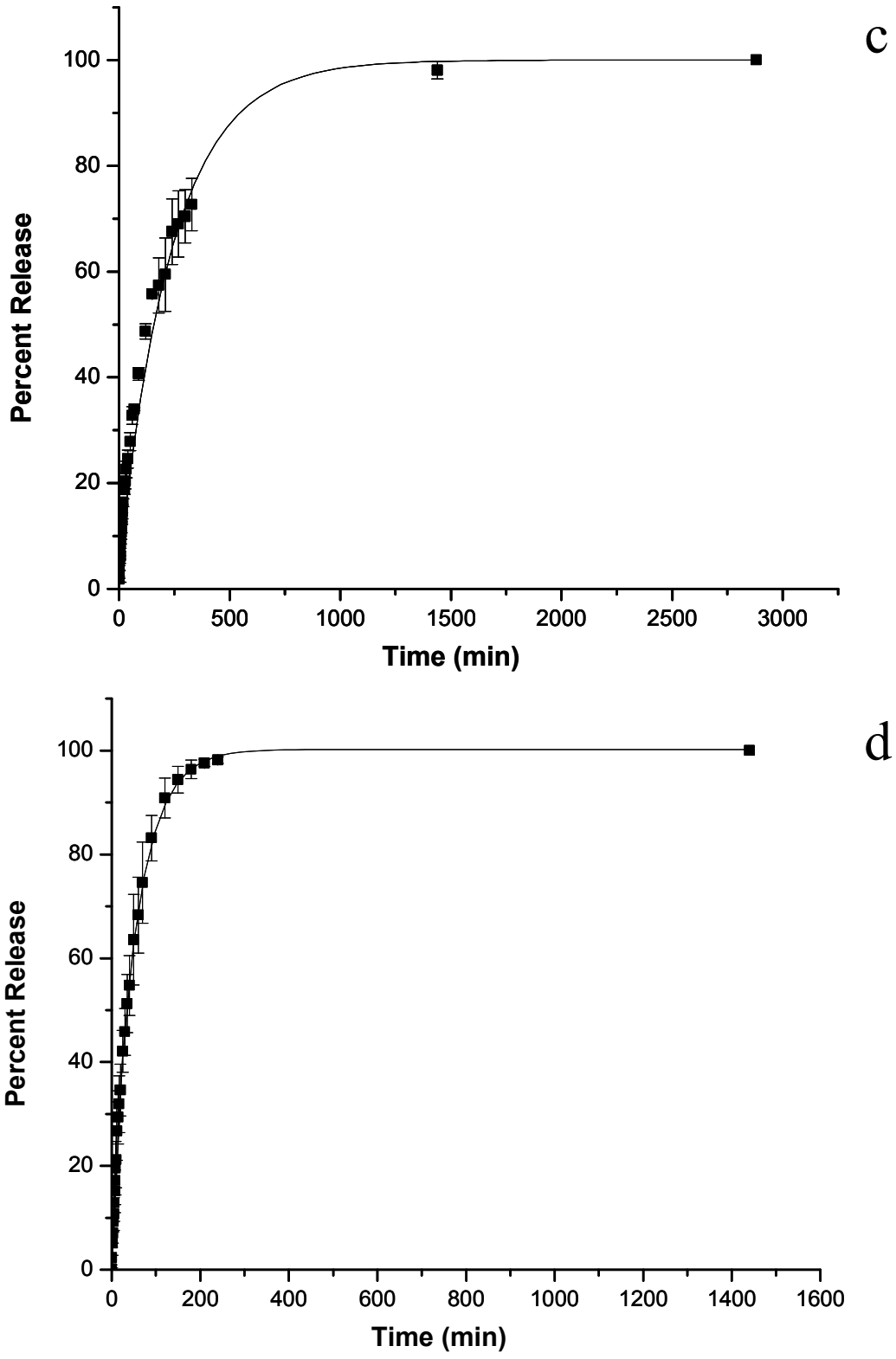

Figure 17. Time course of (c) 6-α-methylprednisolone, (d) cortisone release from composite hydrogels *in vitro*. Data points represent mean ± s.d of $n = 3$ independent trials, and the associated curves are best fit regressions to the form $m(t) = A\,(1 - e^{-t/\tau})$.

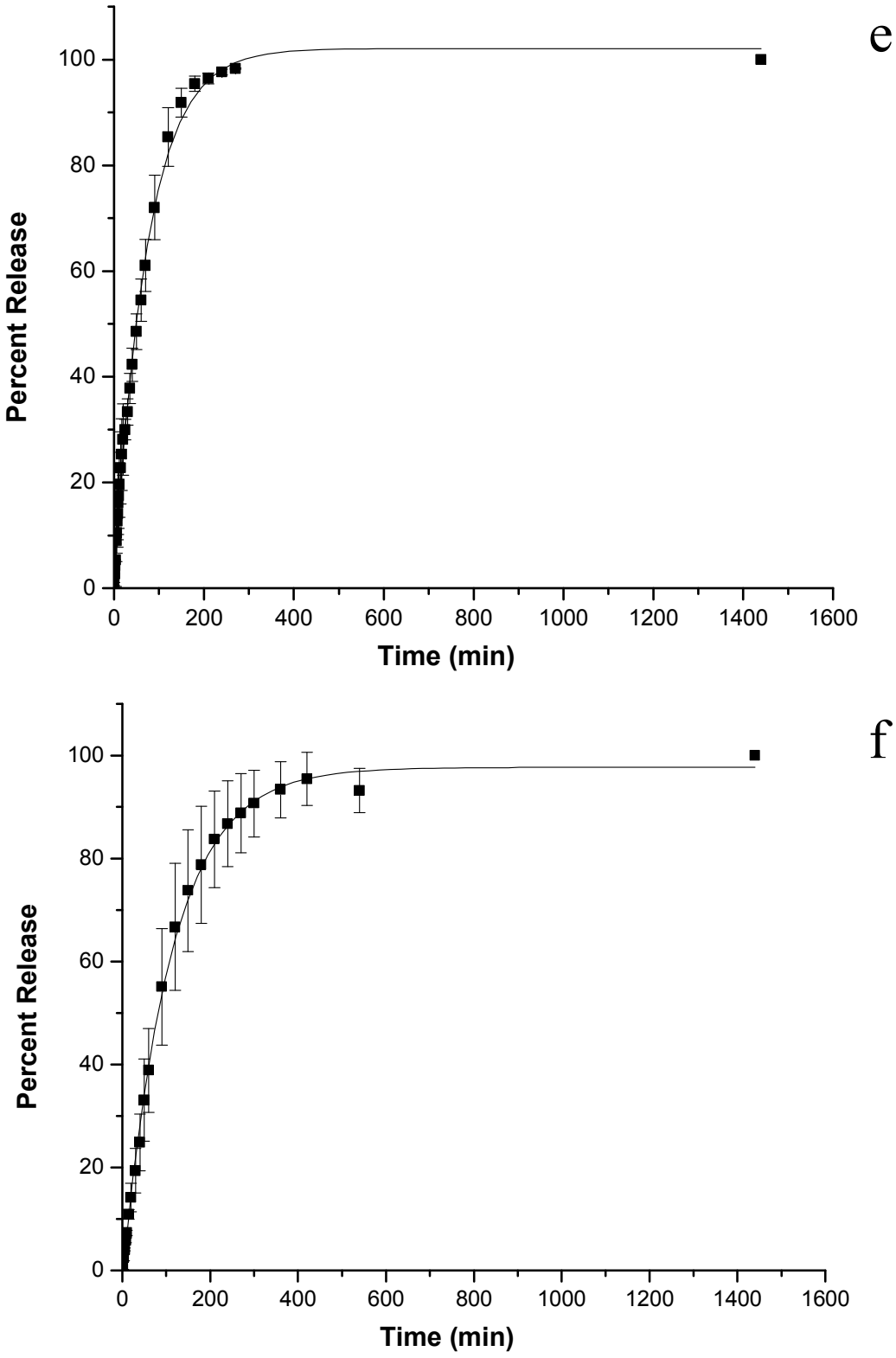

Figure 17. Time course of (e) prednisolone (f) prednisone release from composite hydrogels *in vitro*. Data points represent mean ± s.d of $n = 3$ independent trials, and the associated curves are best fit regressions to the form $m(t) = A\,(1 - e^{-t/\tau})$.

3.2.6.2 *in vitro* VEGF Release

Figure 18 shows the time course of release of VEGF from composite gels *in vitro*, in both the presence and absence of 0.3% thiol-modified heparin in the gel. As in past studies, the presence of immobilized Hp significantly affected the final cumulative VEGF release over the 42 days of the study [109, 132]. The presence of covalently-linked Hp increased total release from 25% to approximately 57% of the initial load. Previous research has suggested that interactions between sulfate groups of the heparin and positively charged lysine and arginine residues of the GF can serve to control release both *in vitro* and *in vivo*[24, 109].

The present results match previously published values for VEGF release from non-Hp containing HA-based gels, showing approximately 30% of loaded VEGF to be released over the 42 day experiment[24]. However, Hp-containing gels did not match previous results which showed delayed release of GFs in Hp presence[24], again presumably due to the presence of glycerol which may be shielding charges on the HA backbone and the Hp chains. Such shielding would effectively minimize attractive forces between the HA/Hp ECM and the positively charged amino acid residues of VEGF[129, 130]. This would produce higher overall release in the presence of glycerol compared to previously published results. Alternatively, glycerol could be occluding the negative sulfate groups on the heparin, interfering with interactions between the GF and heparin, ultimately altering drug retention time[131, 133].

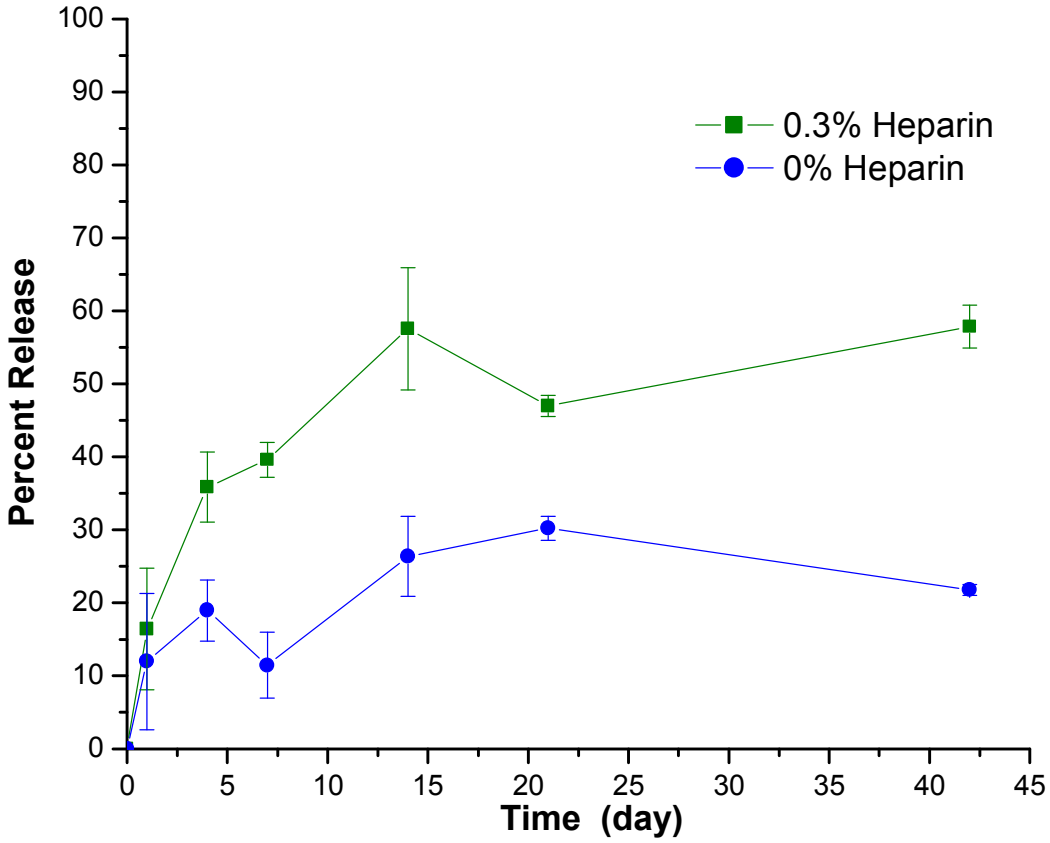

Figure 18. Time course of *in vitro* VEGF release from composite hydrogels containing 0.0% or 0.03 % heparin. Data points represent mean ± s.d of $n = 3$ independent measurements.

3.3 Experiment 3: Encapsulation of cells in Hydrogels

3.3.1 Gel thickness and seeding density

Gels of two distinct thicknesses and seeding densities were created to study the effects of gel thickness and cell density on cell viability. Gel thickness and cell density dictate the distance between cells and the above supernatant and can potentially hinder exchange of nurturance and waste. Hydrogels of 1:1 HA to Gtn,

were cast to a final height of either ~500um or ~70um. The gels were seeded with either a high 50,000 cells/gel density or at a low 25,000 cells/gel density. As described previously growth ratios of cells was used as a measure of cell viability.

Figure 19 shows cell data measured using MTS assays for the four treatment groups over a seven day time course. The graph demonstrates that although the gels with initial seeding density of 25,000 cells/gel did not undergo a significant decrease in growth ratio, they demonstrated little cell growth over the course of the seven day study. In contrast, gels seeded at 50,000 cells/gel underwent a period of 4 days where cell numbers showed a pronounced increase, followed by a steady decrease in cell numbers over the next three days.

Although the use of cell proliferation data makes drastic differences between groups evident, growth ratios allows for easy comparison of otherwise very different treatments. Figure 20 demonstrates that seeding density plays an important role in final cell number in the hydrogels. The gels initially seeded with a high cell density showed significant decrease in cell growth over the seven day time course. The growth ratio dropped 31% for the thick gels, from 1.33 +/- 0.21 on day 3 to 0.91 +/- 0.24 (p <0.05) by day 7. By day 7 thin gels showed a similar significant drop, with 34% decrease in cell growth ratio from 1.17 +/- 0.15 on day 3 to 0.77 +/- 0.243 (p <0.05). Gels seeded at a lower initial cell density did not demonstrate the same significant decrease in cell growth ratio. Cells in the thick gels showed a decrease in growth ratio over the course of the 7 day experiment that was not statistically different from day 3. The thin gels were the only treatment which

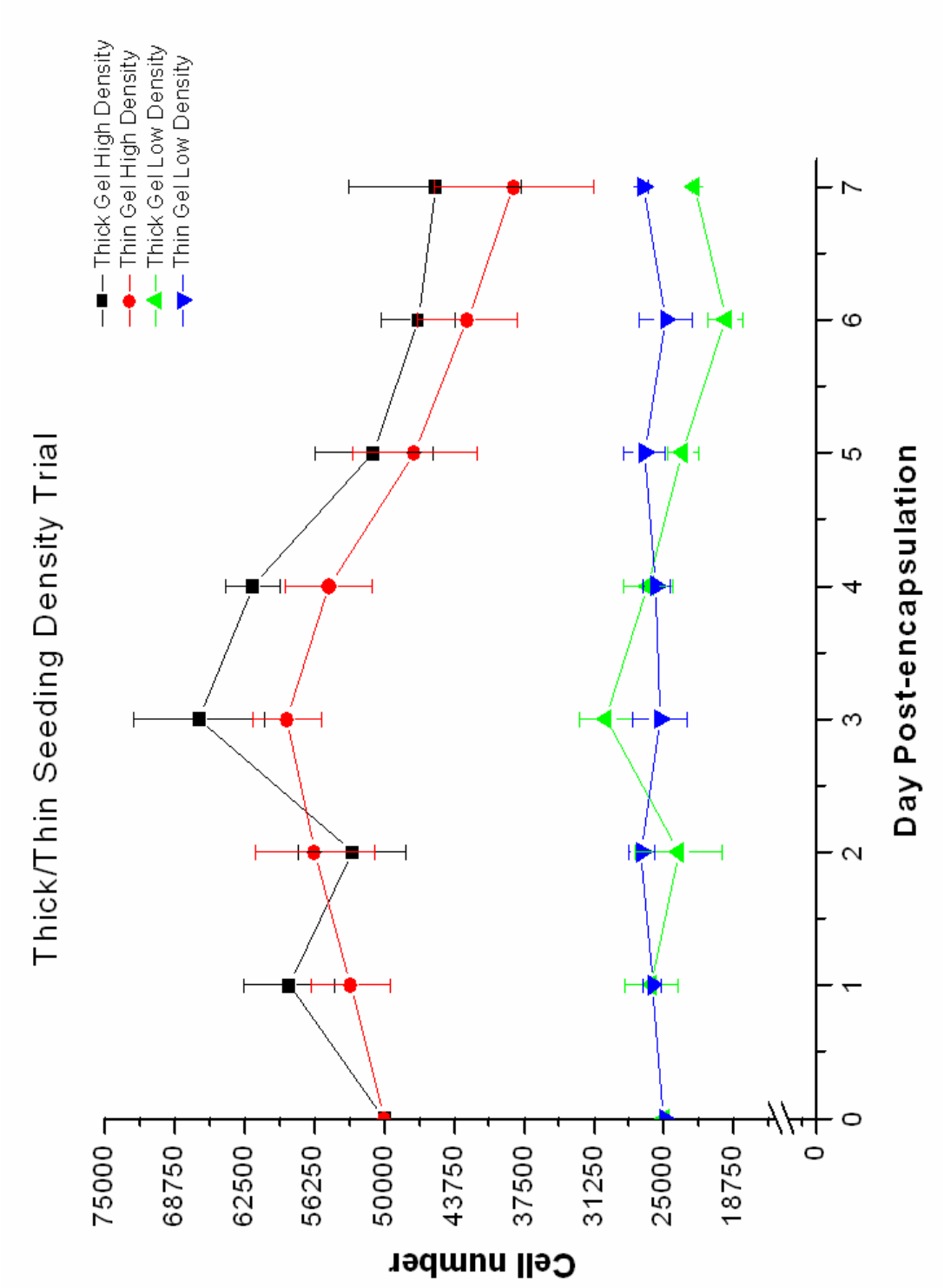

Figure 19. Effect of gel thickness and seeding density on cell numbers. HEK293 cells grown over 7 days in thick (200um) or thin (70um) hydrogels and seeded at either high (50,000 cells/gel) or low (25,000 cells/gel) cell densities. Cell numbers based on MTS assay

demonstrated a slight increase in growth ratio. This 5% increase from day 3 to day 7 was not statistically significant.

The same data is re-plotted in Figure 21, shows that there is no significant difference in final cell growth ratio for either thicknesses regardless of seeding density. With one exception, the growth ratio of all treatments dropped below 1.0 over the course of the experiment, indicating a net loss of cells compared to the initial seeding. Thick gels showed an almost identical growth ratio pattern over the course of the 7 days regardless of seeding density, with a growth rate that decreased to 0.91 +/- 0.25 and to 0.89 +/- 0.19 for the low and high seeding densities respectively. The thin gels with a high cell seeding density showed a 34% drop in growth ratio similar to the thick gels. The thin gels with lower seeding density the showed a slight increase in growth ration over the seven day experiment, however this increase was not significantly different when compared to the seven day growth ratio of thin gels with high initial seeding.

All gels seeded with high cell numbers experienced a sharp decrease in cell number after day 3. Gel thickness appears to influence two factors involved in the growth patterns; the first being the finite physical area available for cells growth and the second is the height of the gel relative to waste and nutrient availability. As with any cell culture the surface on which cell can adhere limits cell growth. Hydrogels, like all bioscaffolds, have a finite area for cell growth. It is likely the case for these gels that after an initial period of cell division, the cells are adequately and evenly distributed throughout the gel, probably around day 3-4. After this point there is limited space for further cell growth and thus cell numbers stabilize for a period of time, before beginning to drop.

The maximum distance for effective diffusion of oxygen and small molecules into actively metabolizing cells is approximately 100-200um[134] . The thick gels are 500μm thick, we can expect that the cells that growing well prior to the first few cell divisions, could be hindered, if not completely deprived of diffusion based molecular exchange. Once cells are evenly distributed throughout the gel, cells closer to the gel surface would survive with little issue, while those farther away from the surface may experience difficulty removing waste products and obtaining nutrients. Although not significant figure 21 shows that the thin gels had the highest overall growth ratio on day 7.

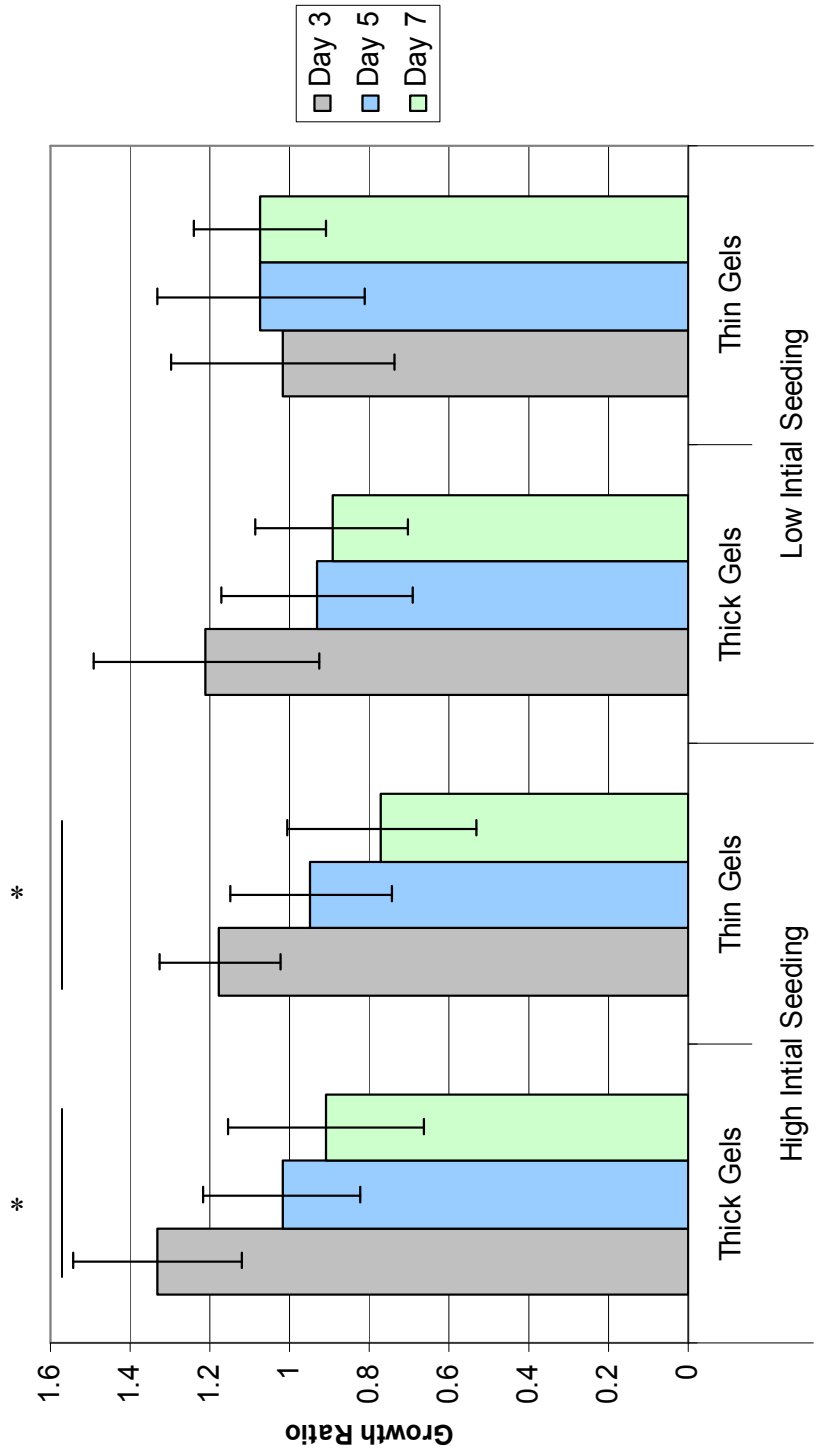

Figure 20. Effects of thickness and seeding density on growth ratios of cells. HEK293 cells were grow over 7 days in thick (200um) or thin (70um) hydrogels and seeded at either high (50,000 cells/gel) or low (25,000 cells/gel) cell densities. * represent statistical significance ($p<0.05$)

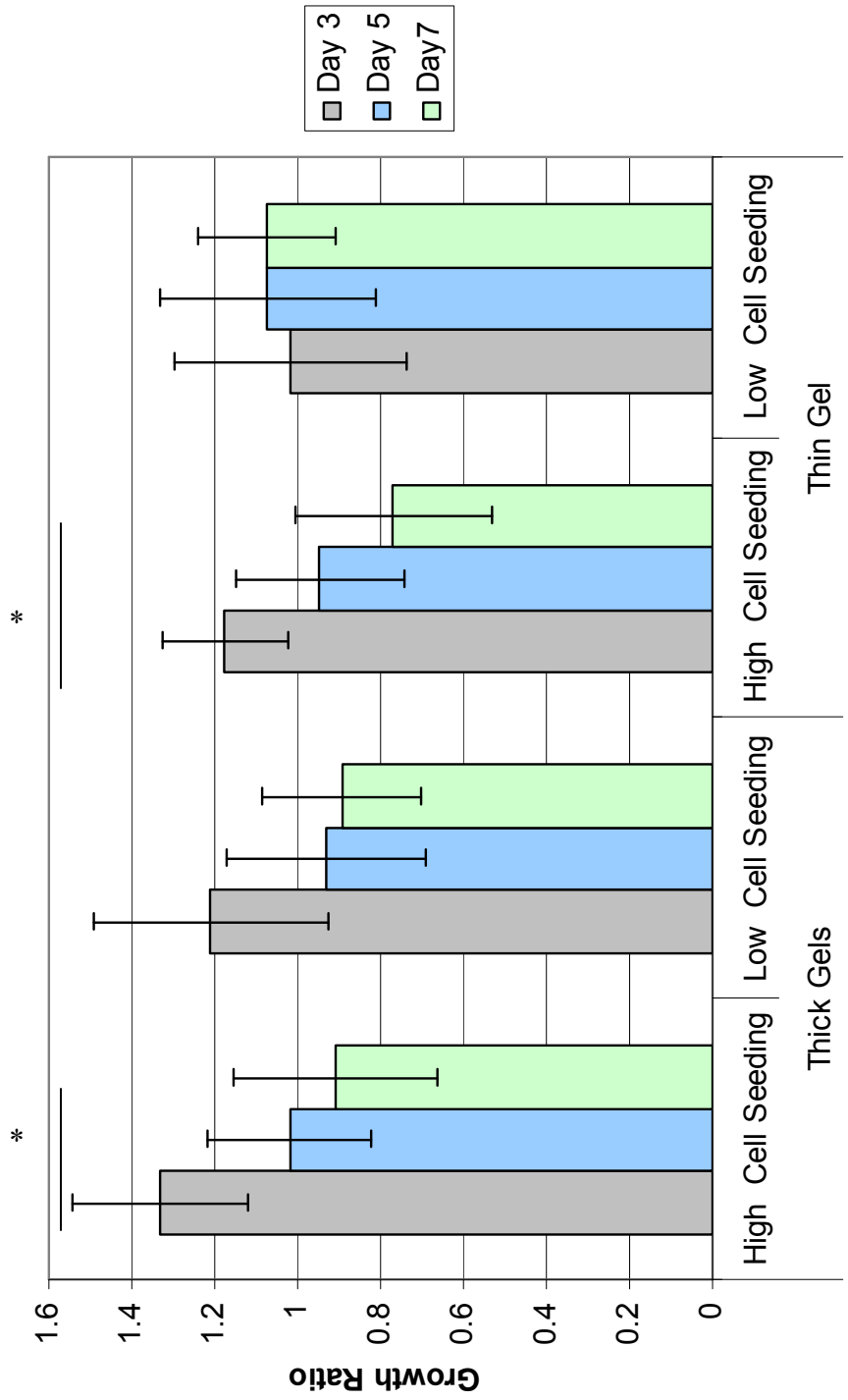

Figure 21. Effects of thickness and seeding density on growth ratios of cells. HEK293 cells were grow over 7 days in thick (200um) or thin (70um) hydrogels and seeded at either high (50,000 cells/gel) or low (25,000 cells/gel) cell densities. * represent statistical significance (p<0.05)

Similarly for the thin gels seeded with 25,000 cells/gel it was observed that cell number stays relatively constant for the full seven days. It is possible that 25,000 cells is very close to the maximum cell capacity for gels of this size. Thus the cells are able to easily exchange metabolic products, but lack of accessible cell-free hydrogel volume limits further growth. An unusual result was obtained from the 500um gel with low seeding density. Based on the above reasoning, one would expect that the cell in these gels have ample room to divide. Additionally, minimal diffusion limited growth should be seen until the cells reach a density closer to full gel volume coverage. In this case it may be that there is too much space for cell settlement and growth. In order to migrate and expand, cells require interactions with the ECM as well as other cells. These interactions are only possible if cells are close enough to make contact[135-137]. It possible that the distribution of the cells throughout the gel was originally very sparse and consequently slow growth was observed[136].

3.3.2 Varying HA:Gtn composition of hydrogel

Hyaluronic-acid based hydrogels with varying Gtn content were seeded with 13,000 cells to determine if gelatin could help support growth of the HEK293 cell line. Each hyrdogel had a final volume of 50 ul, corresponding to approximately 150um in thickness. In all cases the cells survived the hydrogel encapsulation process and remained viable for the full 21 day time course.

Inclusion of gelatin within the hydrogels had an evident effect on the growth of encapsulated cells over the experimental time course (Figure 22). During the first 7 days, the non-encapsulated control cells had the highest average growth rate. These cells reached maximum density between days 4-5, at which point cell numbers began

to decline to zero by day 21. With the exception of the 1:1 HA:Gtn gel all other combinations produced significantly lower growth rate at days 3 and 7 when compared to the non-encapsulated controls ($p < 0.05$ for all direct comparisons). Although the hydrogels with less than 20% gelatin had lower growth ratio compared to the non-encapsulated cells, they were all able to sustain cell growth for the full 21 days.

Overall, the treatment best able to sustain cells and promote growth was found to be the 1:1 HA:Gtn. Figure 22 illustrates that over the course of 14 days these gels produced significantly higher growth ratios compared to all other hydrogel compositions ($p < 0.025$ for all direct comparisons). A peak growth ratio of 2.4 was reached at day 14. However by day 21 all the hydrogels treatments had reached a growth ratio of just above 1. Again, these results are not surprising given that Gtn has often been chosen as an additional scaffold component, because of its role in cell adhesion and expansion [43, 138, 139]. Collagen/gelatin has been shown to contain numerous integrin binding domains which provide adhesion sites for binding via integrin proteins[140-142]. It appears that an increase in gelatin may be providing additional cell binding sites. This would explain the increase in cell viability for gels containing more gelatin. However, there appears be more factors controlling cell viability than just adhesion sites, because gels without gelatin produced cell growth ratios that were often greater than hydrogels containing 10% and 20% gelatin.

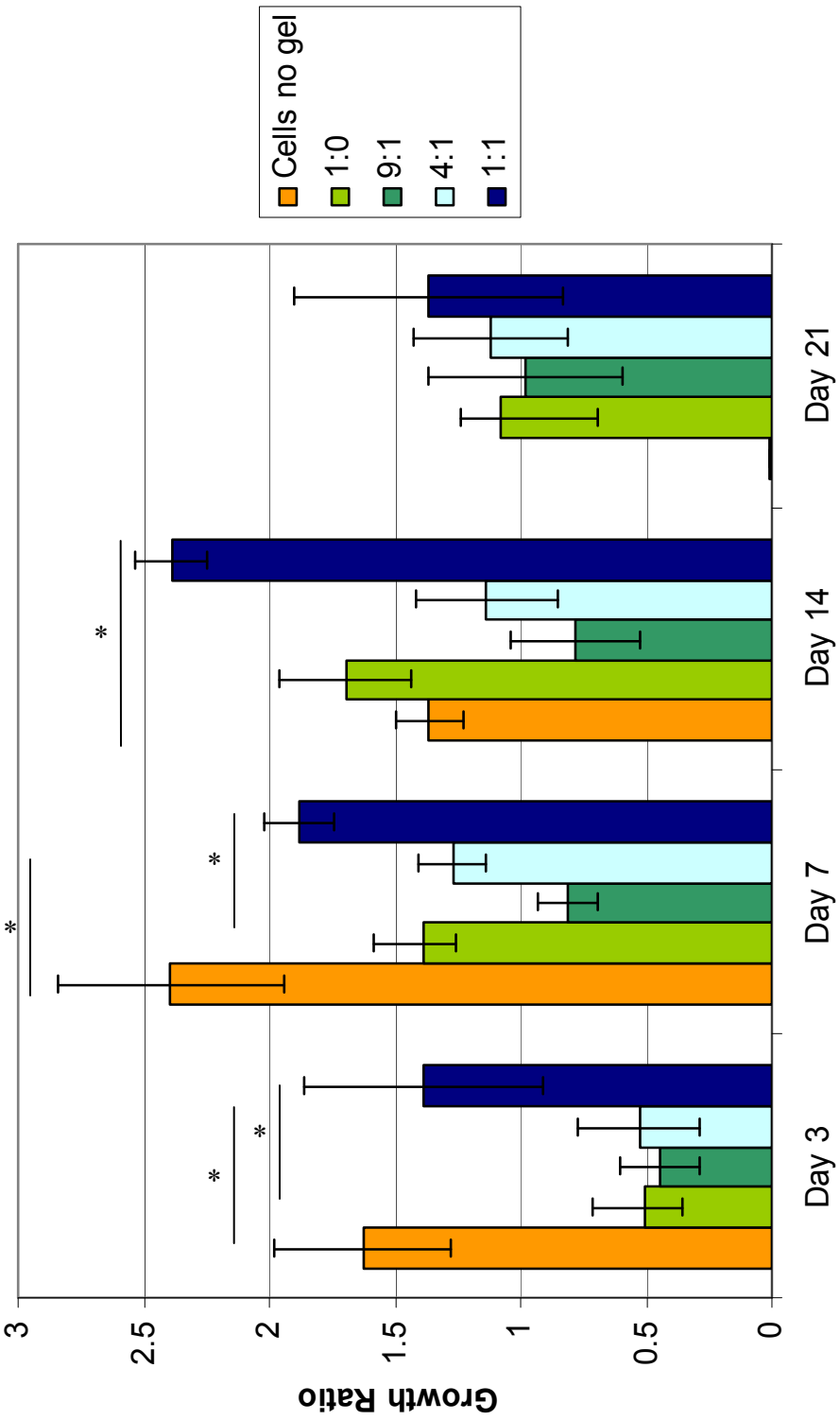

Figure 22. Effect of gelatin content on growth ratios of cells. Cells were grown over 21 days in 100um hydrogels of various HA:Gtn content; 1:0, 9:1, 4:1 or 1:1. Hydrogels all seeded at 13,000 cells/gel. * represent statistical significance (p<0.05)

Focal adhesion (FA) sites are areas of integrin-clustering that serve to link the cell cytoskeleton to the ECM[143]. The primary function of these integrin complexes is to provide physical attachment of the cell to the ECM, and transduce force between the cell and the surrounding environment[144, 145]. It has been shown that exposure to stiff two-dimensional substrates promotes an increase in FA size, as well as promotes cell motility[146-148]. FA sites are involved in numerous signaling cascades that regulate cell proliferation, survival, and migration[137, 143, 149].

With focal adhesion sites transducing force from the ECM to the cells, it is possible that the mechanical characteristics of the cell scaffold, especially the stiffness, may also play a role in cell growth. Studies have shown that mechanical stress imparted onto cells by the surrounding environment has a profound effect on growth, differentiation, migration, ECM remodeling and integrin expression[150-153]. Georges et al. describe varying the effects of mechanical stress based on cell type. Specifically, in this experiment myocytes preferentially grew on a stiffer gel scaffold, while hepatocytes grew on and reorganized softer gels[154-156]. In separate experiments endothelial cells showed a decrease in network-like structures[157, 158], as well as better cell adhesion and spreading on stiffer gels[154]. Epithelial cells, such as those used in these gels, demonstrated significant increases in cell spreading on stiffer gels[148, 159]. Additionally, epithelial cells grown on stiffer acrylamide surfaces showed morphologies similar to cells grown on culture plates, while less stiff acrylamide gels produced cells with an irregular shape[148].

Figure 23 depicts the stiffness of the hydrogels created with varying gelatin content. The addition of gelatin had a marked effect on gel stiffness. The incorporation of 50% gelatin dropped the compressive modulus by over 68% from

3.5 kPa to 1.1 kPa ($p = 0.059$). Even the addition of a small amount of gelatin dropped the modulus by over 32% to 2.4 kPa of the 9:1 hydrogels. The compressive properties of the gels many account for the growth ratios observed in figure 21. Hydrogels without gelatin produced equal or significantly improved cell growth when compared to gels with less than 50% gelatin composition ($p < 0.02$ day 14 1:1 vs 9:1). As described above, stiffness of these gels could account for this difference in cell viability. Although the gelatin gels should contain more cell adhesion sites, they may not be enough, especially in the 9:1 and 4:1 compositions, to account for the accompanied negative effects of gel stiffness.

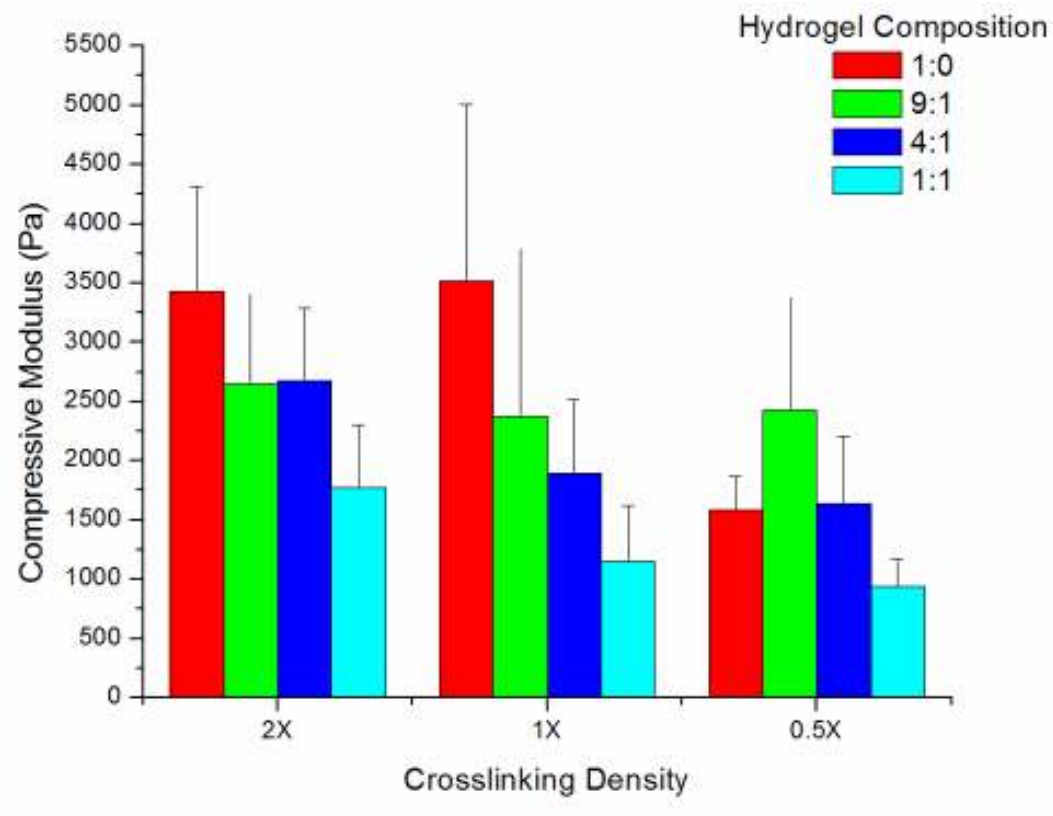

Figure 23. Compression modulus (kPa) of various hydrogels with varying HA:Gtn compositions or PEGDA crosslinker density. * represent statistical significance ($p<0.05$)

3.3.3 Co-encapsulation with growth factors

Hyaluronic based hydrogels containing 1:1 HA:Gtn were seeded with 10,000 cells to determine if co-encapsulation with growth factors could inhibit growth of a HEK293 cell line. Each hyrdogel had a final thickness of approximately 150μm. Angiogenic growth factors (VEGF, Ang-1, KGF, and PDGF-AA) were incorporated into the hydrogels at 25ng/ul doses. In all cases the cells survived the hydrogel encapsulation process, remained viable for the full 21 day time course..

Co-encapsulation of GFs did not have an evident effect on the growth of encapsulated cells over the time course of the experiment (Figure 24). All of the GF containing scaffolds produced cell numbers in line with the non GF containing gels. It appears that the slightly lower seeding density allowed for continued cell growth for the duration of the 21 day study. The non-encapsulated cells reached maximum density after 5-6 days at which point cell numbers began to decline. However unlike the non-gel-encapsulated cells in the gelatin experiments, the culture did not reach zero cells. As controls, gels without cells were fabricated to observe any potential interactions between the Alamar Blue and MTS assays. No interactions were noted, with either assay, and the gels and the absorbance/fluorescence readings obtained from this control experiment were treated as reference points and subtracted from all other treatments.

3.3.3.1 Single GF encapsulation

Figure 24 shows the change in cell number in various single GF loaded gels. All treatments with encapsulated cells show the same trend of steady growth over the 21 days. Cell growth for each GF containing gel was higher compared to the no

GF control gels. However, it was observed that none of the individual treatments were significantly different from each other. The VEGF containing gel showed approximately 15% more cells at the 21 day time point but given the large variability this was not a significant difference ($p = 0.056$).

The effects of single GF delivery on *in vitro* cell viability and proliferation are dependent on, among other factors; cell type, cell density, induced stresses and GF dose[115-120]. PDGF-AA was shown have a strong effect on *in vitro* corneal stromal fibroblast proliferation[115]. This relationship was shown to be strongly dose dependent, and predominantly dictated by cell seeding numbers[115]. In an *in vitro* a wound healing study using NIH3T3 mouse fibroblasts, PDGF-AA presence increased the number of cells moving toward the wound site as well as their migratory speed[117]. Cell type also plays a role in GF function, renal proximal tubular epithelial cells cultured in gel showed strong tubular growth when exposed to hepatocyte growth factor (HGF), however addition of VEGF and PDGA did not influence cell growth[116].

Biliary tract tumor cells exposed to KGF showed an increased proliferation rate, while VEGF and PDGF-AA had no apparent effect[118]. Human keratinocytes exposed to KGF showed a decrease in cell viability in culture[119]; but when the same cells were exposed to oxidative stress the presence of KGF had a protective effect on the cells[119]. In a 2011 study, Tuo et al. used mouse heart myocardial endothelial cells to study the affect of Ang-1 under hyperglycemic stress, a condition associated with high glucose-induced endothelial dysfunction[120, 160]. Ang-1 increased cellular viability under hyperglycemic conditions as well as suppressed starvation-

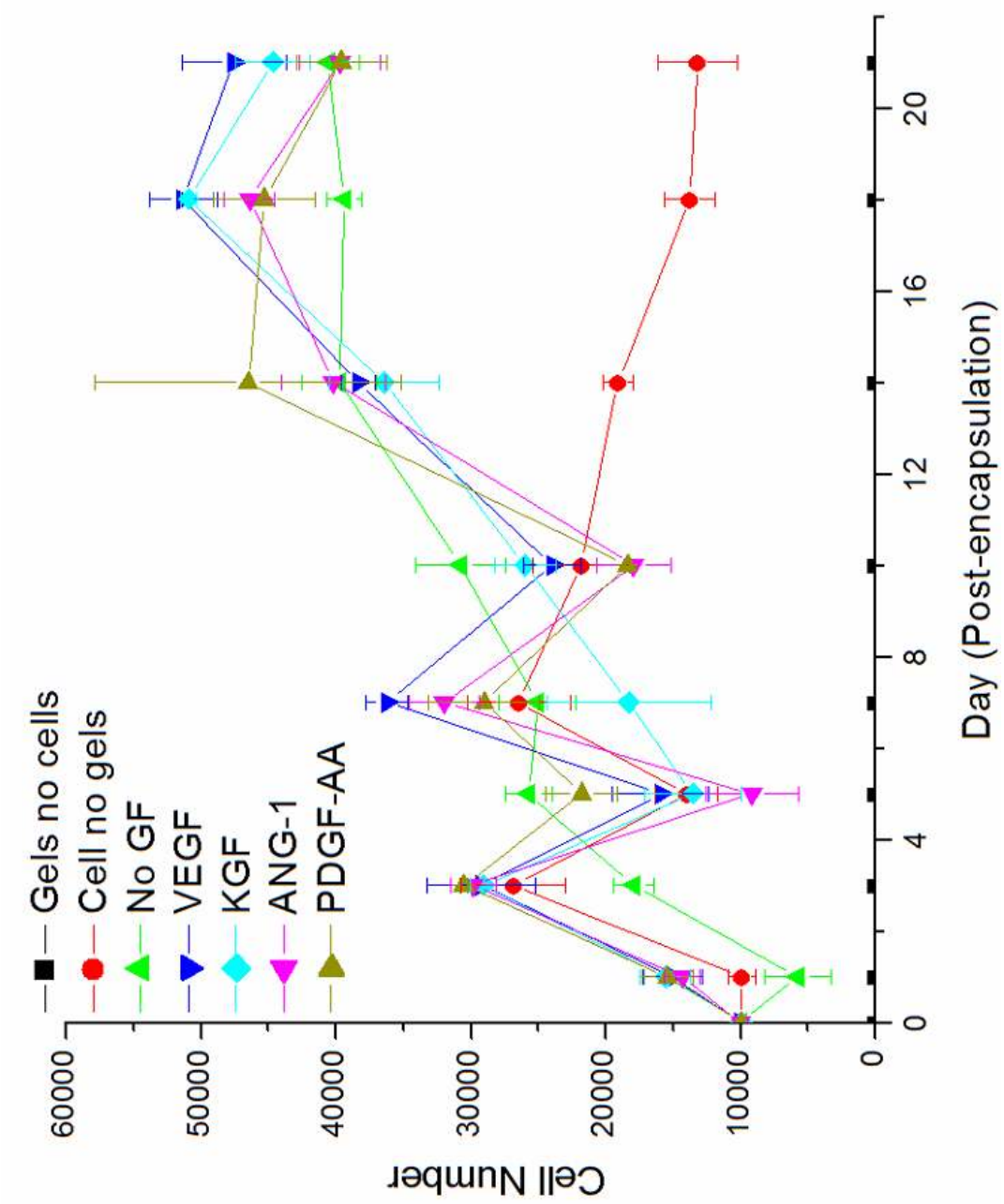

Figure 24. Effects of co-encapsulated single growth factors on cell numbers. Cells were grown over 21 days in 100um 1:1 HA:Gtn, and seeded at an initial density of 10,000 cells/gel.

induced apoptosis[120]. The presence of Ang-1 promoted formation myocardial endothelial tubules even under hyperglycemic conditions; tubular formation was significantly impaired in cultures without Ang-1[161].

GF effects on cells can be suppressive[119], stimulative or not measurably different from control treatments[116]. In our studies we showed that GF incorporation did not inhibit the growth of HEK293 epithelial cells grown in HA hydrogels. It could be that the GFs introduced into these hydrogels have no particular affinity for the epithelial HEK293 cells. As noted above GF function is closely tied to cell type, GFs bind specific receptors, and it is this receptor recognition that allows for observed changes in cells[117, 118]. Additionally GF function is often tied to stress conditions, as was described above for PDGF-AA and KGF[116, 119]. The cells in these experiments were not exposed to any intentional environmental stresses. Although GF activation has been linked to cell seeding densities, no affect on growth was observed, even as cell density increased over the time course of the experiment.

3.3.3.2 Dual GF encapsulation

In co-treatment with dual GFs, it was observed that all dual GF treatments had higher final cell numbers at day 21 than the control. GFs were chosen based on previously obtained *in vivo* results, and each GF delivered at 25ng/ml. Figure 25 demonstrates that the combinations VEGF+Ang-1 and VEGF+PDGF-AA showed a significant increase in cell number compared to the no GF control ($p < 0.04$, $p < 0.03$ respectively).

As with single GF delivery, the interaction between cells and the surrounding growth factor cytokines is dependent on multiple variables. Studies have shown that under the same conditions co-delivery of GFs can significantly alter cell proliferation and cell growth[88, 89]. In human macular inner choroidal endothelial cells the co-

deliver of VEGF and FGF2 produced significantly higher cell proliferation and angiogenic tubule formation than either GF delivered singularly[89]. Similarly formation of capillary sprouts in adrenal-cortex-derived microvascular endothelial cells was significantly greater for co-delivered VEGF and Ang-1[88]. The observed growth was synergistic, in that more sprouts formed then would be expected from additive formation of sprouts via individual GF delivery[88].

Although individual GF delivery did not affect cell growth, co-delivery of all treatment groups showed an increase in final cell number. The combinations of VEGF+Ang-1 and VEGF+PDGF-AA in this study produced a significant increase in final cell number over the course of the 21 days. In fact, even the VEGF-KGF combination showed a 15.6% increase in cell number. The above mentioned *in vitro* experiments demonstrate that in many instances the co-presence of GF is enough to stimulate cell growth[88, 89]. The interactions are often cell- and substrate-specific and difficult to predict. In the case of HA-Gtn hydrogels, various protein binding domains exist and one could imagine a possible ECM-GF-GF-cell interplay. In this scenario, single delivery of GFs may not influance cell activity; however inclusion of the second GF could promote cell ECM interactions. Further testing for molecular markers would be necessary to fully understand the mechanisms behind the augmented cell growth. However, the successful co-encapsulation of cells and growth factors provides evidence that these hydrogels are a viable option for simultaneous delivery of therapeutic cells and GFs.

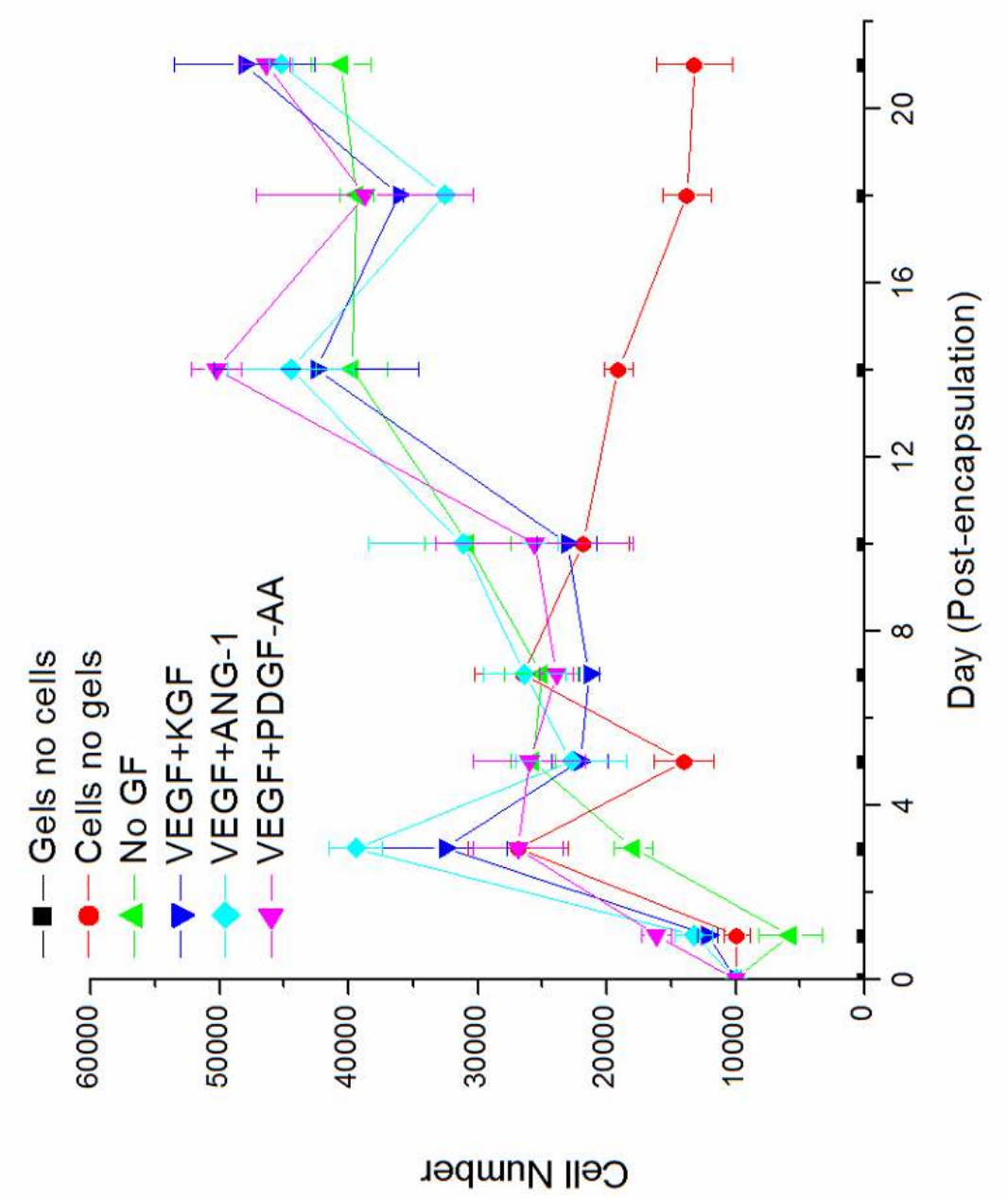

Figure 25. Effects of co-encapsulated dual growth factors on cell numbers. Cells were grown over 21 days in 100um 1:1 HA:Gtn, and seeded at an initial density of 10,000 cells/gel.

4 Conclusions

4.1 Research Summary

A series of experiments were carried out to address the lack in therapeutic cell/drug delivery devices capable of targeting moving tissues and organs.

Experiment 1

Dual growth factor loaded hyaluronic acid-based hydrogels were allowed to cure *in situ*, in mouse ear pinnae, and subsequent *in vivo* angiogenic response was investigated. H&E staining revealed that *in situ* gelled implants were tolerated successfully, with reduced to no inflammation compared to previously investigated films. All implants produced a significant increase in microvessel density compared to the sham surgeries ($p < 0.05$). The presence of both Hp and Gtn produced significantly more microvessels in three of the four tested GF combinations. By day 7 the VEGF+PDGF HA gel containing 0.3% Hp produced the highest microvessel density at 829 microvessels/mm^2. Similarly the highest microvessel density after 14 days was observed in the 0.3% Hp VEGF+KGF gel, which was found to have a final vessel density of 801 microvessels/mm^2. When standardized using the NI these same treatments were again shown to produce the strongest vascularization resonse. The Ni's were 3.52 for the VEGF+PDGF at day 7 and 3.91 for the VEGF+KGF at day 14. In general the largest vascularization responses for both day 7 and 14 were produced by the VEGF+KGF containing gels.

Experiment 2

In order to achieve localized delivery of therapeutic molecules and cells, a securable biocomposite consisting of HA and silk was fabricated. SEM imaging showed that the hydrated composite is porous, and gel surface smooth and largely uniform. Direct and indirect experiments showed that the HA component of composite is controllably degradable *in vitro* by HAse. Tensile testing indicated that the incorporation of a silk electrospun mat into a hydrogel adds the mechanical strength necessary for fastening to tissues and organs *in vivo*. At the same time the silk mat did not seem to interfere with the hydrogels ability to cycle from dehydrated to hydrated states. The composite demonstrated the ability for storage and sustained release of various therapeutically relevant molecules, including GFs.

Experiment 3

The affect of hydrogel composition on viability of encapsulated cells was investigated *in vitro*. Hydrogels initially seeded at a high cell density showed a significant decrease in viability regardless of gel thickness ($p < 0.05$). There was no significant difference in final cell growth ratio for either gel thickness irrespective of original seeding density, with all gels demonstrating a decrease in growth over 7 days. Gtn content had a profound impact on cell viability, with increase in gelatin content corresponding strongly with increased cell viability. Growth factor incorporation studies demonstrated that single GF deliver had no significant effect on viability. Co-delivery of GF however showed that both VEGF+Ang-1 and VEGF+PDGF-AA treatments produced a significant increase in cell numbers by day 21 ($p < 0.05$). Most importantly it was demonstrated that none of the GFs whether delivered

individually or in combination produced an inhibitory effect on HEK 293 epithelial cell growth.

4.2 Future Direction

4.2.1 Hydrogel characterization

This thesis work touched briefly on the impact of cell binding sites and hydrogel stiffness on cell viability. It seemed that both factors played a role in cell growth. The results of gel stiffness were not foreseen and thus the experiments as conducted did not allow the impact of these two variables to be separated. It was however demonstrated that Gtn content and crosslinker density could be manipulated to alter gel rigidity. It would be interesting to perform a series of experiments with varying Gtn content, but constant gel stiffness as well as constant Gtn content with varying gel stiffness. This additional characterization would allow for further improvement of the hydrogel system and its cell sustaining capabilities.

4.2.2 HAse effects

Of critical importance would be study the influence of hyaluronidase on viability of encapsulated cells. First the impact of the enzyme and degradation products on cells should be examined carefully. It is possible that breakdown products interfere with cell growth or function in unexpected ways. Additionally it is also important to know whether the breakdown of the gels is to fast for cells to establish attachment and put down an ECM. If the degradation of the gel is too

rapid, the gels may have to be augmented with another biocompatible material with a longer *in vivo* resonance time possibly Gtn or silk.

4.2.3 Therapeutic cell lines

It was demonstrated here that HA based hydrogels can support growth of a recombinant cell line. The next step in this direction would be to encapsulate and optimize hydrogel conditions for cells of therapeutic relevance such as pancreatic islet cells. This would involve conducting experiments similar to those preformed in this thesis work, with the added consideration of cell specific culture conditions. For therapeutic cells lines it would also be interesting to monitor not only *in vitro* cell growth but function as well. For example, for pancreatic islet cells monitoring insulin levels produced by the incorporated cell would be of great importance for eventual *in vivo* use.

4.2.4 Functionalizing Silk

In the current design the electrospun silk mat serves only as a reinforcing element, designed to give the hydrogel mechanical integrity. Work with silk and in particular electrospun silk has demonstrated the materials ability to release drugs as well as sustain cell growth[57, 72]. It follows that the silk electrospun mats could be used as a secondary source of therapeutic agents, with a distinct, presumably slower, release profile compared to the surrounding gel. Compared to the other composite constituents, the silk mat is expected to have a much longer resonance time *in vivo*[55, 56]. Thus a potential drug loading scheme could include an initial delivery of anti-inflammatory and vascularization inducing GFs, like VEGF, via the hydrogel. This

would be followed by delivery of GFs like KGF, shown to promote maturation of vessels, through the silk mat component. Additionally as the hydrogel component is expected to degrade within a few weeks the silk component may ultimately play a crucial role in survival and proliferation of any encapsulated cells. By functionalizing the silk with a cell binding sequence such as RGD, we can effectively increase the likelihood of cell attachment[108]. *In vitro* and *in vivo* cells growth on silk electrospun mats has been demonstrated[71, 129], and could be exploited for the purposes of a next generation composite.

5 References

1. Pardue EL, I.S., Ramamurthi A, *Role of hyaluronan in angiogenesis and its utility to angiogenic tissue engineering.* Organogenesis, 2008. **4**(4): p. 203-214.
2. Zhang M, M.D., Poppa V, Fujio Y, Walsh K, Murry CE, *Cardiomyocyte grafting for cardiac repair: graft cell death and anti-death strategies.* J Mol Cell Cardiol, 2001. **33**: p. 907-921.
3. Olabisi RM, L.Z., Franco CL, Hall MA, Kwon SK, Sevick-Muraca EM, Hipp JA, Davis AR, lmsted-Davis EA, West JL, *Hydrogel Microsphere Encapsulation of a Cell-Based Gene Therapy System Increases Cell Survival of Injected Cells, Transgene Expression, and Bone Volume in a Model of Heterotopic Ossification.* 2010. **16**(12): p. 3727-3736.
4. Tobias CA, H.S., Shumsky JS, Kim D, Tumolo M, Dhoot NO, Wheatley MA, Fischer I, Tessler A, Murray M., *Alginate encapsulated BDNF-producing fibroblast grafts permit recovery of function after spinal cord injury in the absence of immune suppression.* Journal of Neurotrauma, 2005. **22**(1): p. 138–156.
5. Knudson CB, K.W., *Cartilage proteoglycans.* Semin Cell Dev Biol 2001. **12**: p. 69-78.
6. Luo Y, K.K., Prestwich GD, *Cross-linked hyaluronic acid hydrogel films: new biomaterials for drug delivery.* Journal of Controlled Release, 2000. **69**: p. 169-184.
7. Peattie RA, Nayate AP, Firpo MA, Shelby J, Fisher RJ, Prestwich GD, *Stimulation of in vivo angiogenesis by cytokine-loaded hyaluronic acid hydrogel implants.* Biomaterials 2004. **25**: p. 2789-2798.
8. Butterworth P, B.H., Porter J, *A modification of the Ellman procedure for the estimation of protein sulfhydryl groups.* Arch. Biochem. Biophys, 1967. **118**: p. 716-723.
9. Elbert DL, H.J., *Conjugate addition reactions combined with free-radical cross-linking for the design of materials for tissue engineering.* Biomacromolecules, 2001. **2**.
10. R, S., *Hyaluronan catabolism: a new metabolic pathway.* Eur J Cell Biol 2004. **83**: p. 17-25.
11. West DC, H.I., Arnold F, Kumar S, *Angiogenesis induced by degradation products of hyaluronic acid.* Science 1985. **228**: p. 1324-326.
12. Slevin M, W.D., Kumar P, Rooney P, Kumar S, *Hyaluronan, angiogenesis and malignant disease.* Int J Cancer, 2004. **109**: p. 793-794.
13. PW., N., *Hyaluronan and its catabolic products in tissue injury and repair.* Matrix Biology, 2002. **21**: p. 25-29.
14. Rooney P, K.S., Ponting J, Wang M . *The role of hyaluronan in tumour neovascularization.* Int J Cancer, 1995. **50**: p. 632-636.

15. Schoenfelder M, E.R., *Expression of hyaluronan synthases and corresponding hyaluronan receptors is differentially regulated during oocyte maturation in cattle.* Biol. Reprod, 2003. **69**: p. 269-277.
16. Evanko SP, J.P., Braun KR, Underhill CB, Dudhia J, Wight TN, *Platelet-derived growth factor stimulates the formation of versican-hyaluronan aggregates and pericellular matrix expansion in arterial smooth muscle cells.* Arch Biochem Biophys, 2001. **394**: p. 29-38.
17. Gao F, Y.C., Mo W, Liu YW, He YQ. , *Hyaluronan oligosaccharides are potential stimulators to angiogenesis via RHAMM mediated signal pathway in wound healing.* . Clin Invest Med, 2008. **31**: p. 106-116.
18. Taylor KR, T.J., Rudisill JA, Termeer CC, Simon JC, Gallo RL, *Hyaluronan fragments stimulate endothelial recognition of injury through TLR4.* J Biol Chem, 2004. **279**: p. 17079-17084.
19. Savani RC, C.G., Pooler PM, Zaman A, Zhou Z, DeLisser HM, *Differential involvement of the hyaluronan (HA) receptors CD44 and receptor for HA-mediated motility in endothelial cell function and angiogenesis.* J Biol Chem, 2001. **276**: p. 36770-36778.
20. Canfield AE, S.A., Schor SL, Grant ME, *The biosynthesis of extracellular-matrix components by bovine retinal endothelial cells displaying distinctive morphological phenotypes.* Biochem J, 1986. **235**: p. 375-83.
21. Rodgers LS, L.S., Hardy KM, Xiang X, Broka D, Antin PB, Camenisch TD, *Depolymerized hyaluronan induces vascular endothelial growth factor, a negative regulator of developmental epithelial-to-mesenchymal transformation.* Circ Res., 2006. **99**: p. 583-589.
22. Ohno-Nakahara M, H.K., Tanimoto K, Tanaka N, Doi T, Suzuki A, Yoneno K, Nakatani Y, Ueki M, Ohno S, Knudson W, Knudson CB, Tanne K, *Induction of CD44 and MMP expression by hyaluronidase treatment of articular chondrocytes.* J Biochem, 2004. **135**: p. 567-575.
23. Zhang Y, T.A., Machida K, Ichigotani Y, Naito Y, Hiraiwa Y, Senga T, Sohara Y, Matsuda S, Hamaguchi M. , *Hyaluronan-CD44s signaling regulates matrix metalloproteinase-2 secretion in a human lung carcinoma cell line QG90.* Cancer Res., 2002: p. 3962-3965.
24. Pike DB, Cai S, Pomraning KR, Firpo MA, Fisher RJ, Shu XZ, et al., *Heparin-regulated release of growth factors in vitro and angiogenic response in vivo to implanted hyaluronan hydrogels containing VEGF and bFGF.* Biomaterials, 2006. **27**: p. 5242-5251.
25. Riley CM, F.P., Firpo MA, Shu XZ, Prestwich GD, Peattie RA, *Stimulation of in vivo angiogenesis using dual growth factor-loaded crosslinked glycosaminoglycan hydrogels.* Biomaterials 2006. **27**: p. 5935-5943.
26. Wissink MJB, B.R., Poot AA, Engbers GHM, Beugeling T, van Aken WG, Feijen J, *Improved endothelialization of vascular grafts by local release of growth factor from heparinized collagen matrices.* J Control Rel, 2000. **64**: p. 103-114.
27. Cleland JL, D.E., Park A, Daugherty A, Kahn J, Kowalski J, Cuthbertson A, *Development of poly-(D,L-lactide-coglycolide) microsphere*

formulations containing recombinant human vascular endothelial growth factor to promote local angiogenesis. J. Control. Rel, 2001. **72**: p. 13-24.
28. Godspodarowicz D, C.J., *Heparin protects basic and acidic FGF from inactivation.* J. Cell Physiol., 1986. **128**: p. 475-484.
29. Hosack L. W, F.M.A., Scott A. J, Prestwich G.D, Peattie RA, *Microvascular maturity elicited in tissue treated with cytokine-loaded hyaluronan-based hydrogels.* Biomaterials, 2008. **15**: p. 2336–2347.
30. Peattie RA, Rieke ER, Hewett EM, Fisher RJ, Shu XZ, Prestwich GD, *Dual growth factor-induced angiogenesis in vivo using hyaluronan hydrogel implants.* Biomaterials, 2006. **27**: p. 1868-1875.
31. Shu XZ, A.S., Liu Y, Prestwich GD, *Synthesis and evaluation of injectable, in situ crosslinkable synthetic extracellular matrices for tissue engineering.* J. Biomed. Mat. Res. A 2006. **79**: p. 902-912.
32. Shu XZ, L.Y., Palumbo F, Prestwich GD, *Disulfide-crosslinked hyaluronan-gelatin hydrogel films: a covalent mimic of the extracellular matrix for in vitro cell growth.* Biomaterials, 2003. **24**: p. 3825-3834.
33. Elia R, F.P., VanDelden A, Firpo MA, Prestwich GD, Peattie RA, *Stimulation of in vivo angiogenesis by in situ crosslinked, dual growth factor-loaded, glycosaminoglycan hydrogels.* Biomaterials, 2010. **31**(17): p. 4630-4638.
34. Hernández RM, O.G., Murua A, Pedraz JL, *Microcapsules and microcarriers for in situ cell delivery.* Advanced Drug Delivery Reviews, 2010. **62**: p. 711-730.
35. Maeda M, T.S., Sano A, Fujioka K, *Microstructure and release characteristics of the minipellet, a collagen based drug delivery system for controlled release of protein drugs.* J. Controlled. Rel, 1999. **62**: p. 313-324.
36. Lee CH, S.A., Lee Y, *Biomedical applications of collagen.* International Journal of Pharmaceutics, 2001. **221**: p. 1-22.
37. J, H., *The collagen receptor integrins have distinct ligand recognition and signaling functions.* Matrix Biology, 2000. **19**: p. 319-323.
38. Allison D, G.-A.K., *Hyaluronan: a powerful tissue engineering tool.* Tissue Eng., 2006. **12**(8): p. 2131-2140.
39. Serban MA, P.G., *Making modular extracellular matrices: solutions for the puzzle.* Methods 2008. **45**: p. 93-98.
40. GD, P., *Engineering a clinically-useful matrix for cell therapy.* Organogenesis, 2008. **4**: p. 41-47.
41. GD, P., *Simplifying the extracellular matrix for 3-D cell culture and tissue engineering: a pragmatic approach.* J. Cell. Biochem., 2007. **101**: p. 1370-1383.
42. Liu Y, S.X., Prestwich GD., *Osteochondral defect repair with autologous bone marrow-derived mesenchymal stem cells in an injectable, in situ, cross-linked synthetic extracellular matrix.* Tissue Eng. , 2006 **12**(12): p. 3405-3416.
43. Prestwich GD, K.J.-w., *Chemically-modified HA for therapy and regenerative medicine.* Curr. Pharm. Biotech, 2008. **9**: p. 242-245.

44. Prestwich, G.D., *Engineering a clinically-useful matrix for cell therapy.* Organogenesis, 2008 **4**(1): p. 42–47.
45. Kaplan DL, M.C., Arcidiacono S, et al., *Silk*, in *Protein-based materials*, K.D. McGrath K, Editor 1997: Birkhauser, Boston.
46. Matsumoto A, C.J., Collette AL, Kim U-J, Altman GH, Cebe P, Kaplan DL, *Mechanisms of silk fibroin sol-gel transitions.* J Phys Chem B, 2006. **110**: p. 21630-21638.
47. Altman GH, D.F., Jakuba C, Calabro T, Horan RL, Chen J, Lu H,John Richmond J, Kaplan DL, *Silk-based biomaterials.* Biomaterials, 2003. **24**: p. 401-416.
48. Vepari C, K.D., *Silk as a biomaterial.* Prog Polym Sci 2007. **32**: p. 991-1007.
49. Soong HK, K.K., *Adverse reactions to virgin silk sutures in cataract surgery.* Ophthalmology 1984. **91**: p. 479-483.
50. Perez-Rigueiro J, V.C., Llorca J, Elices M, *Mechanical properties of single-brin silkworm silk.* J Appl Polym Sci, 2000. **75**: p. 1270-1277.
51. Hardy JG, R.L., Scheibel TR., *Polymeric materials based on silk proteins.* Polymer 2008. **49**: p. 4309-43027.
52. Gil ES, P.S., Tien LW, Trimmer B, Hudson SM, Kaplan DL, *Mechanically Robust, Rapidly Actuating, and Biologically Functionalized Macroporous Poly(N-isopropylacrylamide)/Silk Hybrid Hydrogels.* Langmuir 2010 **26**(19).
53. Jin H, F.S., Rutledge GC, Kaplan DL, *Electrospinning Bombyx mori Silk with Poly(ethylene oxide).* Biomacromolecules 2002. **3** p. 1233-1239.
54. Wang X, K.J., Leisk GG, Kaplan DL., *Sonication-induced gelation of silk fibroin for cell encapsulation.* Biomaterials 2008. **29**(8): p. 1054-1064.
55. Horan RL, A.K., Collette AL, Wang Y, Huang J, Moreau JE, Volloch V, Kaplan DL, Altman GH, *In vitro degradation of silk fibroin.* Biomaterials 2005. **26** p. 3385-3393.
56. Wang Y, R.D., Walsh A, Abrahamsen L, Kim HJ, Kim HS, Kirker-Head C, Kaplan DL, *In vivo degradation of three-dimensional silk fibroin scaffolds.* Biomaterials 2008. **29** p. 3415-3428.
57. Zhang X, B.C., Kaplan DL, *In vitro evaluation of electrospun silk fibroin scaffolds for vascular cell growth.* Biomaterials, 2008. **29**: p. 2217-2227.
58. J, Z., *The electrical discharge from liquid points and ahydrostatic method of measuring the electric intensity at their surfaces.* J. Phy. Rev., 1914. **3**: p. 69-91.
59. Fang X, R.D., *DNA fibers by electrospinning.* J. Macromol. Sci., 1997. **Phys. B36**: p. 169-173.
60. Fong H, R.D., *Electrospinning and formation of nanofibers*, in *Structure Formation in Polymeric Fibers*, D.R. Salem, Editor 2001: Hanser, Munich. p. 225-246.
61. Warner S, B.A., Grimler M, Ugbolue S, Rutledge G, Shin M, *Nano fibers.* Natl. Text, Cent. Annu. Rep, 1998: p. 83.

62. Shin YM, H.M., Brenner MP, Rutledge GC, *Electrospinning: a whipping fluid jet generates submicron polymer fibers.* Appl. Phys. Lett., 2001. **78**: p. 1149-1151.
63. Wilson D, V.R., Kaplan DL, *Conformational transitions in model silk peptides.* Biophys. J., 2000. **78** p. 2690-2701.
64. Steinthorsson G, S.B., *Clinical and biological relevance of vein cuff anastomosis.* Acta Chir. Belg., 1999. **99** p. 282-288.
65. Yokoyama T, G.M., Lee YC, Edmiston WA, Kay JH, *Aorta-coronary artery revascularization with an expanded polytetrafluoroethylene vascular graft. A preliminary report.* J. Thorac. Cardiovasc. Surg, 1978. **76** p. 552-555.
66. Sapsford RN, O.G., Talbot S, *Early and late patency of expanded polytetrafluoroethylene vascular grafts in aorta-coronary bypass.* J. Thorac. Cardiovasc. Surg, 1981. **81** p. 860-864.
67. Veith FJ, G.S., Ascer E, White-Flores S, Samson RH, Scher LA, Towne JB, Bernhard VM, Bonier P, Flinn WR, Astelford P, Yao JST, Bergan JJ, *Six year prospective multicenter randomized comparison of autologous saphenous vein and expanded polytetrafluoroethylene grafts in infrainguinal arterial reconstructions.* J. Vasc. Surg. , 1986. **3**: p. 104-114.
68. Min BM, L.G., Kim SH, Nam YS, Lee TS, Park WH, *Electrospinning of silk fibroin nanofibers and its effect on the adhesion and spreading of normal human keratinocytes and fibroblasts in vitro.* Biomaterials 2004. **25** p. 1289-1297.
69. Min BM, J.L., Nam YS, Kim JM, Kim JY, Park WH, *Formation of silk fibroin matrices with different texture and its cellular response to normal human keratinocytes.* Int. J. Biol. Macromol. , 2004. **34** p. 281-288.
70. Min BM, J.L., Lee KY, Park WH, *Regenerated silk fibroin nanofibers: water vapor-induced structural changes and their effects on the behavior of normal human cells.* Macromol. Biosci, 2006. **6**: p. 285-292.
71. Schneider A, W.X., Kaplan DL, Garlick JA, Egles c, *Biofunctionalized electrospun silk mats as a topical bioactive dressing for accelerated wound healing.* Acta Biomaterialia, 2009. **5**: p. 2570-2578.
72. Li C, V.C., Jin H, Kim HJ, Kaplan DL *Electrospun silk-BMP-2 scaffolds for bone tissue engineering.* Biomaterials 2006. **27**: p. 3115-3124.
73. Kim KH, J.L., Park HN, Shin SY, Park WH, Lee SC, Kim TI, Park YJ, Seol YJ, Lee YM, Ku Y, Rhyu IC, Han SB, Chung CP, *Biological efficacy of silk fibroin nanofiber membranes for guided bone regeneration.* J Biotechnol, 2005. **120**(3): p. 327-339.
74. Jin HJ, C.J., Karageorgiou V, Altman GH, Kaplan DL, *Human bone marrow stromal cell responses on electrospun silk fibroin mats.* Biomaterials, 2004. **25** p. 1039-1047.
75. Li WJ, T.R., Okafor C, Derfoul A, Danielson KG, Hall DJ, Tuan RS., *A threedimensional nanofibrous scaffold for cartilage tissue engineering using human mesenchymal stem cells.* Biomaterials 2005. **26** p. 599-609.
76. Baek HS, P.Y., Ki CS, Park JC, Rahd DK, *Enhanced chondrogenic responses of articular chondrocytes onto porous silk fibroin scaffolds*

treated with microwave-induced argon plasma. Surf. Coat. Technol, 2008. **202** p. 5794-5797.
77. Soker S, M.M., Atala A, *Systems for therapeutic angiogenesis in tissue engineering.* World J Urol, 2000. **18**(10-18).
78. Yancopoulos GD, D.S., Gale NW, Rudge JS, Wiegand SJ, Holash J, *Vascular-specific growth factors and blood vessel formation.* Nature, 2000. **407**: p. 242-248.
79. N, F., *Role of vascular endothelial growth factor in physiologic and pathologic angiogenesis: therapeutic implications.* Semin Oncol, 2002. **29**: p. 10-14.
80. RK, J., *Tumor angiogenesis and accessibility: role of vascular endothelial growth factor.* Semin Oncol, 2002. **29**: p. 3-9.
81. Gillis P, S.U., Volpert OV, Jimenez B, Waters CM, Panos RJ, Bouck NP *Keratinocyte growth factor induces angiogenesis and protects endothelial barrier function.* J Cell Sci, 1999. **112**(12): p. 2049-2057.
82. Thurston G, R.J., Ioffe E, Zhou H, Ross L, Croll SD, Glazer N, Holash J, McDonald DM, Yancopoulos GD, *Angiopoietin-1 protects the adult vasculature against plasma leakage.* Nat Med., 2000. **6**: p. 460-463.
83. Thurston G, W.Q., Baffert F, Rudge J, Papadopoulos N, Jean-Guillaume D, Wiegand S, Yancopoulos GD, McDonald DM, *Angiopoietin1 causes vessel enlargement, without angiogenic sprouting, during a critical developmental period.* Development, 2005. **132**: p. 3317-3326.
84. Cho C-H, K.R., Lee HJ, Yasunaga K, Kim K-T, Choi H-H, Kim W, Kim SH, Park SK, Lee GM, Koh GY, *Designed angiopoietin-1 variant, COMP-Ang1, protects against radiation-induced endothelial cell apoptosis.* Proc Natl Acad Sci USA, 2004. **101**: p. 5553-5558.
85. T, F.N.a.D.-S., *The biology of vascular endothelial growth factor.* Endocr Rev, 1997 **18**(1): p. 4-25.
86. Neufeld G, C.T., Gengrinovitch S, Poltorak Z, *Vascular endothelial growth factor (VEGF) and its receptors.* FASEB Journal. **13**(1): p. 9-22.
87. Shikada Y, Y.Y., Koga T, Onimaru M, Nakano T, Okano S, Sata S, Nakagawa K, Yoshino I, Maehara Y, Sueishi K., *Platelet-Derived Growth Factor-AA Is an Essential and Autocrine Regulator of Vascular Endothelial Growth Factor Expression in Non-Small Cell Lung Carcinomas.* Cancer Res 2005. **65**(16): p. 7241-7248.
88. Koblizek TI, W.C., Yancopoulos GD, Deutsch U, Risau W, *Angiopoietin-1 induces sprouting angiogenesis in vitro.* Current Biology, 1998. **8**: p. 529-532.
89. Browning AC, D.H., Amoaku WM, *The effects of growth factors on the proliferation and in vitro angiogenesis of human macular inner choroidal endothelial cells.* Br J Ophthalmol, 2008. **92**: p. 1003-1008.
90. Rodgers LS, L.S., Hardy KM, Xiang X, Broka D, Antin PB, Camenisch TD, *Depolymerized hyaluronan induces vascular endothelial growth factor, a negative regulator of developmental epithelial-to-mesenchymal transformation.* Circ Res., 2006 **99**(6): p. 583-589.

91. Collins SD, B.R., Waksman R, *Cell therapy in myocardial infarction.* Cardiovasc. Revasc. Med., 2007: p. 43-51.
92. Goren A, D.N., Goren E, Baruch L, Machluf M, *Encapsulated human mesenchymal stem cells: a unique hypoimmunogenic platform for long-term cellular therapy.* FASEB J., 2010. **24**: p. 22-31.
93. Godier-Furnémont AF, M.T., Koeckert MS, Wan L, Parks J, Arai K, Zhang G, Hudson B, Homma S, Vunjak-Novakovic G., *Composite scaffold provides a cell delivery platform for cardiovascular repair.* Proc Natl Acad Sci USA, 2011. **108**(19): p. 7974-7979.
94. Song JJ, O.H., *Organ engineering based on decellularized matrix scaffolds.* Trends Mol Med., 2011 **xx**: p. 1–9.
95. Brown JW, E.R., Clarke DR, Tweddell JS, Huddleston CB, Doty JR, Fehrenbacher JW, Takkenberg JJ, *Performance of the CryoValve SG human decellularized pulmonary valve in 342 patients relative to the conventional CryoValve at a mean follow-up of four years.* J. Thorac. Cardiovasc.Surg., 2010. **139**: p. 339-348.
96. Schmidt CE, B.J., *Acellular vascular tissues: natural biomaterials for tissue repair and tissue engineering.* Biomaterials 2000. **21** p. 2215-2231.
97. Reing JE, B.B., Daly KA, Freund JM, Gilbert TW, Hsiong SX, Huber A, Kullas KE, Tottey S, Wolf MT, Badylak SF, *The effects of processing methods upon mechanical and biologic properties of porcine dermal extracellular matrix scaffolds.* Biomaterials 2010. **31** p. 8626-8633.
98. Olde Damink LH, D.P., Van Luyn MJ, Van Wachem PB, Nieuwenhuis P, Feijen J, *Influence of ethylene oxide gas treatment on the in vitro degradation behavior of dermal sheep collagen.* J. Biomed. Mater. Res., 1995. **29** p. 149-155.
99. Freytes DO, S.R., Badylak SF, *Uniaxial and biaxial properties of terminally sterilized porcine urinary bladder matrix scaffolds.* J. Biomed. Mater. Res. B: Appl. Biomater., 2008. **84**: p. 408-414.
100. Freytes DO, B.S., Webster TJ, Geddes LA, Rundell AE, *Biaxial strength of multilaminated extracellular matrix scaffolds.* Biomaterials 2004. **25** p. 2353-2361.
101. Orive G, H.R., Rodríguez Gascón A, Calafiore R, Chang TM, de Vos P, Hortelano G, Hunkeler D, Lacík I, Pedraz JL., *History, challenges and perspectives of cell microencapsulation.* Trends Biotechnol., 2004. **22** p. 87-92.
102. Geller RL, L.T., Neuenfeldt S, Johnson RC, Brauker JH, *Use of an immunoisolation device for cell transplantation and tumor immunotherapy.* Ann. N. Y. Acad. Sci., 1997. **831** p. 438-451.
103. Orive G, T.S., Pedraz JL, Hallé JP, *Biocompatibility of alginate-poly-L-lysine microcapsules for cell therapy.* Biomaterials 2006. **20** p. 3691-3700.
104. Bünger CM, T.B., Jahnke A, Gerlach C, Freier T, Schmitz KP, Hopt UT, Schareck W, Klar E, de Vos P, *Deletion of the tissue response against alginate-pll capsules by temporary release of co-encapsulated steroids.* Biomaterials 2005. **26**: p. 2353-2360.

105. Figliuzzi M, P.T., Cornolti R, Adobati F, Fagiani A, Rossi L, Remuzzi G, Remuzzi A., *Biocompatibility and function of microencapsulated pancreatic islets.* Acta Biomater, 2006. **2**(2): p. 221-227.
106. Chuealee R, A.P., Noipha K, Srichana T., *Bioactivity and toxicity studies of amphotericin B incorporated in liquid crystals.* European Journal of Pharmaceutical Sciences, 2011(In Press).
107. Jin HJ, P.J., Karageorgiou V, Kim UJ, Valluzzi R, Kaplan DL, *Water-Stable Silk Films with Reduced β-Sheet Content.* Adv. Funct. Mater., 2005. **15** p. 1241-1247.
108. Chen J, A.G., Karageorgiou V, Horan R, Collette A, Volloch V, Colabro T, Kaplan DL, *Human bone marrow stromal cell and ligament fibroblast responses on RGD-modified silk fibers.* J Biomed Mater Res A, 2003. **67**: p. 559-570.
109. Peattie RA, Y.B., Cai S, Firpo MA, Pike DB, Fisher RJ, et al, *Effect of gelatin on heparin regulation of cytokine release from hyaluronan-based hydrogels.* Drug Delivery 2008. **15**: p. 363-371.
110. Uemura A, O.M., Hirashima M, Fujiwara T, Koyama S, Takagi H, et al., *Recombinant angiopoietin-1 restores higher-order architecture of growing blood vessels in mice in the absence of mural cells.* J. Clin. Invest., 2002. **110**: p. 1619-1628.
111. B, T., *Glycosaminoglycans in morphogenesis*, in *Cell Biology of the Extracellular Matrix*, H.E.e. . Editor 1982, Plenum Press New York p. 259-294.
112. Mast BA, D.R., Krummel TM, Cohen IK *Scarless wound healing in the mammalian fetus.* Surg. Gynecol. Obstet., 1992. **174:**: p. 441-451.
113. Zhang L, U.C., Chen L *Hyaluronan on the surface of tumor cells is correlated with metastatic behavior.* Cancer Res., 1995. **55**: p. 428-433.
114. Raman R, V.G., Ernst S, Sasisekharan V, Saasisekharan R, *Structural specificity of heparin binding in the fibroblast growth factor family of proteins.* Proc.Natl. Acad. Sci. , 2003. **100**: p. 2357-2362.
115. Denk PO, K.M., *he in vitro effect of platelet-derived growth factor isoforms on the proliferation of bovine corneal stromal fibroblasts depends on cell density.* Graefe's Arch Clin Exp Ophthalmol, 1997. **235**: p. 530-534.
116. Miya M, M.A., Mishima K, Sakurai N, Ikeuchi H, kuroiwa T, Hiromura K, Yokoo H, Nojima Y, *Enhancement of In Vitro Human Tubulogenesis by Endothelial Cell-derived Factors: Implications for In Vivo Tubular Regeneration after Injury* Am J Physiol Renal Physiol, 2011.
117. Schneider L, C.M., Lehman J, Nielsen SK, Guerra CF, Veland IR, Stock C, Hoffmann EL, Yoder BK, Schwab A, Satir P, Christensen ST, *Directional cell migration and chemotaxis in wound healing response to PDGF-AA are coordinated by the primary cilium in fibroblasts.* Cell Physiol Biochem, 2010 **25**(2-3): p. 279-292.
118. Amano R, Y.N., Doi Y, Yashiro M, Ohira M, ATSUSHI Miwa A, Hirakawa K. , *Significance of Keratinocyte Growth Factor Receptor in the*

Proliferation of Biliary Tract Cancer. Anticancer Research, 2010. **30**: p. 4115-4122.
119. Gragnani A, R.M., Albuquerque JCM, Brito GSS, Aloise AC, Ferreira LM, *Keratinocyte growth factor protected cultured human keratinocytes exposed to oxidative stress.* Acta Cir Bras., 2010. **25**(1): p. 93-97.
120. Tuo Q-h, X.G.-z., Zeng H, Yu H-d, Sun S-w, Ling H-y, Zhu B-y, Liao D-f, Chen J-x, *Angiopoietin-1 protects myocardial endothelial cell function blunted by angiopoietin-2 and high glucose condition.* Acta Pharmacologica Sinica, 2011. **32**: p. 45-51.
121. Shu XZ, L.Y., Palumbo FS, Luo Y, Prestwich GD, *In situ crosslinkable hyaluronan hydrogels for tissue engineering.* Biomaterials, 2004. **25** p. 1339-1348.
122. Lu Q, Z.B., Li M, Zuo B, Kaplan DL, Huang Y et al., *Degradation Mechanism and Control of Silk Fibroin.* Biomacromolecules, 2011. **12**: p. 1080-1086.
123. Beek MV, J.L., Sheardown H, *Hyaluronic acid containing hydrogels for the reduction of protein adsorption.* Biomaterials, 2008. **29**: p. 780-789.
124. Xiao H, K.D., Cebe P, *Effect of water on the thermal properties of silk fibroin.* Thermochimica Acta, 2007. **461**: p. 137-144.
125. Lim ST, F.B., Berry DJ, Martin GP, Brown MB, *In vivo evaluation of novel hyaluronan/chitosan microparticulate delivery systems for the nasal delivery of gentamicin in rabbits.* Int. J. Pharm., 2002. **231**: p. 73-82.
126. Luo Y, K.K., Prestwich GD, *Cross-linked hyaluronic acid hydrogel films: new biomaterials for drug delivery.* J Control Rel 2000. **69**: p. 169-184.
127. Dave V, T.M., Focher B, *Hyaluronic Acid- (Hydroxyproppyl) cellulose Blends: A solution and solid state study.* Macromolecules, 1995. **28** p. 3531-3539.
128. Cloyd JM, M.N., Weng L, Chen W, Mauck RL, Elliott DM, *Material properties in unconfined compression of human nucleus pulposus, injectable hyaluronic acid-based hydrogels and tissue engineering scaffolds.* Eur Spine J, 2007. **16**: p. 1892-1898.
129. Zhang XZ, W.D., Chu CC, *Synthesis, characterization and controlled drug release of thermosensitive IPN-PNIPAAm hydrogels.* Biomaterials, 2004. **25**: p. 3793-3805.
130. Niederer SA, B.M., Pullan AJ, Smith NP. *Computing Work in the Ischemic Heart*. in *Proceedings 26th Annual International Conference of the IEEE EMBS*. 2004.
131. Makai M, C.E., Németh Z, Pálinkás J, Eros I, *Structure and drug release of lamellar liquid crystals containing glycerol.* International Journal of Pharmaceutics, 2003. **256** p. 95-107.
132. Cai S, L.Y., Shu X, Prestwich GD, *Injectable glycosaminoglycan hydrogels for controlled release of human basic fibroblast growth factor.* Biomaterials 2005. **26**(30): p. 6054-6067.
133. Wissink MJB, B.R., Poot AA, Engbers GHM, Beugeling T, van Aken WG et al., *Improved endothelialization of vascular grafts by local release*

of growth factor from heparinized collagen matrices. J Control Rel, 2000. **64** p. 103-114.
134. Bernhard 0. Palsson, S.N.B., *Tissue Engineering*2004: Pearson Prentice Hall.
135. M, T., *The cadherins: cell-cell adhesion molecules controlling animal morphogenesis.* Development, 1988. **102**: p. 639-655.
136. Sharon , L.H., *Lectins as Cell Recognition Molecules.* Science, 1989. **246**: p. 227-234.
137. Mitra SK, H.D., Schlaepfer DD. , *Focal Adhesion Kinase in Command and Control of Cell Motility.* Nat Rev Mol Cell Biol., 2005. **6**: p. 56-68.
138. Shu XZ, A.S., Liu Y, Prestwich GD. . ;():902e12., *Synthesis and evaluation of injectable, in situ crosslinkable synthetic extracellular matrices for tissue engineering.* J Biomed Mater Res A, 2006. **79**(4): p. 902-912.
139. Lee CH, S.A., Lee Y, *Biomedical applications of collagen.* Int J Pharm, 2001. **22**: p. 1-22.
140. J, H., *The collagen receptor integrins have distinct ligand recognition and signaling functions.* Matrix Biology 2000. **19**: p. 319-323.
141. RO, H., *Integrins: Bidirectional, Allosteric Signaling Machines.* Cell, 2002. **110**: p. 673-687.
142. A. Howe, A.E.A., S.K. Alahari and R.L. Juliano,, *Integrin signaling and cell growth control.* Curr Opin Cell Biol, 1998. **10**(2): p. 220–231.
143. Burridge K, F.K., Kelly T, Nuckolls G, Turner C, *Focal adhesions: transmembrane junctions between the extracellular matrix and the cytoskeleton.* Annu Rev Cell Biol, 1988. **4**: p. 487-525.
144. Burridge K, C.-W.M., *Focal Adhesions, Contractility, and Signaling.* Annu Rev Cell Dev Biol., 1996. **12**: p. 463-519.
145. Provenzano PP, I.D., Eliceiri KW, Keely PJ, *Matrix density-induced mechanoregulation of breast cell phenotype, signaling, and gene expression through a FAK-ERK linkage.* Oncogene, 2009 **28**(49): p. 4326-4343.
146. Choquet D, F.D., Sheetz MP, *Extracellular Matrix Rigidity Causes Strengthening of Integrin–Cytoskeleton Linkages.* Cell, 1997. **88**: p. 39-48.
147. Galbraith CG, Y.K., Sheetz MP, *The relationship between force and focal complex development.* J Cell Biol., 2002. **159**: p. 695-705.
148. Pelham RJ, W.Y.-L., *Cell locomotion and focal adhesions are regulated by substrate flexibility.* Cell Biology, 1997. **94**: p. 13661-13665.
149. Geiger B, B.A., Pankov R, Yamada KM, *Transmembrane Extracellular Matrix-Cytoskeleton Crosstalk.* Nat Rev Mol Cell Biol., 2001(2): p. 793-805.
150. Suzuki N, Y.Y., Deyama Y, Suzuki K, Kitagawa Y, *Mechanical stress directly suppresses osteoclast differentiation in RAW264.7 cells.* Int. Jour. of Mole. Med., 2008. **21**: p. 291-296.
151. Jean C, G.P., Fournie JJ, Laurent G, *Influence of stress on extracellular matrix and integrin biology.* Oncogene, 2011: p. 1-10.

152. Matthew G. Haugh, C.M.M., Ross C. McKiernan, Cornelia Altenbuchner, Fergal J. O'Brien. Part A. May 2011, (9-10): . *Crosslinking and Mechanical Properties Significantly Influence Cell Attachment, Proliferation, and Migration Within Collagen Glycosaminoglycan Scaffolds.* Tissue Engineering: Part A 2011. **17**(9-10): p. 1201-1208.
153. Discher DE, J.P., Wang Y-L, *Tissue Cells Feel and Respond to the Stiffness of Their Substrate.* Science, 2005. **310**: p. 1139-1143.
154. Georges PC, J.P., *Cell type-specific response to growth on soft materials.* J Appl Physiol, 2005. **98**: p. 1547-1553.
155. Engler AJ, G.M., Sen S, Bonnemann CG, Sweeney HL, Discher DE, *Myotubes differentiate optimally on substrates with tissue like stiffness: pathological implications for soft or stiff microenvironments.* J Cell Biol, 2004. **166**: p. 877-887.
156. Coger R, T.M., Moghe PV, Ezzell RM, and Yarmush ML, *Hepatocyte aggregation and reorganization of EHS matrix gel.* Tissue Engineering: Part A, 1997. **3**: p. 375-390.
157. Vailhe B, R.X., Tracqui P, Usson Y, Tranqui L, *In vitro angiogenesis is modulated by the mechanical properties of fibrin gels and is related to alpha(v)beta3 integrin localization.* In Vitro Cell Dev Biol Anim, 1997. **33**: p. 763-773.
158. Vernon RB, A.J., Iruela-Arispe ML, Lane TF, Sage EH, *Reorganization of basement membrane matrices by cellular traction promotes the formation of cellular networks in vitro.* Lab Invest, 1992. **66**: p. 536-547.
159. Tilghman RW, C.C., Mih JD, Koryakina Y, Gioeli D, et al. . *Matrix Rigidity Regulates Cancer Cell Growth and Cellular Phenotype.* PLoS ONE, 2010 **5**(9): p. 1-13.
160. Farhangkhoee H, K.Z., Kaur H, Xin X, Chen S, Chakrabarti S, *Vascular endothelial dysfunction in diabetic cardiomyopathy: pathogenesis and potential treatment targets.* Pharmacol Ther, 2006. **111**: p. 384-99.
161. Lovren F, P.Y., Shukla PC, Quan A, Teoh H, Szmitko PE, et al., *Visfatin activates eNOS via Akt and MAP kinases and improves endothelial cell function and angiogenesis in vitro and in vivo: translational implications for atherosclerosis.* Am J Physiol Endocrinol Metab, 2009. **296**: p. E1440-1449.